



2015

Influence of Calcium Sulfoaluminate Cement on the Pullout Performance of Reinforcing Fibers: An Evaluation of the Micro-Mechanical Behavior

Robert B. Jewell

University of Kentucky, bob.jewell@uky.edu

Recommended Citation

Jewell, Robert B., "Influence of Calcium Sulfoaluminate Cement on the Pullout Performance of Reinforcing Fibers: An Evaluation of the Micro-Mechanical Behavior" (2015). *Theses and Dissertations--Civil Engineering*. 27.
http://uknowledge.uky.edu/ce_etds/27

This Doctoral Dissertation is brought to you for free and open access by the Civil Engineering at UKnowledge. It has been accepted for inclusion in Theses and Dissertations--Civil Engineering by an authorized administrator of UKnowledge. For more information, please contact UKnowledge@lsv.uky.edu.

STUDENT AGREEMENT:

I represent that my thesis or dissertation and abstract are my original work. Proper attribution has been given to all outside sources. I understand that I am solely responsible for obtaining any needed copyright permissions. I have obtained needed written permission statement(s) from the owner(s) of each third-party copyrighted matter to be included in my work, allowing electronic distribution (if such use is not permitted by the fair use doctrine) which will be submitted to UKnowledge as Additional File.

I hereby grant to The University of Kentucky and its agents the irrevocable, non-exclusive, and royalty-free license to archive and make accessible my work in whole or in part in all forms of media, now or hereafter known. I agree that the document mentioned above may be made available immediately for worldwide access unless an embargo applies.

I retain all other ownership rights to the copyright of my work. I also retain the right to use in future works (such as articles or books) all or part of my work. I understand that I am free to register the copyright to my work.

REVIEW, APPROVAL AND ACCEPTANCE

The document mentioned above has been reviewed and accepted by the student's advisor, on behalf of the advisory committee, and by the Director of Graduate Studies (DGS), on behalf of the program; we verify that this is the final, approved version of the student's thesis including all changes required by the advisory committee. The undersigned agree to abide by the statements above.

Robert B. Jewell, Student

Dr. Kamyar C. Mahboub, Major Professor

Dr. Yi-Tin Wang, Director of Graduate Studies

INFLUENCE OF CALCIUM SULFOALUMINATE CEMENT ON THE PULLOUT
PERFORMANCE OF REINFORCING FIBERS: AN EVALUATION OF THE
MICRO-MECHANICAL BEHAVIOR

DISSERTATION

A dissertation submitted in partial fulfillment of the requirements for the degree of
Doctor of Philosophy in the College of Engineering at the University of Kentucky

By

Robert Benjamin Jewell

Lexington, Kentucky

Director: Dr. Kamyar Mahboub, Associate Dean of Engineering and Lawson Professor
of Civil Engineering, University of Kentucky

Lexington, Kentucky

2015

Copyright © Robert Benjamin Jewell 2015

ABSTRACT OF DISSERTATION

INFLUENCE OF CALCIUM SULFOALUMINATE CEMENT ON THE PULLOUT PERFORMANCE OF REINFORCING FIBERS: AN EVALUATION OF THE MICRO-MECHANICAL BEHAVIOR

The objective of this research was to determine the influence of calcium sulfoaluminate (CSA) cement on reinforcing fibers by evaluating the fiber pullout behavior, and bonding characteristics, of a single fiber embedded in a cementitious paste matrix. Four types of fibers commonly used in industry were evaluated: 1) Polyvinyl alcohol; 2) Polypropylene; 3) Coated Steel; and 4) Plain Steel.

Upward trends in energy costs and potential greenhouse gas regulations favor an increased use of construction materials that require lower energy and lower CO₂ emissions to fabricate, such as CSA cement, as opposed to the production of ordinary portland cement (OPC), which is more energy intensive and produces more CO₂ emissions. However, widespread use of CSA cement requires a more in-depth understanding of the engineering characteristics that govern its performance, including interaction with reinforcing fibers.

The overarching objective of this research was to provide the engineering base needed for the utilization of reinforcing fibers in CSA cement-based construction materials. The aims of the research were (1) to develop an ettringite-rich calcium sulfoaluminate cement, and (2) evaluate the pullout characteristics of reinforcing fibers embedded in a CSA-cement matrix. Key elements of the strategy included (1) Compare the performance of a laboratory-fabricated CSA cement to a commercial CSA cement and OPC, (2) Evaluate the peak load, and toughness of reinforcing fibers in CSA cement and OPC, (3) Evaluate the debonding-energy density and multiple-cracking behavior of fibers in CSA cement and OPC, and (4) Evaluate the shear bond strength of reinforcing fibers in CSA cement and OPC.

Based on the findings of this PhD dissertation, calcium sulfoaluminate cement has a significant influence on the characteristics and behavior of embedded reinforcing fibers. An important factor contributing to the bond strength between fiber and matrix was the ability to transfer interfacial stresses from fiber to matrix. The more rigid-dense morphology of the CSA cement paste related to the ettringite crystal structure yielded

higher peak loads, toughness, debonding-energy densities and shear-bond strengths for both steel and synthetic fibers. In addition to cement phase morphology, the reduction of the fiber/matrix elastic modulus ratio was found to be a primary factor affecting the performance and behavior of fibers embedded in a cementitious matrix.

KEYWORDS: Calcium Sulfoaluminate Cement, Single-Fiber Pullout, Interfacial Bond, Reinforcing Fibers, Fiber-Matrix Bond

Robert Benjamin Jewell

Student's Signature

4/17/2015

Date

INFLUENCE OF CALCIUM SULFOALUMINATE CEMENT ON THE PULLOUT
PERFORMANCE OF REINFORCING FIBERS: AN EVALUATION OF THE
MICRO-MECHANICAL BEHAVIOR

By

Robert Benjamin Jewell

Dr. Kamyar C. Mahboub

Co-Director of Dissertation

Dr. Yi-Tin Wang

Director of Graduate Studies

4/17/2015

Date

This dissertation is dedicated to my wife Meghan and my sons, Elliott and Isaac

ACKNOWLEDGMENTS

I would never have been able to finish my dissertation without the guidance of my committee members and support from my wife, children and family.

I would like to express my gratitude to my advisor, Dr. Kamyar Mahboub, for his time, support and patience during my doctoral education. I would like to thank my supervisor Dr. Thomas Robl for encouraging me to seek a PhD, and for creating the flexibility in my job that provided time for classwork and research. I would also like to thank Dr. Harik, Dr. Bryson, and Dr. Bathke for guiding my research and for providing sound advice on the doctoral process. I am very appreciative for the time, teaching, and expertise of Dr. Wood on finalizing the statistical analyses.

Finally, I would like to thank my wife, Meghan Jewell. She is my greatest supporter and walked beside me the entire way. To my sons, Elliott and Isaac, for their unconditional love and understanding of my absence on this journey.

The work reported in this dissertation was supported by the University of Kentucky Center for Applied Energy Research and the National Institute for Hometown Security.

TABLE OF CONTENTS

ACKNOWLEDGMENTS.....	iii
TABLE OF CONTENTS.....	iv
LIST OF TABLES.....	x
LIST OF FIGURES.....	xii
CHAPTER 1 : INTRODUCTION.....	1
1.1. Introduction.....	1
1.2. Background.....	4
1.2.1. Calcium Sulfoaluminate Cements.....	4
1.2.2. Engineered Cementitious Composites.....	6
1.3. Literature Review.....	7
1.3.1. Reinforcing Fibers in Concrete.....	8
1.3.2. Calcium Sulfoaluminate Cements and Fabrication from CCBs.....	8
1.3.3. Engineered Cementitious Composite and the Single-Fiber Pullout Test Method.....	10
1.3.4. Multiple Cracking Behavior of ECCs.....	12
1.3.5. Interfacial-Shear Strength of ECCs.....	12
1.4. Nomenclature.....	13

1.4.1. Cement Chemistry Notation.....	13
1.4.2. Acronyms.....	15
CHAPTER 2 : MATERIALS AND METHODS.....	16
2.1. Materials.....	16
2.1.1. Calcium Sulfoaluminate Cement.....	17
2.1.2. Ordinary Portland Cement.....	18
2.1.3. Polyvinyl-Alcohol Fiber.....	18
2.1.4. Polypropylene Fiber.....	20
2.1.5. Steel Fibers.....	20
2.2. Methods.....	21
2.2.1. Calcium Sulfoaluminate Cement Fabrication.....	21
2.2.2. Sample Characterization.....	22
2.2.3. Single-Fiber Pullout Test Setup.....	23
2.2.4. Preparation of Test Specimens.....	25
2.2.5. Statistical Analysis.....	27
CHAPTER 3 : FABRICATION AND TESTING OF LOW-ENERGY CSAB CEMENTS THAT UTILIZE CIRCULATING FLUIDIZED BED COMBUSTION BYPRODUCTS.....	28

3.1. Introduction.....	28
3.2. Fabrication of CSAB Cement from CCBs.....	32
3.3. Paste Study – Effect of Gypsum Content.....	37
3.4. Fabrication of Bulk CSAB Clinker Cement.....	43
3.5. Strength Testing of CSAB Mortar.....	44
3.5.1. Set Time.....	44
3.5.2. Strength of Commercial CSA Cement Mortar.....	45
3.5.3. Strength of Laboratory CSA Cement Mortar.....	46
3.6. Conclusions.....	50
CHAPTER 4 : INTERFACIAL BOND BETWEEN REINFORCING FIBERS AND CSA CEMENTS: FIBER PULLOUT CHARACTERISTICS.....	52
4.1. Introduction.....	52
4.2. Research Significance – Chapter 4.....	55
4.3. Experimental Results and Discussion.....	56
4.3.1. Single-Fiber Pullout Test.....	56
4.3.2. PVA fiber.....	58
4.3.3. Polypropylene fiber.....	59
4.3.4. Coated steel fiber.....	60

4.4. Peak Load Analysis.....	61
4.4.1. Ordinary Portland Cement.....	61
4.4.2. Commercial CSAB cement.....	63
4.4.3. CAER CSAB cement.....	66
4.5. Energy Consumption Analysis.....	68
4.5.1. Ordinary Portland Cement.....	68
4.5.2. Commercial CSAB Cement.....	70
4.5.3. CAER CSAB Cement.....	71
4.6. Statistical Analysis.....	72
4.6.1 Peak Load.....	73
4.6.2. Pullout Energy Consumption.....	74
4.6.3. Synthesis of the Statistical Analysis.....	75
4.7. Conclusions.....	76
 CHAPTER 5 : INFLUENCE OF CEMENT TYPE ON MULTIPLE CRACKING BEHAVIOR IN FIBER COMPOSITES.....	
5.1. Introduction.....	79
5.2. Research Significance – Chapter 5.....	83
5.3. Experimental Program.....	84

5.4. Experimental Results and Discussion.....	85
5.4.1. Fiber/Matrix Debond-Energy Density.....	85
5.4.2. Influence of Hydrated Cement Morphology.....	93
5.4.3. Fiber Bridging Stress.....	96
5.4.4. Toughening Mechanisms.....	106
5.5. Statistical Analysis.....	108
5.5.1. Steel Fiber Results.....	110
5.5.2. Synthetic Fiber Results.....	113
5.6. Conclusion.....	116
 CHAPTER 6 : INFLUENCE OF CEMENT TYPE ON FIBER-MATRIX INTERFACE	
BOND STRENGTH.....	118
6.1. Introduction.....	118
6.2. Research Significance – Chapter 6.....	122
6.3. Experimental program.....	123
6.4. Experimental Results and Discussion.....	124
6.4.1. Influence of Hydrated Cement Morphology.....	124
6.4.2. Interface Shear Strength.....	127
6.4.3. Shear-Bond Stress.....	130

6.4.4. Axial-Bond Stresses.....	136
6.4.5. Influence of Interface Stresses on Composite Toughness.....	140
6.5. Statistical Analysis.....	143
6.5.1. Steel Fiber Results.....	145
6.5.2. Synthetic Fiber Results.....	148
6.6. Conclusion.....	151
CHAPTER 7 : CONCLUSIONS AND FUTURE WORK.....	152
7.1. General Conclusions.....	152
7.2. Future Work.....	154
APPENDICES.....	156
APPENDIX A : STATISTICAL ANALYSIS.....	156
APPENDIX B : SINGLE-FIBER PULLOUT TEST DATA.....	159
REFERENCES.....	181
VITA.....	189

LIST OF TABLES

Table 1-1. Cement abbreviations, chemical formulae and scientific names of cement components and phases.....	14
Table 1-2. List of acronyms.....	15
Table 2-1. Properties of reinforcing fibers (data from product technical datasheet.....)	17
Table 2-2. Description of raw materials.....	22
Table 2-3. Chemical composition of CCBs.....	23
Table 3-1. Comparison of clinker phases.....	36
Table 3-2. CSAB cement formulations.....	37
Table 3-3. CSAB cement composition from XRF analysis.....	37
Table 3-4. Mortar mix proportions following ASTM C 305 and C 109 protocols.....	44
Table 3-5. Effect of set retarder on the set time of CSAB, from China, cement mortar.....	45
Table 4-1. Peak load (N) and energy consumption values (mJ).....	57
Table 4-2. Analysis of variance on peak load.....	74
Table 4-3. Analysis of variance on energy consumption.....	74
Table 4-4. Synthesis of statistical analysis.....	75
Table 5-1. Coefficient of determination before and after log transformation.....	109
Table 5-2. ANOVA results for effect of cement type and levels of days of curing on debonding-energy density for the plain-steel fiber.....	110
Table 5-3. ANOVA results for effect of cement type and levels of days of curing on debonding-energy density for the coated-steel fiber.....	112
Table 5-4. ANOVA results for effect of cement type and levels of days of curing on debonding-energy density for the polypropylene fiber.....	113
Table 5-5. ANOVA results for effect of cement type and levels of days of curing on debonding-energy density for the polyvinyl-alcohol fiber.....	115
Table 6-1. Matrix strength and elastic modulus results.....	135
Table 6-2. E_f/E_m ratios.....	139
Table 6-3. Coefficient of determination before and after log transformation.....	144

Table 6-4. Type I ANOVA for effect of cement type and levels of days of curing on shear strength for the plain-steel fiber.....	145
Table 6-5. Type I ANOVA for effect of cement type and levels of days of curing on shear strength for the coated-steel fiber.....	147
Table 6-6. Type I ANOVA for effect of cement type and levels of days of curing on shear stress for the polypropylene fiber.....	148
Table 6-7. Type I ANOVA for effect of cement type and levels of days of curing on shear stress for the polyvinyl-alcohol fiber.....	150

LIST OF FIGURES

Figure 1-1. The crystalline structure of ettringite modified from Hartman and Berliner (2006); the c-axis is vertical.....	9
Figure 2-1. SEM image of a coated steel fiber, 400x magnification.....	21
Figure 2-2. <i>Left</i>) Tensile testing machine setup; <i>Right</i>) Screw-type grips for securing specimen.....	25
Figure 2-3. Specimen preparation; fiber embedded in paste plug.....	26
Figure 2-4. Fiber pullout specimen preparation: <i>Left</i>) Schematic of mold used to form each cement plug; <i>Right</i>) Grips with fiber-plug specimen.....	27
Figure 3-1. XRD profiles of the three laboratory synthesized clinkers compared to the commercially available CSAB cements. K = Klein's Compound; An = anhydrite; B = belite (C ₂ S).....	34
Figure 3-2. CSAB clinker demonstrating color variation and mass loss based on oven-firing temperature.....	35
Figure 3-3. SEM image of ettringite crystals within the CSAB#2 paste, taken at 3000x magnification.....	39
Figure 3-4. XRD profiles for the hydration of the CSAB#2, 15% gypsum, cement. Gp = gypsum; K = Klein's Compound; B = belite; Et = ettringite. On the right, an SEM image, under 2500x magnification, showing the formation of ettringite crystals in the CSAB#2, 15% gypsum cement after 7-days of curing.....	40
Figure 3-5. XRD profiles for the hydration of the CSAB#2, 20% gypsum, cement. On the right, an SEM image, under 2500x magnification, showing the formation of well-defined ettringite crystals in the CSAB#2, 20% gypsum, cement after 7-days of curing.....	41
Figure 3-6. XRD profiles for the hydration of the CSAB#2, 20% gypsum with 1% lime, cement. On the right, an SEM image, under 2500x magnification, showing the formation of ettringite crystals in the CSAB#2, 20% gypsum 1% lime, cement after 7-days of curing.....	42
Figure 3-7. Compressive strength of mortar cubes using the CSAB#2 cement with the addition of gypsum and lime.....	43
Figure 3-8. Compressive strength of mortar cubes made with commercially available CSAB cement.....	47
Figure 3-9. Compressive strength of the CSAB#4 cement mortar.....	49

Figure 3-10. <i>Left</i> : SEM image, under 700x magnification, of ettringite crystals in the CSAB#4 cement mortar. <i>Right</i> : SEM image, under 1500x magnification, showing ettringite crystals within the CSAB#4 cement paste.....	49
Figure 3-11. SEM image of the CSAB#4 cement used in mortar with sand grains clearly embedded in the paste; with a zoomed view of the sand grain surface.....	50
Figure 4-1. Typical load-displacement curves for each fiber type.....	57
Figure 4-2. Clusters of ettringite crystals adhered to a single PVA fiber after 3-days of curing.....	59
Figure 4-3. <i>Left</i> : Polypropylene fiber after the pullout test. <i>Right</i> : Surface of fiber with valley-and-ridge structure.....	60
Figure 4-4. SEM images of a copper-coated steel fiber: (A) Copper coating peeled from fiber surface; (B) Fiber end with crack in copper coating; (C) Zoomed image of crack with defined boundary between copper coating and steel surface.....	61
Figure 4-5. Peak load development of PVA, PP and steel fibers embedded in an OPC matrix; standard error of the mean are indicated for each column.....	62
Figure 4-6. SEM images of fibers pulled from the OPC matrix (500x magnification): (A) PVA; (B) PP; (C) Steel.....	63
Figure 4-7. SEM image of the matrix morphology for the commercial CSAB Cement.....	64
Figure 4-8. Peak load development of PVA, PP and steel fibers in the Commercial CSAB matrix.....	65
Figure 4-9. SEM images of fibers pulled from the Commercial CSAB matrix (500x magnification): (A) PVA; (B) PP; (C) Steel.....	66
Figure 4-10. SEM image of the CAER CSAB cement with long needle-like ettringite Crystals.....	67
Figure 4-11. Peak load development of PVA, PP and steel fibers in the CAER CSAB cement.....	67
Figure 4-12. SEM images of fibers pulled from the CAER CSAB matrix (500x magnification): (A) PVA; (B) PP; (C) Steel.....	68
Figure 4-13. Energy consumption development of PVA, PP and steel fibers in the OPC matrix.....	69

Figure 4-14. Energy consumption development of PVA, PP and steel fibers in the Commercial CSAB cement.....	71
Figure 4-15. Energy consumption development of PVA, PP and steel fibers in the CAER CSAB cement.....	72
Figure 5-1. Fiber-matrix debond-energy density as a function of curing time for the steel fibers.....	90
Figure 5-2. Fiber-matrix debond-energy density as a function of curing time for the synthetic fibers.....	92
Figure 5-3. SEM image of OPC paste showing irregular structure of C-S-H phases; 9000x magnification.....	94
Figure 5-4. SEM images of hydrated CSA cement: <i>Top</i> : Commercial CSA, 2500x magnification; <i>Bottom</i>) CSAB#4, 1500x magnification.....	95
Figure 5-5. Fiber bridging stress as a function of curing time in the OPC paste.....	100
Figure 5-6. Fiber bridging stress as a function of curing time in the Commercial CSA cement paste.....	103
Figure 5-7. Fiber bridging stress as a function of curing time in the CSAB#4 cement paste.....	105
Figure 5-8. Chart illustrating relationship between fiber strain and fiber-bridging stress.....	108
Figure 5-9. Analysis of variance for debonding-energy density for the plain-steel fiber.....	111
Figure 5-10. Analysis of variance for debonding-energy density for the coated-steel fiber.....	112
Figure 5-11. Analysis of variance for debonding-energy density for the polypropylene fiber.....	114
Figure 5-12. Analysis of variance for debonding-energy density for the polyvinyl-alcohol fiber.....	115
Figure 6-1. Fiber pullout specimen.....	120
Figure 6-2. SEM image of OPC paste showing irregular structure of CSH phases, magnification is 9000x.....	125
Figure 6-3. SEM image of CSA cement paste showing acicular ettringite structure, magnification is 1500x.....	126

Figure 6-4. Representative load-displacement highlighting key points in the fiber pullout process.....	129
Figure 6-5. Relationship between E_f/E_m ratio and shear-bond stress of coated-steel fibers.....	132
Figure 6-6. Relationship between E_f/E_m ratio and shear-bond stress of plain-steel fibers.....	133
Figure 6-7. Relationship between E_f/E_m ratio and shear-bond stress of PVA fibers.....	134
Figure 6-8. Relationship between E_f/E_m ratio and shear-bond stress of PP fibers.....	135
Figure 6-9. Normalized axial stress as a function of normalized axial position for the Coated-Steel Fiber in OPC at different E_f/E_m ratios.....	138
Figure 6-10. Normalized interfacial shear stress as a function of normalized axial position for the Coated-Steel Fiber in OPC at different E_f/E_m ratios.....	139
Figure 6-11. Influence of cement and fiber type on fiber-matrix axial stresses.....	140
Figure 6-12. Comparing the relationship between energy consumption from total fiber pullout to total fracture toughness as a function of interface shear bond.....	142
Figure 6-13. Analysis of variance response curves of shear strength for the plain-steel fiber.....	146
Figure 6-14. Analysis of variance response curves of shear stress for the coated-steel fiber.....	147
Figure 6-15. Analysis of variance response curves of shear stress for the polypropylene fiber.....	149
Figure 6-16. Analysis of variance response curves of shear stress for the polyvinyl-alcohol fiber.....	150

CHAPTER 1 : INTRODUCTION

1.1. Introduction

The primary reason for the addition of fibers to cementitious matrices is to delay and contain cracking (Naaman, Namur et al. 1991, Lin and Li 1997, ACI 2010). While it is generally believed that the inclusion of fibers enhances the pre-cracking behavior of cement composites by increasing its cracking strength, the effect of fiber addition becomes evident only after cracking (Naaman, Namur et al. 1991, Lin and Li 1997, ACI 2010). Fibers bridge the cracked parts of the matrix, thus delaying sudden global failure of the composite (Lin and Li 1997). Therefore, in the post-cracking stage the fiber behavior is governed by the interfacial bond stress response as being subjected to pull-out loads (Naaman, Namur et al. 1991). The bond between fiber and matrix is important, if fibers have a weak bond with the matrix they can slip out at low loads and do not contribute to preventing the propagation of cracks. However, if the bond is too strong then the fibers may rupture before they can contribute to the post-crack strength of the matrix material.

Fiber-reinforced composites (FRC) resist tensile forces through a composite action, whereby part of the tensile force is resisted by the matrix, while the balance is taken by the fibers (Naaman, Namur et al. 1991). The transmission of forces between the fiber and the matrix is achieved through a bond defined as the shearing stress at the interface between the fiber and the surrounding matrix (Naaman, Namur et al. 1991). The fiber contribution to increasing the toughness (total energy absorbed with a unit mJ) of the composite is primarily dictated by the mechanisms of fiber pullout (Naaman, Namur et al. 1991, Brown, Shukla et al. 2002). Fiber pull-out tests are often used to study the

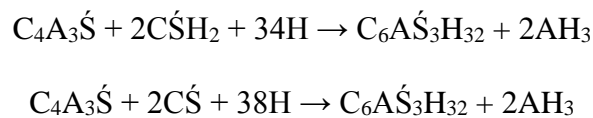
fiber-matrix bond behavior in fiber reinforced cement composites. This test simulates the fiber bridging-pull-out mechanism during the failure process of FRC (Wang, Li et al. 1988). In relating pullout test results with the fiber-matrix bond characteristics, numerous studies have been completed to demonstrate the reliability of the data (Bentur, Mindess et al. 1989, Naaman, Namur et al. 1991, Herrera-Franco and Drzal 1992, Betterman, Ouyang et al. 1995, Mobasher and Cheng Yu 1996, Zucchini and Hui 1996, Wille and Naaman 2012).

Composites made with brittle fibers, such as steel, and brittle matrices, i.e. calcium sulfoaluminate cement, can exhibit high toughness when failure occurs preferentially along the interface before fibers fail in tension. Most of the important toughening mechanisms are a direct result of the interface-related shear failure which gives rise to an improved energy absorption capability with a sustained crack growth stability through crack surface bridging and crack tip blunting (Li and Stang 1997). The prevalent type of cracking depends on the properties of the interface relative to the fiber and matrix (Kim and Mai 1998). According to Kim and Mai (1998), when a crack approaches an isolated fiber, the following failure mechanisms may be expected to take place: 1) fiber-matrix interface debonding; 2) post-debonding friction; 3) fiber tensile failure; 4) stress redistribution and 5) fiber pullout.

The cement-fiber interfacial bond results from some combination of mechanical interlocking of cement hydration products with the fiber surface and chemical reaction between fiber and cement paste within the interstitial transition zone (Kim and Mai 1998, Brown, Shukla et al. 2002, Chan and Chu 2004, Markovic 2006). In FRC materials, the principal factor governing load transfer from the matrix to the fiber is shear strength of

the interfacial bond between the two components. Broken specimens of fiber-reinforced concrete show that failure takes place primarily due to fiber pullout or debonding. Generally fiber pullout rather than rupture confers a larger ductility to the fiber reinforced composites (Li and Stang 1997, Lin and Li 1997). Unlike plain concrete, a fiber-reinforced concrete specimen does not break immediately after initiation of the first crack; thereby increasing the work of failure, or toughness. Within the cracked section, the matrix does not resist any tension and the fibers carry the entire load applied to the composite. With an increasing load on the composite, fibers will tend to transfer additional stress to the matrix through bond stresses. If these bond stresses do not exceed the bond strength, then there may be additional cracking in the matrix. This process of multiple cracking will continue until either the fibers fail or accumulated local debonding will lead to fiber pullout (Shah 1991, Mehta and Monteiro 2006).

The principal phases of CSA clinker are $4\text{CaO}\cdot 3\text{Al}_2\text{O}_3\cdot \text{SO}_3$ ($\text{C}_4\text{A}_3\text{S}$), also called Klein's compound or yeelimite, Ca_2SiO_4 (C_2S) or belite, and C_4AF (or brownmillerite) (Arjunan, Silsbee et al. 1999). Other phases such as calcium aluminates (e.g. C_{12}A_7 or $\text{C}_{11}\text{A}_7\text{CaF}_2$) are sometimes present. Unlike portland cement, which gains its strength from the hydration of calcium silicates, alite (C_3S) and belite (C_2S), CSA cement gains strength from the hydration of Klein's compound with calcium sulfate (such as gypsum $\text{C}\text{S}\text{H}_2$ or anhydrite CS) to form ettringite via these reactions (Arjunan, Silsbee et al. 1999, Marroccoli, Nobili et al. 2007):



These reactions are relatively fast, and are nearly complete within one month. When the sulfate anion is depleted, ettringite $C_6A\dot{S}_3H_{32}$ (AFt phase) is converted to monosulfate $C_4A\dot{S}H_{12}$ (AFm phase or “mono” phase) which reduces the strength of the cement.

1.2. Background

1.2.1. Calcium Sulfoaluminate Cements

The production of portland cement requires a large amounts of energy, mainly because of the high temperatures required to partially melt and fuse the raw materials into clinker. Portland cement clinker, which is comprised mainly of calcium silicates, is also very hard and requires considerable energy to grind to the final product (Arjunan, Silsbee et al. 1999). Furthermore, limestone is the predominant raw material used to produce Portland cement and releases large amounts of CO_2 during the thermal processing. In order to attain substantial reductions in energy consumption and CO_2 emissions, significantly lowering the clinkering temperature and the proportion of limestone in the feed is necessary (Damtoft, Lukasik et al. 2008, Gartner and Macphee 2011, Schneider, Romer et al. 2011). This is unfortunately not possible with portland cement. However, energy-conserving or “low-energy” cements can be produced at lower temperatures and using much less limestone than portland cement. They can also be much softer and easier to grind (Beretka, de Vito et al. 1993). An additional environmental benefit is that CSA cements can be prepared using substantial amounts of coal combustion wastes as the raw materials. These include FGD gypsum, pulverized coal combustion (PCC) fly ash, and fluidized bed combustion (FBC) ash. There are several types or classes of low-energy, low- CO_2 cements (Juenger, Winnefeld et al. 2011). The proposed research focuses on

one type: calcium sulfoaluminate (CSA) cements however portland cement specimens will be tested for comparative purposes.

Currently in the U.S., there are approximately 60 fluidized bed combustion boilers used to generate electricity. Although FBC boilers can substantially reduce SO_x and NO_x emissions relative to a pulverized coal combustion (PCC) boiler, they generate a much larger quantity of solid byproducts. FBC burns coal in a fluidized bed of sorbent, usually limestone, which removes most of the SO_x emissions. The resultant byproducts are thus mainly composed of calcium sulfate, and also contain lesser amounts of unreacted sorbent i.e. lime or CaO. There are two types of byproducts produced in an FBC boiler: spent bed material, which is a coarse sandy material, and fly ash, which is a much finer material that is captured from the flue gas. The spent bed material generally contains a higher proportion of lime and calcium sulfate than the fly ash, whereas the latter contains more alumina and silica because of the presence of ash from the combusted coal. The lime, alumina and calcium sulfate within FBC byproducts imparts a cementitious nature when they are mixed with water. The cementitious properties are largely the result of the formation of two hydrated phases: gypsum and ettringite. Gypsum is formed from the hydration of the anhydrous calcium sulfate, anhydrite (Marroccoli, Nobili et al. 2007). Ettringite is a calcium aluminum sulfate hydrate that forms in a high pH environment, i.e. that occurring from the dissolution of lime in the FBC ash.

In China, CSA cements have been used primarily to replace portland cement in mortars and concrete when rapid strength gain, self-stressing properties or sulfate resistance is desired. Approximately 1 million tons per year are manufactured in China which has special standards for the cements (Zhang and Glasser 1999, Zhang, Su et al. 1999,

Damtoft, Lukasik et al. 2008, Ukrainczyk, Frankoviæ Mihelj et al. 2013). CSA-type cements have a long history of use in the United Kingdom for specialty applications such as in the mining industry. Brown (1993) described a wide range of formulations for products used in construction, for example, general purpose low shrinkage cement, shrinkage compensated concrete slabs, mortar coatings for concrete pipes, rapid repair and setting m mortars, anchor bolt grouts and glass fiber reinforced cement products (Brown 1993). The proposed work will use a combination of ordinary portland cement, a CSA cement manufactured in the United States and a CSA cement fabricated from coal-combustion byproducts at the Center for Applied Energy Research

1.2.2. Engineered Cementitious Composites

The increasing interest in researching and utilizing ultrahigh performance concrete (UHPC) as a means for moving away to lessen or remove the need for reinforcing steel in the construction process. Cementitious matrices have been developed that are capable of surpassing structural strengths within the first day of curing; in some cases, within the first few hours after mixing. After 28 days of curing these same mixes have attained strengths, both compressive and flexural, that can potentially replace steel members in a structure. As cementitious matrices continue to be engineered to perform at ultrahigh compressive and flexural strengths there is an underlying need for the characterization of how these enhanced systems interact with reinforcing fibers. High-strength cementitious systems are brittle and exhibit low-energy absorption or toughness as a result of their inability to sustain deformation and crack resistance. The proposed research intends to illustrate how the fiber-matrix composite is influenced from the utilization of high-strength cementitious systems, specifically calcium sulfoaluminate cements. As

compared to lower-strength systems, like that of an ordinary portland cement. Moreover, there is a need to understand better the pullout process and the energy absorbing mechanisms associated with increased toughness in composites.

The most crucial link between the properties of fiber, matrix and fiber-matrix interface and that of a composite is the crack bridging stress-crack opening relation. This relation defines the ultimate stress and strain of a uniaxial tensile stress-strain curve and the energy consumption due to fiber bridging, which in turn control the strength, ductility and toughness of a structural member (Lin and Li 1997).

The bond between the fiber and matrix is important, if the fibers have a weak bond with the matrix they can slip out at low loads and do not contribute to preventing the propagation of cracks. However, if the bond is too strong then the fibers will rupture before they can contribute to the post-crack strength of the matrix material and will exhibit a low complementary energy.

1.3. Literature Review

Published literature on the subject of reinforcing fiber in calcium sulfoaluminate cement is not available, and is the main thrust for pursuing this research opportunity. There is a great deal of published work on the bonding characteristics of reinforcing fibers in a portland cement matrix.

1.3.1. Reinforcing Fibers in Concrete

The length and volume of fibers present in a concrete mix are critical in controlling the flexural strength and toughness of the hardened concrete, including the prevention of

crack propagation. Generally, the composite will carry increasing loads after the first cracking of the matrix if the pull-out resistance of the fibers at the first crack is greater than the load at first cracking. Within the cracked section, the matrix does not resist any tension and the fibers carry the entire load taken by the composite. With an increasing load on the composite, the fibers will tend to transfer the additional stress to the matrix through bond stresses. If these bond stresses do not exceed the bond strength, then there may be additional cracking in the matrix. This process of multiple cracking will continue until either the fibers fail or the accumulated local debonding will lead to fiber pullout (Shah 1991, Mehta and Monteiro 2006).

1.3.2. Calcium Sulfoaluminate Cements and Fabrication from CCBs

There are several types or classes of low-energy, low-CO₂ cements (Juenger, Winnefeld et al. 2011). The proposed research focuses on one type: calcium sulfoaluminate (CSA) cements which gain strength primarily from the formation of a calcium aluminum sulfate hydrate called ettringite (Beretka, de Vito et al. 1993, Sherman, Beretka et al. 1994, Arjunan, Silsbee et al. 1999, Janotka, Krajci et al. 2003, Bernardo, Telesca et al. 2006). Because of the rapid rate of formation of ettringite, CSA cements gain strength very quickly. The research described herein will involve the formulation, production and evaluation of an FBC byproduct-based product: CSAB cement produced by heating the FBC spent bed in the presence of limestone, bauxite and PCC fly ash. The formulation, production and performance testing, in relation to reinforcing fibers are described in the proposed research.

Ettringite is a hexagonal hydrated calcium aluminum sulfate ($a = 11.26$, $c = 21.48$ Å, space group $P31c$, $Z = 2$; Figure 1-1) (Moore and Taylor 1968, Grier, Jarabek et al. 2002, Hartman and Berliner 2006, Stark, Möser et al. 2007). Numerous analogous compounds exist for ettringite, where carbonate (CO_3^{2-}), sulfite (SO_3^{2-}), borate (BO_3^{3-}), and other oxyanions may replace sulfate, and Fe^{3+} , Cr^{3+} , and other cations substitute for Al^{3+} (Grier, Jarabek et al. 2002).

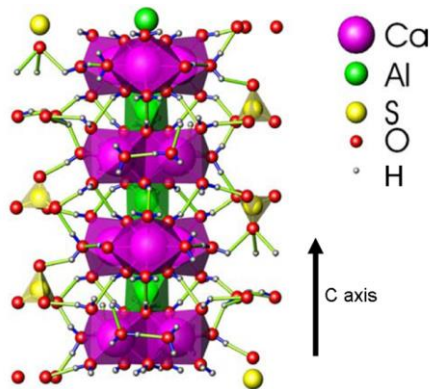


Figure 1-1. The crystalline structure of ettringite modified from Hartman and Berliner (2006); the c -axis is vertical.

The sizes and shapes of ettringite crystals in cements depend on chemical conditions and whether the ettringite forms early or later in curing, or during weathering in commercial products. Different chemical reactions produce ettringite crystals of variable sizes and habits, including needle-like, fibrous and prismatic forms (Xu and Stark 2005, Hartman and Berliner 2006). In one set of experiments, Xu and Stark (2005) noticed that small prismatic crystals of ettringite formed within ~30 minutes after the initiation of curing of ordinary portland cement. The addition of an alkaline shotcrete accelerator, mainly consisting of sodium aluminate ($\text{NaAl}[\text{OH}]_4$) and sodium hydroxide (NaOH), produced

fiber- and needle-like ettringite within 0.5 to 8 hours of curing (Xu and Stark 2005). The high strength, dense crystal structure, of ettringite-rich CSA cements underscore the reason for exploring their interaction with reinforcing fibers. Therefore a CSA produced by Buzzi Unicem USA for rapid repair of concrete structures will be used along with a low-energy, low-CO₂ CSA cement produced from coal-combustion byproducts.

1.3.3. Engineered Cementitious Composite and the Single-Fiber Pullout Test

Method

The design of engineered cementitious composites (ECC) is targeted at creating a fiber reinforced cementitious material with a deformation behavior analogous to that of metals, specifically at achieving pseudo strain-hardening and cracking behaviors after first cracking (Li and Leung 1992, Lin and Li 1997, Li and Fischer 2002). Unlike plain concrete, a fiber-reinforced concrete specimen does not break immediately after initiation of the first crack. This has the effect of increasing the work of failure, or toughness.

Fiber-reinforced composites (FRC) resist tensile forces through a composite action, whereby part of the tensile force is resisted by the matrix, while the balance is taken by the fibers (Naaman, Namur et al. 1991). The transmission of forces between the fiber and the matrix is achieved through bond defined as the shearing stress at the interface between the fiber and the surrounding matrix (Naaman, Namur et al. 1991). It is generally agreed that the fiber contribution to increasing the toughness of the composite is primarily dictated by the mechanisms of fiber pullout (Naaman, Namur et al. 1991). The term toughness, which represents the crack resistance capability of concrete, or the total energy absorbed prior to complete failure; or the critical potential energy release rate

of a composite specimen with a unit mJ (Brown, Shukla et al. 2002). Toughness is also one of the fundamental parameters in failure analysis (Xu and Zhang 2008).

A popular interface characterization test is the single-fiber pullout test (Nairn, Liu et al. 2001). In the single-fiber pullout test, the end of a fiber is embedded in a cement matrix and pulled out while the matrix is held in place. The peak force, P , required to debond the fiber is typically recorded as a function of time; and will be correlated to curing time in the proposed research. The pullout test is also important by itself as it simulates the fiber bridging-pull-out mechanism during the failure process of FRC (Wang, Li et al. 1988). In relating the pullout test results with the fiber-matrix bond characteristics, numerous models have been developed and many of them have been reviewed (Bartos 1981, Bentur, Mindess et al. 1989, Hsueh 1990, Leung and Li 1990, Kim and Mai 1991, Naaman, Namur et al. 1991, Herrera-Franco and Drzal 1992, Nairn 1992, Chu, Robertson et al. 1994, Betterman, Ouyang et al. 1995, Mobasher and Cheng Yu 1996, Zucchini and Hui 1996, Li and Stang 1997, Kanda and Li 1998).

1.3.4. Multiple Cracking Behavior of ECCs

The crack-bridging behavior and associated complementary energy concept first proposed by Marshall and Cox (1988) is used as the linking concept between interfacial bond and composite failure behavior (Marshall, Cox et al. 1985, Marshall and Cox 1988, Li, Kanda et al. 1997).

Xu and Zhang (2008) defined crack propagation in concrete as having three distinguished stages: crack initiation, stable crack propagation and unstable failure (Leung and Li 1990, Betterman, Ouyang et al. 1995, Xu and Zhang 2008). After first-cracking, provided the fibers are strong enough, the material can take further loading (by the fibers themselves) until ultimate failure occurs. With increased loading beyond the first-cracking strength, multiple cracks will be formed, giving rise to pseudo-ductility of the material (Leung and Li 1990). Pseudo strain-hardening and multiple cracking have been observed in continuously reinforced ceramic and cement matrices with aligned fibers (Li and Wu 1992).

1.3.5. Interfacial-Shear Strength of ECCs

The cement-fiber interfacial bond results from some combination of mechanical interlocking of cement hydration products with the fiber surface and chemical reaction between fiber and cement paste within the interstitial transition zone (Kim and Mai 1998, Brown, Shukla et al. 2002). In fiber reinforced composite materials, the principal factor governing load transfer from the matrix to the fiber is the shear strength of the interfacial bond between the two components. Broken specimens of fiber-reinforced concrete shows that failure takes place primarily due to fiber pullout or debonding. Generally

fiber pullout rather than rupture confers a larger ductility to the fiber reinforced composites (Li and Stang 1997, Lin and Li 1997).

The mechanical properties of mortars are influenced by microstructure development through changes induced during cement hydration and hardening of the bonding system in the cement paste during curing (Janotka, Krajci et al. 2003). Uniform shear bond strength between the fiber and the matrix is often assumed in FRC models and the bond strength from pull-out tests is frequently reported in terms of the average value over the embedded fiber surface area (Kim and Mai 1998, Johnston 2001, Mehta and Monteiro 2006).

1.4. Nomenclature

Due to the frequent recurrence of the hydration phases and cement chemical formulations within the text, abbreviations commonly used in the cement industry, as-well-as acronyms, are used to simplify the language of this dissertation and are displayed in Sections 1.4.1 and 1.4.2.

1.4.1. Cement Chemistry Notation

The cement abbreviations, chemical formulae and scientific names for each cement component and hydrated phases are presented in Table 1-1.

Table 1-1. Cement abbreviations, chemical formulae and scientific names of cement components and phases

Cement Abbreviations	Chemical Formulae	Scientific Name (Cement Name)
C	CaO	Calcium Oxide (Lime)
S	SiO ₂	Silicon Dioxide
A	Al ₂ O ₃	Aluminum Oxide
F	Fe ₂ O ₃	Iron Oxide
H	H ₂ O	Water
Ś	SO ₃	Sulfur Trioxide
Ĉ	CO ₂	Carbon Dioxide
M	MgO	Magnesium Oxide (Periclase)
T	TiO ₂	Titanium Dioxide
K	K ₂ O	Potassium Oxide
N	Na ₂ O	Sodium Oxide
C₃S	3CaO·SiO ₂	Tricalcium Silicate (Alite)
C₂S	2CaO·SiO ₂	Dicalcium Silicate (Belite)
C₃A	3CaO·Al ₂ O ₃	Tricalcium Aluminate
C₄AF	4CaO·Al ₂ O ₃ ·Fe ₂ O ₃	Tetracalcium Aluminoferrite (Brownmillerite)
C₄A₃Ś	4CaO·3Al ₂ O ₃ ·SO ₃	Calcium Sulfoaluminate or CSA (Yeelimite)
CŚ	CaO·SO ₃	Calcium Sulfate (Anhydrite)
CŚH_{0.5}	CaO·SO ₃ ·0.5H ₂ O	Calcium Sulfate Hemihydrate (Hemihydrate)
CŚH₂	CaO·SO ₃ ·2H ₂ O	Calcium Sulfate Dihydrate (Gypsum)
C₆A₃H₃₂	6CaO·Al ₂ O ₃ ·3SO ₃ ·32H ₂ O	Ettringite
C₄AŚH₁₂	4CaO·Al ₂ O ₃ ·SO ₃ ·12H ₂ O	Monosulfate (Kuzelite)
CH	CaO·H ₂ O or Ca(OH) ₂	Calcium Hydroxide (Portlandite)
CĈ	CaO·CO ₂ or CaCO ₃	Calcite
C-S-H	Detailed structure not completely known	Calcium Silicate Hydrate

1.4.2. Acronyms

Acronyms used through this dissertation are shown in Table 1-2.

Table 1-2. List of acronyms

Acronym	Signification
OPC	Ordinary Portland Cement
CSA	Calcium Sulfoaluminate
FGD Gypsum	Flue Gas Desulfurization Gypsum
AFm	$Al_2O_3 \cdot Fe_2O_3$ -mono
AFt	$Al_2O_3 \cdot Fe_2O_3$ -tri
XRD	X-Ray Diffraction
SEM	Scanning Electron Microscope
wt. %	Weight percentage
TZ	Transition Zone
UHPC	Ultra High Performance Concrete
ECC	Engineered Cementitious Composites
FRC	Fiber Reinforced Composites
PVA	Polyvinyl Alcohol
PP	Polypropylene





CHAPTER 2 : MATERIALS AND METHODS

The single-fiber pullout test will be performed to investigate the peak pullout load and corresponding energy consumption, or toughness, shear-bond strength, debonding-energy density and fiber-bridging stress. The major parameter that will be investigated is the bond developed to various fiber types, over time, with sulfate-based hydration products as compared to silicate-based hydration products.

2.1. Materials

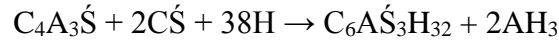
Three types of cements were investigated; ordinary portland cement, a commercially available CSA cement, and a CSA cement fabricated from coal combustion byproducts, at the University of Kentucky Center for Applied Energy Research (CAER), referred to in this study as CSAB#4. Polypropylene (PP) fiber, from Propex Inc., polyvinyl alcohol (PVA) produced by Nycon, Type-1 copper-coated steel fibers (Nycon-SF[®]) from Kuraray Company, and plain steel fibers from Bekaert were used in the tests, fiber properties are listed in Table 2-1.

Table 2-1. Properties of reinforcing fibers (data from product technical datasheet)

Fiber Type	Polypropylene	Polyvinyl Alcohol	Plain Steel	Coated Steel
Image				
Tensile Strength, MPa	600	1200	2000	2660
Modulus of Elasticity, GPa	5	30	200	220
Fiber Elongation, %	25	7	5	5
Density g/cm ³	0.91	1.30	7.80	7.80
Fiber Surface Area mm ² (6 mm length)	6.75	1.89	2.85	2.85
Fiber Length, mm	15	12	13	13

2.1.1. Calcium Sulfoaluminate Cement

The principal phases of CSA clinker are $C_4A_3\dot{S}$ (also called Klein's compound or yeelimite), C_2S (dicalcium silicate, i.e. belite), and C_4AF (tetracalcium aluminoferrite, i.e. brownmillerite)(Arjunan, Silsbee et al. 1999). Other phases such as calcium aluminates (e.g. $C_{12}A_7$ or $C_{11}A_7CaF_2$) are sometimes present. CSA cement gains strength from the hydration of Klein's compound with calcium sulfate (such as gypsum CSH_2 or anhydrite CS) to form ettringite via these reactions (Marroccoli, Nobili et al. 2007):



These reactions are relatively fast, and are nearly complete within one month. When the sulfate anion is depleted, ettringite $C_6A\dot{S}_3H_{32}$ (AFt phase) is converted to monosulfate $C_4A\dot{S}H_{12}$ (AFm phase or “mono” phase) which reduces the strength of the cement (Ikeda 1980).

2.1.2. Ordinary Portland Cement

Unlike CSA cement portland cement gains its strength from the hydration of C_3S (tricalcium silicate, i.e. alite), C_2S , C_3A (tricalcium aluminate), and C_4AF , in the presence of a sulfate source, i.e. gypsum or anhydrite (Richardson 1999, Woodson 2012). These main binding phases in portland cement-based systems are referred to as calcium silicate hydrates (CSH). In addition to CSH, calcium hydroxide is also formed.

2.1.3. Polyvinyl-Alcohol Fiber

The breaking of the chemical bond is evident in the first significant load drop. The second increase in load with fiber pullout has resulted from a slip hardening affect; this behavior is achieved through multiple cracking of the reinforced matrix (Redon, Li et al. 2001). However, as the matrix continues to hydrate and chemically bonds to the fiber surface fiber failure is experienced more often. This type of failure occurs when the fiber-matrix bond is greater than the load capacity of the fiber, thus the fiber ruptures in the fiber-free zone or debonded region of the fiber.

PVA fibers are hydrophilic and have the ability to chemically bond to the surrounding matrix along the interface boundary (Chu, Robertson et al. 1994, Betterman, Ouyang et al. 1995, Redon, Li et al. 2001). The hydrogen bond is formed by the available hydroxyl-groups on the PVA fiber. The chemical bond creates a cohesive fracture (matrix phase adheres to the fiber) when the fiber is pulled from the matrix (Hertzberg 1996). Another possibility for the increased bond with PVA fibers is attributed to the PVA fiber providing nucleation sites for the crystallization of hydrated cement phases (Cadek, Coleman et al. 2002, Bin, Mine et al. 2006, Naebe, Lin et al. 2008).

The use of PVA fibers has caused the mechanism of failure to change. The strong bond between the fiber and matrix has caused the failure site to move from the fiber surface to the more porous matrix region. The porous region is most likely more brittle by comparison with the ductile interfacial layer with steel fibers (Chu, Robertson et al. 1994). In some cases the matrix strength and the fiber-matrix bond exceed the yield strength of the fiber, and rupture results. If fibers rupture the energy experienced by the composite cannot be dissipated through pullout. In this case, the fibers behave as non-active inclusions leading to only marginal improvement in the mechanical properties (Mehta and Monteiro 2006).

2.1.4. Polypropylene Fiber

A typical polypropylene-fiber pullout curve shows a broad curve with a large area value below the curve, demonstrating the PP fiber's ability to increase the toughness of the composite. The PP fiber does not chemically bond to the surrounding matrix, they are hydrophobic and non-polar; therefore fractures form with the matrix in an adhesive (no matrix phase residue on the fiber) manner (Hertzberg 1996, Brogren and Karlsson 1997). The surface morphology of the PP fiber allows for surface irregularities ideal for matrix bonding; in addition to the potential for increased frictional loading, during fiber pullout, due to the valley-and-ridges found on fiber surface.

2.1.5. Steel Fibers

A typical single steel fiber pullout curve displays high peak loads, relative to the PVA and PP fibers, along with a shallow-sloping slip hardening curve; providing a large energy density as illustrated by the area beneath the curve. The coated-steel fibers are coated in copper for corrosion resistance as stated by the manufacturer's product specifications. The plain-steel fiber has not been coated. A scanning electron micrograph is shown in Figure 2-1, where the coating can be seen peeling away from the coated-fiber surface.

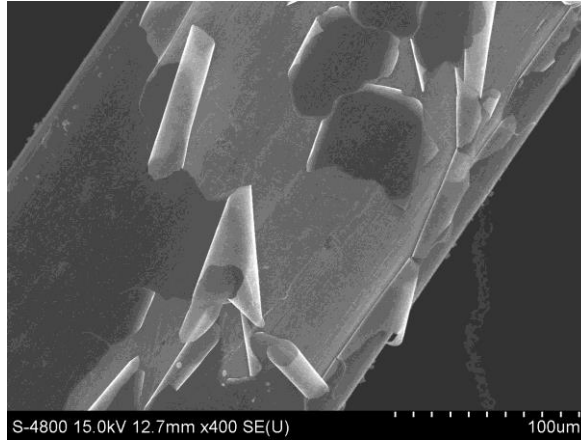


Figure 2-1. SEM image of a coated steel fiber, 400x magnification.

2.2. Methods

2.2.1. Calcium Sulfoaluminate Cement Fabrication

Bulk samples of FBC spent bed and fly ash were collected from a Kentucky FBC unit at the start of the project. These samples were sealed in mylar bags and stored in polyethylene drums. Bauxite was obtained from Ward's Scientific Inc. and stored in closed polyethylene buckets. Class F fly ash was obtained from a Kentucky PCC plant, which is located at the same site as the FBC unit. The limestone used in some of the cement formulations was acquired from a local quarry, and hydrated lime was obtained from a local supplier. Commercial CSAB from China was obtained from the Shenzhen Chenggong Trade supplier. Two additional commercial CSA cements that are produced in North America were also obtained for testing. Cemex Type I ordinary portland cement (OPC) was purchased from a local distributor. All cements were stored in heat-sealed mylar bags.

Flue gas desulfurization (FGD) gypsum was acquired from a power plant in northern Kentucky. An ultra-fine Class F fly ash (UFA) was produced at the CAER from material obtained at a coal ash impoundment in northern Kentucky. Table 2- provides a list of the raw materials used in the project.

Table 2-2. Description of raw materials

Material Name	Type of Material	Source
FBC Spent Bed Material	Coarse FBC Byproduct	Kentucky FBC plant
FBC Fly Ash	Fine FBC Byproduct	Kentucky FBC plant
Class F Fly Ash	Low-calcium coal ash	Kentucky PCC plant
Class C Fly Ash	High-calcium coal ash	Indiana PCC plant
Ultra-Fine Fly Ash (UFA)	Processed Class F ash	Kentucky PCC plant ash pond
Gypsum	FGD Byproduct	Proprietary source
Bauxite	Quarried raw material	Ward's
Limestone	Quarried raw material	Local quarry
Hydrated Lime	Agricultural lime	Southern States

2.2.2. Sample Characterization

The major oxide composition of the materials was determined using x-ray fluorescence following ASTM D 4326 protocols. The loss on ignition (LOI) is important when proportioning the feed materials for CSAB production because the weight loss during heating must be accounted for. During production of the CSAB cement, limestone loses primarily carbon dioxide, whereas the bauxite evolves water from dehydroxylation of the aluminum hydroxide. The majority of LOI for the Class F fly ash and the Gilbert byproducts was derived from combustion of coal. For this study, the LOI of the materials was conducted at 950°C. Density was determined on selected samples using a LeChatelier flask (ASTM C 188). The major oxide compositions of the coal combustion byproducts (CCBs) and native raw materials are shown in Table 2-3.

Table 2-3. Chemical composition of CCBs

	FBC Spent Bed	FBC Fly Ash	Class F FA	Class C FA	UFA	FGD Gypsum	Ward's Bauxite	Limestone	Hydrated Lime
SiO₂	12.77	25.62	57.44	41.65	50.88	4.54	10.61	7.41	4.99
Al₂O₃	5.25	10.34	29.97	22.28	26.98	1.09	78.75	2.76	2.03
Fe₂O₃	3.15	9.08	4.94	5.97	4.85	0.60	5.25	0.77	0.59
CaO	48.23	33.74	1.09	19.32	1.21	40.15	0.28	81.62	89.19
MgO	2.47	4.09	0.79	4.43	0.91	0.37	0.18	3.31	2.69
Na₂O	0.05	0.13	0.15	1.09	0.38	<0.01	0.01	0.04	0.16
K₂O	0.36	1.24	2.73	1.24	2.70	0.06	0.03	0.61	0.12
P₂O₅	0.13	0.14	0.11	0.89	0.25	0.04	0.32	0.03	0.03
TiO₂	0.26	0.42	1.64	1.32	1.72	0.13	3.67	0.15	0.13
SO₃	27.83	16.97	0.11	1.18	<0.01	53.67	1.58	0.82	0.19
LOI	2.00	n.d.	1.61	0.43	3.36	19.05	26.21	41.59	23.27
Free Lime	23.0	10.0	Na	na	na	na	na	na	na
Density (g/cm³)	2.98	2.82			2.41	2.37			

Particle-size distribution was determined using a Malvern Mastersizer 2000 laser diffraction analyzer. Refractive and absorption indices of the materials were determined prior to diffraction analysis. The crystalline phases present in the raw materials were determined using a PANalytical XPert x-ray diffraction (XRD) spectrometer. Hydrated cement pastes and mortars were ground in a mortar and pestle prior to analysis and were either analyzed wet, or after treatment in acetone (to stop hydration) and oven drying at 50-60°C for 1 hour. Scanning electron microscope (SEM) analysis was conducted on samples that had been treated using the acetone-drying method.

2.2.3. Single-Fiber Pullout Test Setup

Fiber pull-out tests are often used to study the fiber-matrix bond behavior in fiber reinforced cement composites. The pullout test is also important by itself as it simulates the fiber bridging-pull-out mechanism during the fracture process of FRC (Wang, Li et al. 1988). In relating the pullout test results with the fiber-matrix bond characteristics,

numerous models have been developed and many of them have been reviewed (Bartos 1981, Bentur, Mindess et al. 1989, Hsueh 1990, Leung and Li 1990, Kim and Mai 1991, Naaman, Namur et al. 1991, Herrera-Franco and Drzal 1992, Nairn 1992, Chu, Robertson et al. 1994, Betterman, Ouyang et al. 1995, Mobasher and Cheng Yu 1996, Zucchini and Hui 1996, Li and Stang 1997, Kanda and Li 1998). Uniform shear bond strength between the fiber and the matrix is often assumed in FRC models and the bond strength from pull-out tests is frequently reported in terms of the average value over the embedded fiber surface area (Gray 1984, Kim and Mai 1998, Johnston 2001, Mehta and Monteiro 2006, Subramani and Gaurav 2012).

The pullout tests were conducted on an Instron 600DX universal testing machine (Figure 2-2). A 2 kN load cell was used to measure the pullout load of the fibers with a displacement rate of 0.02 mm/s. Fiber-free length was kept at a maximum of 1 mm to reduce the effects of fiber elongation. The fibers were embedded 6 mm into a paste plug, which was held in place with a screw-type grip that was secured into the 2 kN (450 lbf) load cell (Figure 2-3). The fiber-free end was glued to a plastic-anchor plate and then secured in the jaws of the upper grip.

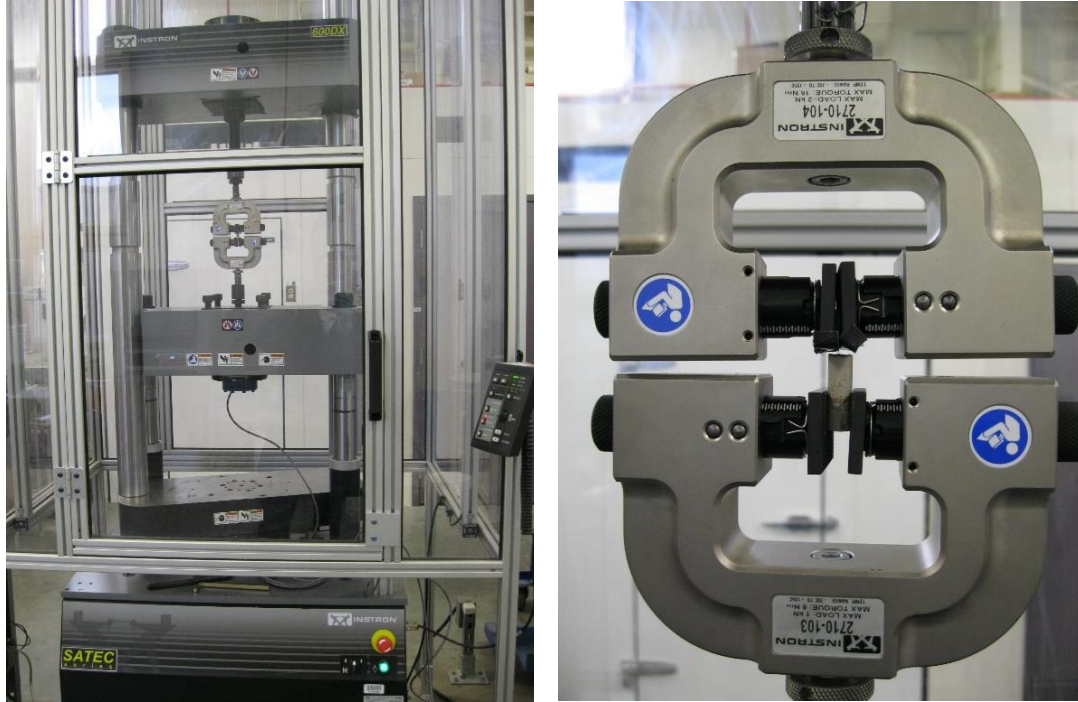


Figure 2-2. *Left)* Tensile testing machine setup; *Right)* Screw-type grips for securing specimen.

2.2.4. Preparation of Test Specimens

Test specimens were embedded in a paste plug (water:cement = 0.45) with an 8 mm (0.31 in) diameter and 25 mm (0.98 in) length (Figure 2-3 and Figure 2-4). The shortest fiber was 12 mm (0.47 in) in length; therefore a depth of 6 mm (0.24 in) was selected to maximize the available fiber-matrix bond surface to allow for quantitative comparison. Fiber characterization and properties are listed in Table 2-1. A depth gauge ensured fibers were embedded to 6 mm (0.24 in) and perpendicularly aligned to the mold surface. Specimens were removed from molds and placed in a temperature and humidity controlled environment and tested at 1, 7, 21, 28 and 56 days.

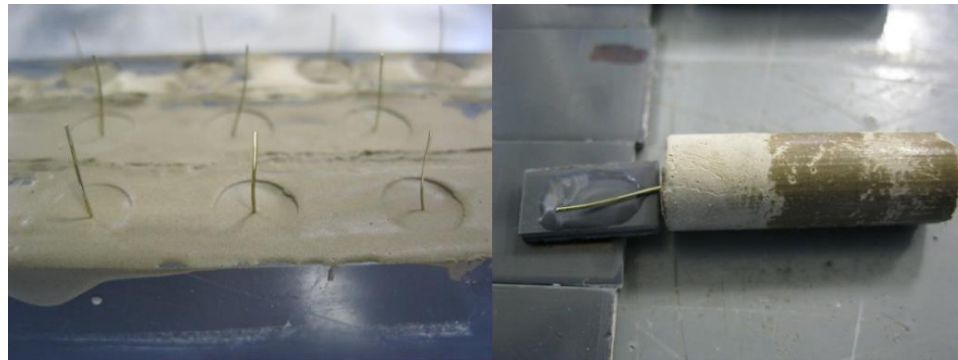
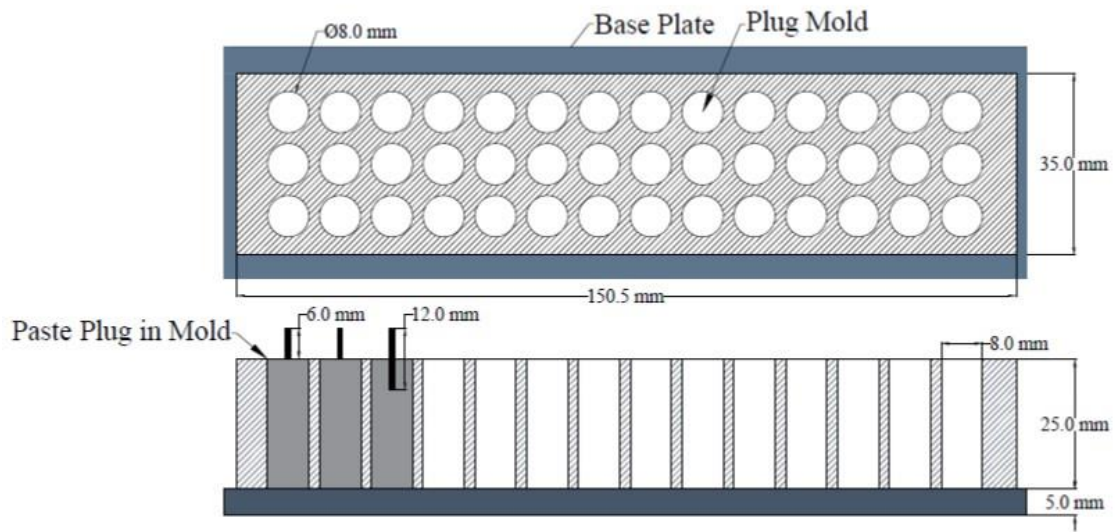


Figure 2-3. Specimen preparation; fiber embedded in paste plug.

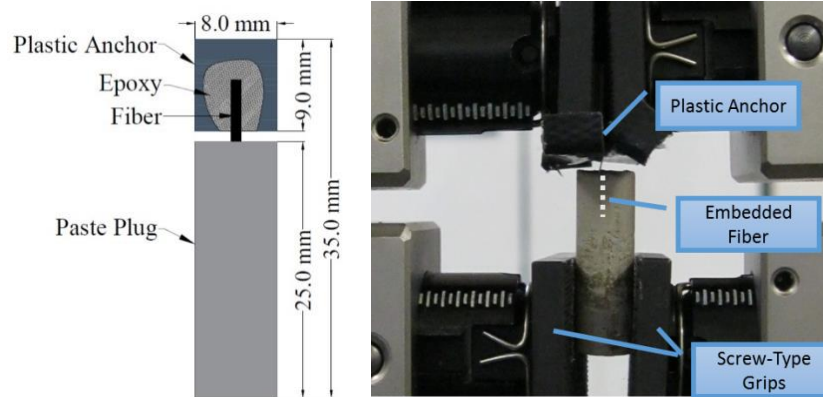


Figure 2-4. Fiber pullout specimen preparation: *Left*) Schematic of mold used to form each cement plug; *Right*) Grips with fiber-plug specimen.

2.2.5. Statistical Analysis

Common to all fiber pullout tests is a certain amount of data scatter in the experimental results; therefore five specimens were prepared for each test. Data scatter is attributed to the presence of naturally occurring random fiber flaws and the lack of uniformity in the surface characteristics along the length of each fiber. The data in Chapter 4 were statistically analyzed using a 3-way analysis of variance (ANOVA) (cement type, fiber type and days of curing). Additionally, the nonparametric rank-based ANOVA-type test proposed by Brunner et al. (1997) was used to confirm the results from the parametric ANOVA. The nonparametric test does not assume normality or homoscedastic errors. Therefore, its agreement with the parametric ANOVA can be interpreted as a confirmation that the latter's assumptions were not grossly violated. Also, the nonparametric ANOVA-type test is invariant under monotone transformations of the data, meaning in particular that it doesn't matter whether the original data or log-transformed data is analyzed.

CHAPTER 3 : FABRICATION AND TESTING OF LOW-ENERGY CSAB CEMENTS THAT UTILIZE CIRCULATING FLUIDIZED BED COMBUSTION BYPRODUCTS

3.1. Introduction

The utilization of circulating fluidized bed combustion (CFBC) ash to make cement products that provide added value and offset CO₂ production is the objective of this research. CFBC burns coal in the presence of a bed of slaked limestone, which effectively absorbs sulfur dioxide (SO₂) to form anhydrite (CaSO₄). CFBC produces two kinds of spent bed materials, coarse bottom ash and a much finer fly ash. Both of these products are very high in calcium. When properly conditioned these materials are capable of acting as hydraulic cements, forming both calcium aluminosulfate minerals, most importantly ettringite, as well as calcium-alumina-silica gels, like that formed from portland cement.

The research to generate calcium sulfoaluminate-belite (CSAB) cement was centered on two components. The first was the production of a cement that maximizes the proportion of coal combustion byproducts while achieving acceptable strength development. The second component focused on optimizing the laboratory-derived CSAB cement to have comparable strength characteristics with commercial CSAB cements.

The production of portland cement requires a large amounts of energy, mainly because of the high temperatures required to sinter the raw materials into clinker. Portland cement clinker, which is comprised mainly of calcium silicates, is also very hard and requires considerable energy to grind to the final product (Arjunan, Silsbee et al. 1999).

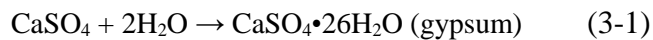
Furthermore, limestone is a major raw material used to produce portland cement and

releases large amounts of CO₂ during the thermal processing. In order to attain substantial reductions in energy consumption and CO₂ emissions, significantly lowering the clinkering temperature and the proportion of limestone in the feed is necessary (Damtoft, Lukasik et al. 2008, Gartner and Macphee 2011, Schneider, Romer et al. 2011). This is unfortunately not possible with portland cement. However, energy-conserving or “low-energy” cements can be produced at lower temperatures and using much less limestone than portland cement. They can also be much softer and easier to grind (Beretka, de Vito et al. 1993). An additional environmental benefit is that calcium sulfoaluminate (CSA) cements can be prepared using substantial amounts of coal combustion wastes as the raw materials. These include flue-gas desulfurization (FGD) gypsum, pulverized coal combustion (PCC) fly ash, and fluidized bed combustion (FBC) ash.

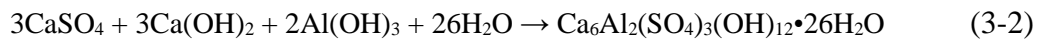
There are several types or classes of low-energy, low-CO₂ cements (Juenger, Winnefeld et al. 2011). This study focuses on one type: CSA cements which gain strength primarily from the formation of a calcium aluminum sulfate hydrate called ettringite (Beretka, de Vito et al. 1993, Sherman, Beretka et al. 1994, Arjunan, Silsbee et al. 1999, Janotka, Krajci et al. 2003, Bernardo, Telesca et al. 2006). Because of the rapid rate of formation of ettringite, CSA cements gain strength very quickly. The research described herein involved the formulation, production and evaluation of an FBC byproduct-based cements: CSAB cement produced by heating the FBC spent bed in the presence of limestone, bauxite and PCC fly ash. The formulation, production and performance testing of this material are described in this study.

Currently in the United States, there are approximately 60 fluidized bed combustion (FBC) boilers used to generate electricity. Although FBC boilers can substantially reduce SO_x and NO_x emissions relative to a PCC boiler, they generate a much larger quantity of solid byproducts. FBC burns coal in a fluidized bed of sorbent, usually limestone, which removes most of the SO_x emissions. The resultant byproducts are thus mainly composed of calcium sulfate, and also contain lesser amounts of unreacted sorbent i.e. lime or CaO. There are two types of byproducts produced in an FBC boiler: spent bed material, which is a coarse sandy material, and fly ash, which is a much finer material that is captured from the flue gas. The spent bed material generally contains a higher proportion of lime and calcium sulfate than the fly ash, whereas the latter contains more alumina and silica because of the presence of ash from the combusted coal.

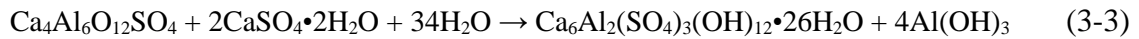
The lime, alumina and calcium sulfate within FBC byproducts imparts a cementitious nature when they are mixed with water. The cementitious properties are largely the result of the formation of two hydrated phases: gypsum and ettringite. Gypsum is formed from the hydration of the anhydrous calcium sulfate, anhydrite (Marroccoli, Nobili et al. 2007). This reaction can be slow because of the “hard burned” nature of the FBC anhydrite, which results from the high temperatures within the boiler. Nevertheless, the hydration reaction is:



Ettringite is a calcium aluminum sulfate hydrate that forms in a high pH environment (i.e. that occurring from the dissolution of lime in the FBC ash) by the following reaction:



One potential pathway to the utilization of FBC byproducts is to produce a CSAB cement via a high temperature clinkering process, similar to the production of portland cement. In contrast to portland cement, which derives its strength from the formation of calcium silicate hydrates, CSAB cement concrete hardens and gains strength primarily through the hydration of Klein's compound ($\text{Ca}_4\text{Al}_6\text{O}_{12}\text{SO}_4$) and calcium sulfate to form ettringite (Arjunan, Silsbee et al. 1999, Janotka, Krajci et al. 2003, Bernardo, Marroccoli et al. 2004, Torre, Aranda et al. 2005):



A compound similar to ettringite called "monosulfate" can also form under sulfate-deficient conditions and its role as a cementitious component in CSA cement is not well understood (Ikeda 1980, Glasser and Zhang 2001). Belite is usually present in CSA cements, but its hydration is typically slow and only provides additional long-term strength (Glasser and Zhang 2001, Torre, Aranda et al. 2005). Because of the rapid rate of formation of ettringite, CSA cements gain strength very quickly. If enough lime ($\text{Ca}(\text{OH})_2$) and calcium sulfate are present in the system, then additional ettringite is formed through reaction with the aluminum hydroxide. However, with excess lime the system can become expansive to the degree that it is destructive to the hardened material (Mehta 1973).

In China, CSA cements have been used primarily to replace portland cement in mortars and concrete when rapid strength gain, self-stressing properties or sulfate resistance is desired. Approximately one million tons per year are manufactured in China which has special standards for the cements (Zhang and Glasser 1999, Zhang, Su et al. 1999,

Damtoft, Lukasik et al. 2008). CSA-type cements have a long history of use in the United Kingdom for specialty applications such as in the mining industry. Brown (1993) described a wide range of formulations for products used in construction, for example, general purpose low shrinkage cement, shrinkage compensated concrete slabs, mortar coatings for concrete pipes, rapid repair and setting m mortars, anchor bolt grouts and glass fiber reinforced cement products.

In summary, CSA cements can potentially present considerable environmental advantages compared to portland cement because of the lower energy use, lower CO₂ emissions and use of coal combustion wastes as raw materials. In order to support widespread introduction of the cements in the marketplace there are several issues that must be addressed, namely, high cost, durability issues, and appropriate applications. As was discussed above, although only a limited amount of research has been conducted on the durability of CSA cements, there is sufficient information indicating that the cements can be quite durable in certain environments.

The research described herein has focused on the production of one class of FBC byproduct-based cement: CSAB cement produced by heating the FBC spent bed in the presence of limestone, bauxite, and PCC fly ash. The formulation, production and performance testing of this class of material are described.

3.2. Fabrication of CSAB Cement from CCBs

Mixtures of FBC spent bed material, PCC fly ash; bauxite and limestone were interground for clinkering. The clinker tests were conducted from 1000°C to 1250°C and

included compositions in the stability fields of Klein's compound and belite. Mineral composition of the cements was determined by X-ray diffraction.

The first cement formulation was calculated using Bogue equations that were modified for phases in CSAB clinker; this formulation is termed "CSAB#1" (Arjunan, Silsbee et al. 1999). The phases assumed to be present were Klein's compound, belite, ferrite (C_4AF), calcium sulfate, and a minor amount of lime ($<0.5\%$). However, it was found that the normative equations could not be used to optimize the CSAB compositions, probably because of the formation of minor amounts of other phases such as gehlenite, and the simplistic assumption that the aluminum:iron ratio in the ferrite phase = 1. Therefore, adjustments were made to the formulations to meet several objectives: 1) minimize the proportion of limestone used and thus the free lime formed (CaO), 2) maximize the proportions of byproducts (i.e. CFBC and PCC ash), and 3) produce a cement that will approach the performance of the commercial CSAB cement. The adjustments were made by analyzing each clinker using XRD until the desired composition was achieved resulting in the synthesis of formulations termed "CSAB#2" and "CSAB#4". Figure 3-1 shows the XRD profiles of the laboratory synthesized clinkers compared to three commercial CSAB cements: a CSAB manufactured in China, Commercial CSAB#1, and Commercial CSAB#2.

The FBC material is a potential source of CaO and SO_3 and thus was used as a partial substitute for gypsum and limestone in the laboratory CSAB raw materials. The effects of firing temperature were examined by XRD using the CSAB#1 clinker formulation. The firing programs consisted of heating the raw mix at $1175^\circ C$, $1200^\circ C$, $1225^\circ C$ and $1250^\circ C$ for one hour each. The resulting clinkers were slowly cooled within the furnace.

Visually there was a progressively darker and notable volume loss with increasing firing temperature as seen in Figure 3-2. The darkening color reflects the increased levels of sintering.

Each clinker was milled in a ball mill along with gypsum, which is used to “activate” the Klein’s compound to form additional ettringite during hydration. Class F fly ash was also milled with the clinker to serve as a filler for certain formulations. The milling of gypsum and/or fly ash with the clinker to make the final cement product is known as “process addition”.

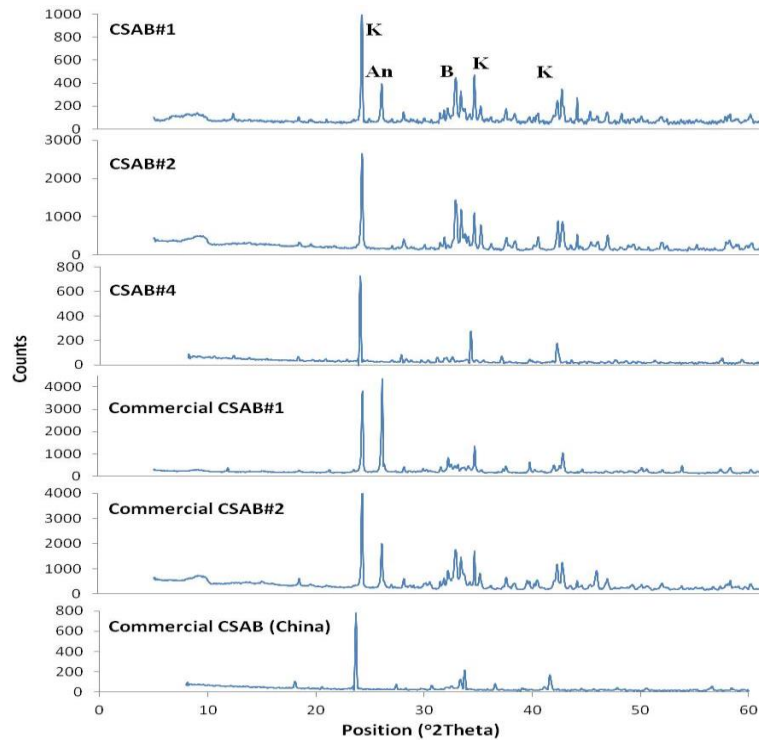


Figure 3-1. XRD profiles of the three laboratory synthesized clinkers compared to the commercially available CSAB cements. K = Klein’s Compound; An = anhydrite; B = belite (C₂S).

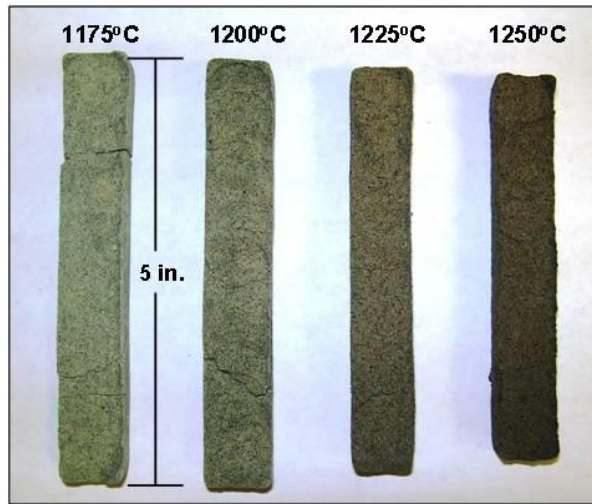


Figure 3-2. CSAB clinker demonstrating color variation and mass loss based on oven-firing temperature.

The optimum firing temperature for the FBC material based CSAB cement was chosen to be 1250°C. At this temperature the maximum amount of Klein's compound and belite was formed with minimal quantities of silicosulfate, an unreactive phase (Roy, Silsbee et al. 1999, Winnefeld and Lothenbach 2010). Table 3-1 provides a list of phases present in the cement formulations.

Table 3-1. Comparison of clinker phases

Phase	Composition	OPC	China CSAB	CSAB#1	CSAB#2	CSAB#4
C ₄ A ₃ S`	Ca ₄ Al ₆ O ₁₂ SO ₄	—	√	√	√	√
C ₂ S	Ca ₂ SiO ₄	√	√	√	√	√
C ₄ AF	Ca ₂ (Al,Fe ⁺³) ₂ O ₅	√	—	√	√	—
CS`	CaSO ₄	√	√	√	—	—
C	CaO	—	—	√	—	—
C ₂ AS	Ca ₂ Al _{2.22} Si _{1.78} O _{6.79} (OH) _{.22}	—	—	●	—	—

√ = Major phase present
 ● = Minor phase
 — = Not detected or trace

The first two formulations (CSAB#1 and CSAB#2) had relatively high contents of belite. CSAB#1 was formulated using 32% FBC bottom ash, 8% Class C fly ash, 15% bauxite and 45% limestone. The major compounds in the clinker were Klein's compound, belite, anhydrite, ferrite and lime. The major compounds in CSAB#2 were Klein's compound and belite, with only a minor amount of free lime.

The third CSAB cement formulation, CSAB#4, is comprised of limestone, bauxite and spent bed material. Unlike CSAB#1 and CSAB#2, Class F fly ash was not added to the raw mixture. However, it was added as a filler during mortar mixing. The CSAB#4 clinker was interground with 35% gypsum, by weight, to provide the necessary sulfate for the formulation of ettringite (Winnefeld and Lothenbach 2010). The amount of gypsum was calculated based on stoichiometry of ettringite formation from Klein's compound. The raw materials used for each formulation are shown in Table 3-2. Each of the cement-clinker formulations were analyzed chemically to compare the major oxides present (Table 3-3) with those that were calculated using modified Bogue

equations (Arjunan, Silsbee et al. 1999). The proportions of raw materials were adjusted accordingly so the resulting clinker composition closely resembled the calculated composition. This was done in order to achieve the phases shown in Table 3-1.

Table 3-2. CSAB cement formulations

Cement Formulations (% on a final product basis)					
Raw Material		CSAB#1	CSAB#2	CSAB#4	CSAB#4 FA
Clinker	Limestone	39.0	46.0	29.6	24.6
	Bauxite	13.1	15.2	30.2	25.0
	Gilbert FBC Spent Bed	27.7	13.1	19.6	16.3
	Class F Fly Ash	-	12.9	-	-
	Class-C PCC Fly Ash	6.9	-	-	-
Process Addition	Gypsum	13.3	12.8	20.6	17.1
	Ultra Fine Ash	-	-	0.0	17.1
% Coal Byproducts in Cement		40.2	38.8	40.2	50.4

Table 3-3. CSAB cement composition from XRF analysis

Cement Composition (%)								
<i>Cement</i>	SiO ₂	Al ₂ O ₃	Fe ₂ O ₃	CaO	MgO	Na ₂ O	K ₂ O	SO ₃
<i>OPC</i>	20.5	5.4	2.6	63.9	2.1	0.61	0.21	3.0
<i>CSAB from China</i>	11.12	26.94	1.76	44.99	3.18	0.04	0.19	12.23
<i>Commercial CSAB#1</i>	5.89	20.48	2.53	42.29	0.78	0.1	0.15	25.71
<i>Commercial CSAB#2</i>	14.92	16.12	1.32	48.91	1.63	0.24	0.49	15.46
<i>CSAB#1</i>	12.91	15.16	2.58	51.24	2.89	0.08	0.47	14.10
<i>CSAB#2</i>	16.90	16.95	2.39	47.10	2.25	0.15	0.68	13.52
<i>CSAB#4 (CAER CSA)</i>	8.21	24.30	2.59	40.02	1.32	0.14	0.62	22.30

3.3. Paste Study – Effect of Gypsum Content

Numerous hydration studies have already been done on the influence of gypsum, calcium sulfate hemihydrate (referred to as “hemihydrate”) and anhydrite on the hydration of CSA clinker containing C₂S and C₄A₃S̄ as main phases (Juenger, Winnefeld et al. 2011).

According to Majling, Znásik et al. (1985) anhydrite (depending on the heating

temperature and mechanochemical activation) is necessary for the high rate of initial strength development. Furthermore, Shah (1991), Sahu and Majling (1994), Winnefeld and Lothenbach (2010), Juenger (2011) and Winnefeld et al. (2011) found that ettringite formation depends on the reactivity of the calcium sulfate used. With hemihydrate or gypsum, ettringite formation is very intensive and can cover the aluminate phases, which retards their hydration. Conversely with anhydrite, there is no “supersaturation” and the hydration continues.

The effect of gypsum addition on the cement strength was determined using the CSAB#2 clinkers. Hydration of the materials was studied using paste prepared with a water:solids ratio of 0.37 and stored at 100% relative humidity and 23°C. At specific hydration intervals, samples of paste were obtained and analyzed using XRD. Hydration experiments were conducted on four paste mixtures: 15%, 20% and 25% gypsum, and 20% gypsum + 1% Ca(OH)₂. This latter mixture was prepared to study the influence of lime availability on the formation of ettringite (Figure 3-3) and expansion characteristics. Figure 3-4, Figure 3-5 and Figure 3-6 show the hydration process over a 56-day curing period. With the addition of 5% more gypsum to the CSAB#2 clinker, from 15% to 20%, there was more sulfate available for the continued formation of ettringite. This can be seen by the decreasing gypsum peak with increasing time, at approximately 11.5° 2theta. Most of the gypsum was consumed after 1-day of curing in the 15% gypsum paste, whereas approximately a third of the peak intensity remains in the 20% gypsum paste. Representative scanning electron microscope (SEM) images after 7-days of curing are shown in Figure 3-4, Figure 3-5 and Figure 3-6. The 15% gypsum paste, Figure 3-4, has ettringite crystals with an average length of 6 microns, with some areas of more crystals

appearing more massive and colloidal. The 20% gypsum paste, Figure 3-5, has well-defined acicular ettringite crystals with an average length of 10 microns; with some areas appearing massive and colloidal. The 20% gypsum 1% lime paste, Figure 3-6, contains ettringite crystals that are mainly small and fibrous with an average length of 3 microns. The smaller ettringite crystals in the presence of lime is consistent with the literature, e.g. (Mehta 1973). The lime would also react with aluminum hydroxide (equation 3-3) to form additional ettringite, which may have caused the slightly higher compressive strength of this mortar (discussed below).

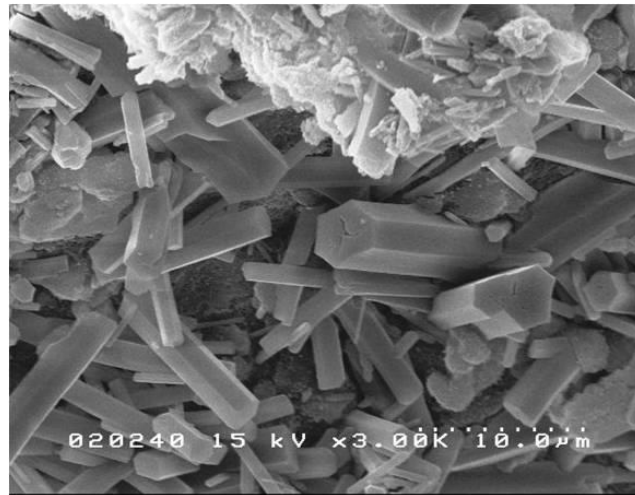


Figure 3-3. SEM image of ettringite crystals within the CSAB#2 paste, taken at 3000x magnification.

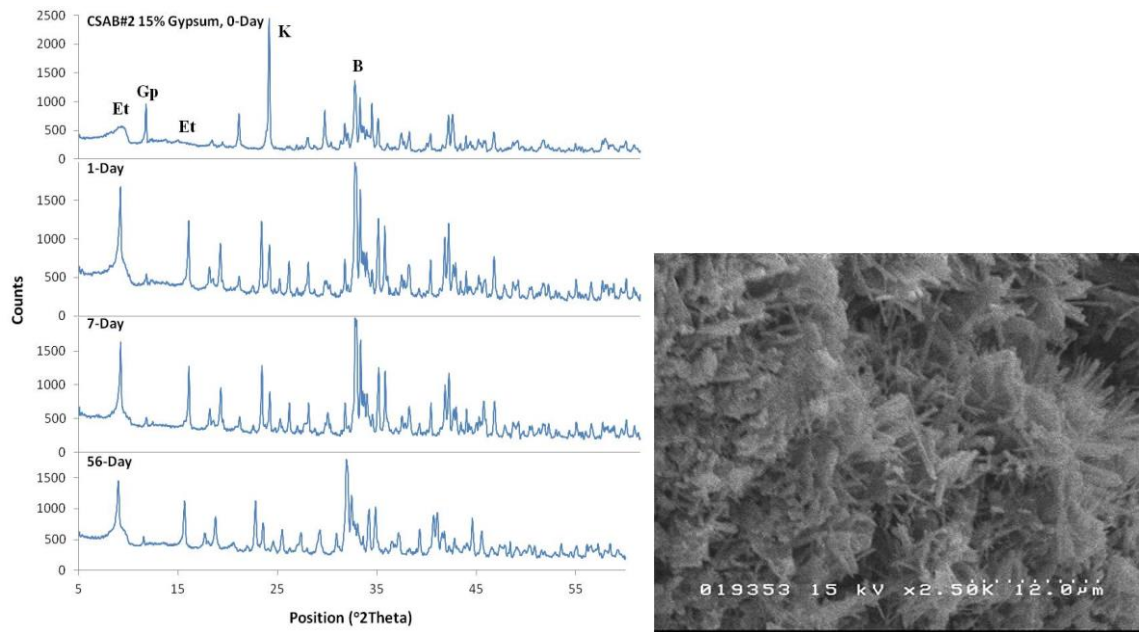


Figure 3-4. XRD profiles for the hydration of the CSAB#2, 15% gypsum, cement. Gp = gypsum; K = Klein's Compound; B = belite; Et = ettringite. On the right, an SEM image, under 2500x magnification, showing the formation of ettringite crystals in the CSAB#2, 15% gypsum cement after 7-days of curing.

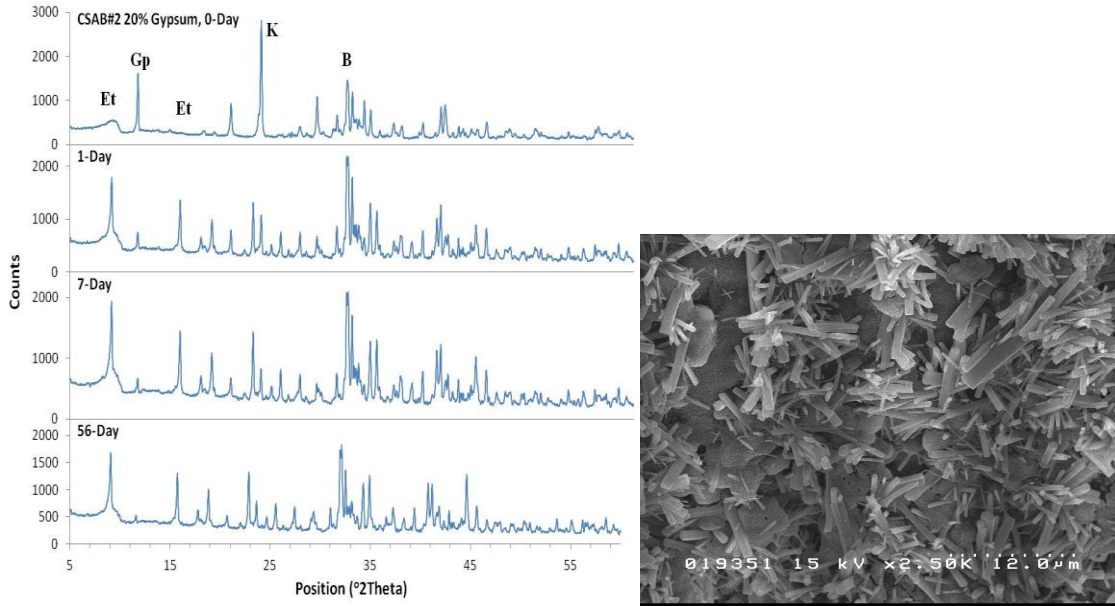


Figure 3-5. XRD profiles for the hydration of the CSAB#2, 20% gypsum, cement. On the right, an SEM image, under 2500x magnification, showing the formation of well-defined ettringite crystals in the CSAB#2, 20% gypsum, cement after 7-days of curing.

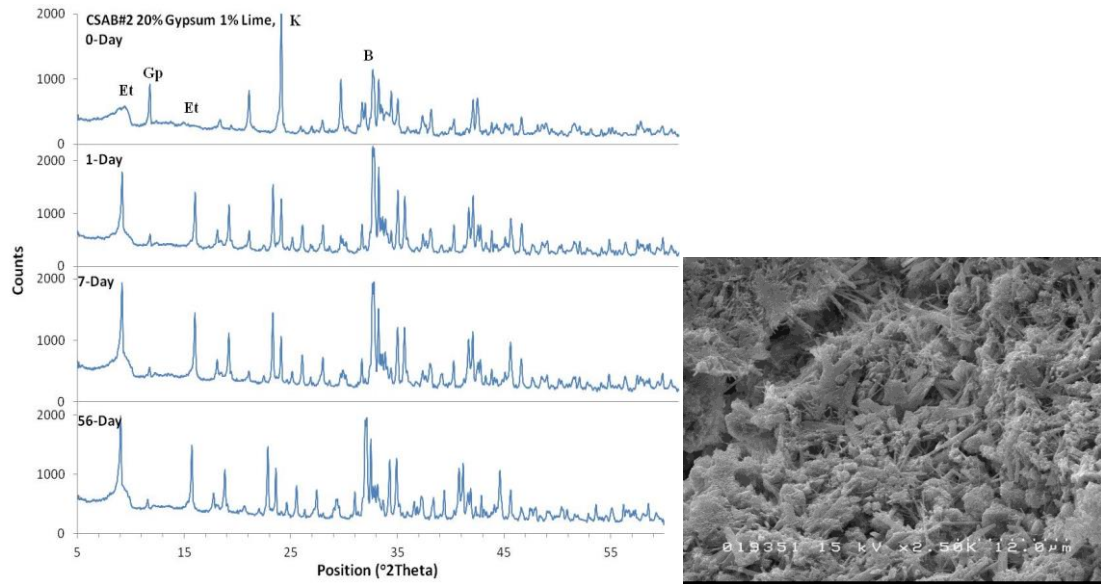


Figure 3-6. XRD profiles for the hydration of the CSAB#2, 20% gypsum with 1% lime, cement. On the right, an SEM image, under 2500x magnification, showing the formation of ettringite crystals in the CSAB#2, 20% gypsum 1% lime, cement after 7-days of curing.

The strength characteristics of the three cement blends, with the addition of a blend using 25% gypsum, were tested in mortar following ASTM C 109 and C 305. Figure 3-7 shows that the compressive strengths of the four blends were quite similar. The 1-day strengths ranged between 15.9 MPa and 18.6 MPa, with the 20% gypsum mortars producing the higher strengths. The 15% gypsum mortar started around 16.6 MPa and gained strength steadily to 28.3 MPa after 56-days. The mortars with 20% gypsum had the highest 1-day strength, approximately 18.6 MPa, and reached 30.0 MPa after 56-days of curing. The addition of lime had very little influence on the strength characteristics of the 20% gypsum mortar (Figure 3-7). The 25% gypsum mortar had the lowest 1-day strength of 16.4 MPa and followed a similar strength-gain trend as the 15% gypsum

mortar. However, at 56 days of curing the mortar experienced a decrease in strength down to 14.5 MPa. This decrease in strength results from a lack of water as seen by the persistence of unhydrated phases in Figure 3-4, Figure 3-5 and Figure 3-6 (Bernardo, Telesca et al. 2006). The continued strength gain for the remaining three pastes results from the hydration of additional phases, in particular, belite (Glasser and Zhang 2001)

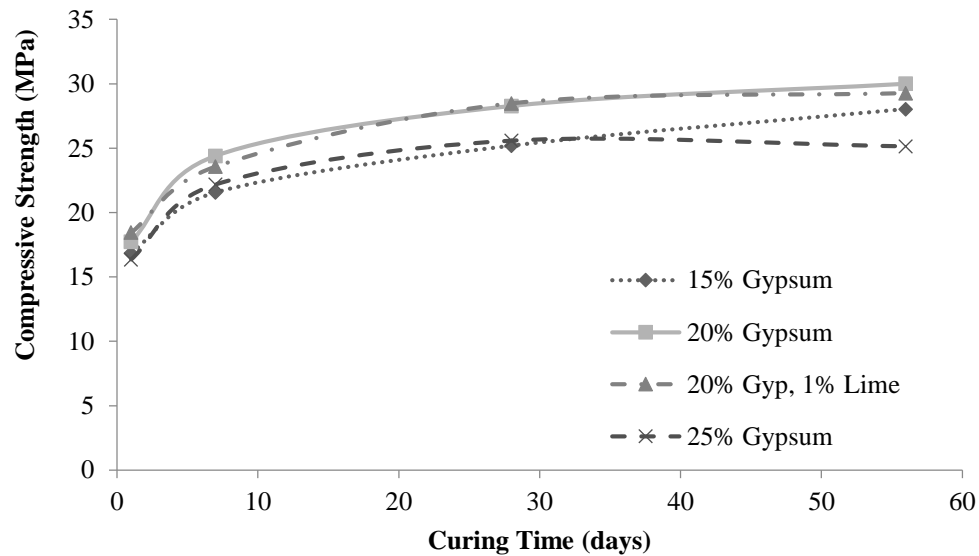


Figure 3-7. Compressive strength of mortar cubes using the CSAB#2 cement with the addition of gypsum and lime.

3.4. Fabrication of Bulk CSAB Clinker Cement

The material formulation was used to create larger samples of FBC-derived CSAB cement for mortar testing. Based on the calculated mix proportions determined from the modified Bogue equations, the raw materials were proportioned and ground in a ball mill to reach an approximate particle size of 16 microns. The ground mix was then placed into zirconia crucibles and fired in an electric furnace at 1250°C for one hour and then air-cooled. The resulting clinker was soft and required little effort to grind to cement

fineness. The ground clinker was analyzed to check that the expected phases were present. Calcium sulfate (CaSO_4) is necessary in CSAB cement to promote strength development through the formation of ettringite (Glasser and Zhang 2001). The calcium sulfate can be added by proportioning the CSAB clinker to contain excess CaSO_4 as anhydrite, or by intergrinding gypsum or anhydrite with the CSAB clinker; the cement mixes within this study were fabricated by intergrinding FGD gypsum (Taylor, Famy et al. 2001).

3.5. Strength Testing of CSAB Mortar

3.5.1. Set Time

The initial set time was established for cement mortars following ASTM C 807 procedures, and the data are shown in Table 3-4. The CSAB cement (from China) cement mortar set earlier than OPC, but was still workable. The set time for the laboratory CSAB cement mortars were substantially shorter than OPC and were dependent on the content of Klein's compound. The set time of the CSAB#4 cement mortars ranged from approximately 70 to 90 minutes, with no discernible trend with increasing process additions (Table 3-4).

Table 3-4. Mortar mix proportions following ASTM C 305 and C 109 protocols

Component	OPC	CSAB from China	CSAB#1	CSAB#2	CSAB#4	CSAB#4 FA
Cement (g)	500	500	500	450	500	500
Sand (g)	1375	1375	1375	1237.5	1375	1375
Water (g)	242	242	238.8	217.8	242	215
Flow (%)	112	112	81	117	120	109
Time of set (min)	189	116	-	88	91	67

The effectiveness of retarding admixtures on initial set time of CSAB cement mortar was conducted using Grace Recover[®], which is an ASTM Type D set retarding admixture.

The dosages were specified based on recommendations from the manufacturer. Table 3-5 provides the set time data for the CSAB cement from China and indicates that the retarder was very effective in slowing the set time of CSAB cement.

Table 3-5. Effect of set retarder on the set time of CSAB, from China, cement mortar

Set Retarder Dosage (ml/500 g cement)	Initial Set (min)
0	116
0.75	180
1.5	237
3.0	330

3.5.2. Strength of Commercial CSA Cement Mortar

To establish benchmarks for strength performance, the commercial CSAB cements described earlier were tested. Mortar cubes were prepared for the cement formulations following ASTM C 305 and C 109 protocols. The mortar mix proportions are provided in Table 3-4. The data for the commercially available CSAB cements are shown in Figure 3-8. As expected for rapid-setting cements, the 1-day strength significantly exceeded that of OPC. The rapid strength gain, accompanied by rapid heat evolution, is characteristic of CSA cements (Glasser and Zhang 2001). This is primarily due to the presence of a large amount of Klein's compound, which readily forms ettringite upon hydration. At 28-days of curing the cement from China matched the strength of the OPC but was then surpassed by the latter. The leveling-off of strength gain for the CSAB mortars was a result of the consumption of the available ettringite-forming compounds. The extremely-high strength of the Commercial#1 cement is attributed to the large amount of Klein's compound and anhydrite available in the cement. However, the Commercial#2 cement has a large amount of Klein's compound but half of the available

anhydrite, based on peak intensity. The lesser amount of anhydrite in the cement explains the slower strength gain after 1-day of curing compared to Commercial#1.

3.5.3. Strength of Laboratory CSA Cement Mortar

After compressive strength testing of the commercial CSA cement mortars, the laboratory CSAB#2 clinker was interground with 20% by mass FGD gypsum and mortars prepared according to ASTM C 109. The mortar prepared with this cement did not experience expansive cracking but exhibited considerably lower strength than the commercial cements (Figure 3-8), probably because it contained substantially more belite. However, its strength gain was good and it would likely qualify as a general rapid hardening (GRH) or medium rapid hardening (MRH) cement under ASTM C 1600 requirements. Of particular interest is that the performance was achieved with cement that comprises approximately 40% coal combustion byproduct.

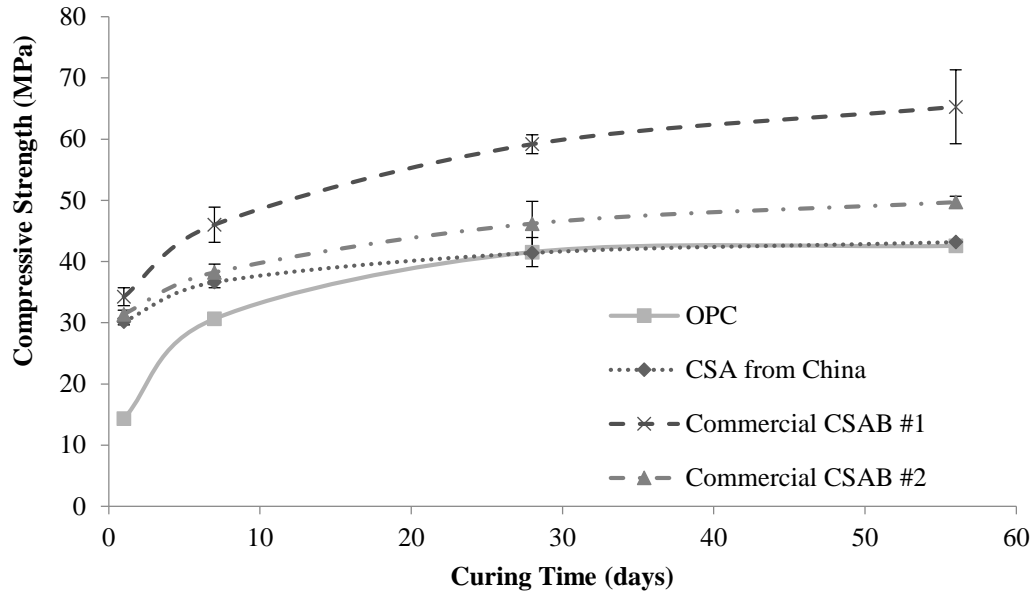


Figure 3-8. Compressive strength of mortar cubes made with commercially available CSAB cement.

The compressive strength development of CSAB#4 mortar was comparable to the CSAB cement from China (Figure 3-9), which is not surprising since both contained a large amount of Klein's compound (Figure 3-1). CSAB#4 mortar cubes matched the performance of the CSAB cement from China cubes from 1 to 7-days, and then from 28 to 112-days they greatly exceeded the CSAB cement from China cubes. The continued strength gain exhibited by the CSAB#4 cubes can likely be attributed to the presence of the active belite phase in the clinker. Based on ASTM C 1600, CSAB#4 would qualify as a very rapid hardening (VRH) cement.

CSAB#4 FA produced a mortar that achieved approximately 26.2 MPa in 1 day, 31.7 MPa in 7 days and 34.5 MPa in 28 days, which meets the criteria for a VRH cement. It is

interesting that this cement gains strength more rapidly than the CSAB#2 formulation despite the higher percentage of byproduct in CSAB#4 FA.

Figure 3-10 and Figure 3-11 depict the growth of ettringite crystals in the CSAB#4 mortar. Figure 3-10 is an image of ettringite crystals with an average length of 10 to 20 microns. The predominantly visible crystals formed in the space between the sand grains and cement paste. However in the bottom-left corner of the image the outline of several ettringite crystals can be seen within the cement paste. Figure 3-10 shows ettringite crystals with an average length of 5 to 20 microns that have formed within the cement paste and created a dense network of interlocking crystals and paste. The rapid-strength gain of CSA cements can be attributed to this geometry. Figure 3-11 shows an SEM image on the right, under 70x magnification, of the CSAB#4 mortar with grains of sand clearly embedded in the cement paste. By increasing the magnification to 3000x and focusing on the surface of one sand grain ettringite crystals, approximately 10 microns in length, have melded to the surface of the sand grain, thereby bridging the interfacial zone between the grain and the surrounding paste.

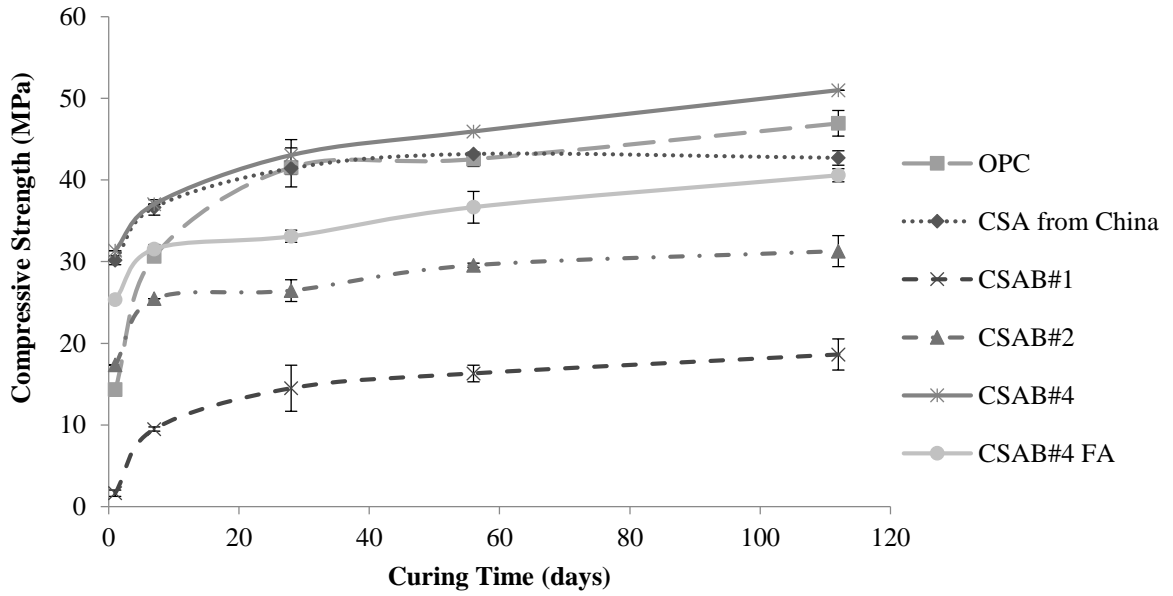


Figure 3-9. Compressive strength of the CSAB#4 cement mortar.

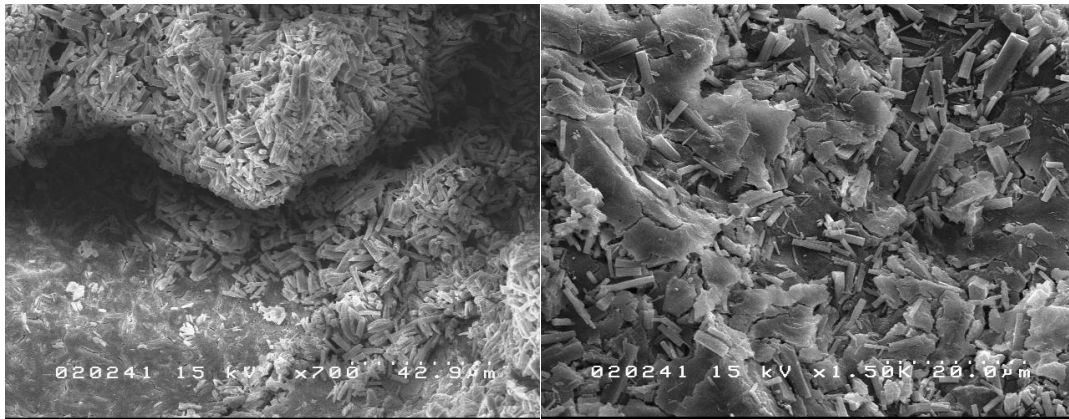


Figure 3-10. *Left*: SEM image, under 700x magnification, of ettringite crystals in the CSAB#4 cement mortar. *Right*: SEM image, under 1500x magnification, showing ettringite crystals within the CSAB#4 cement paste.

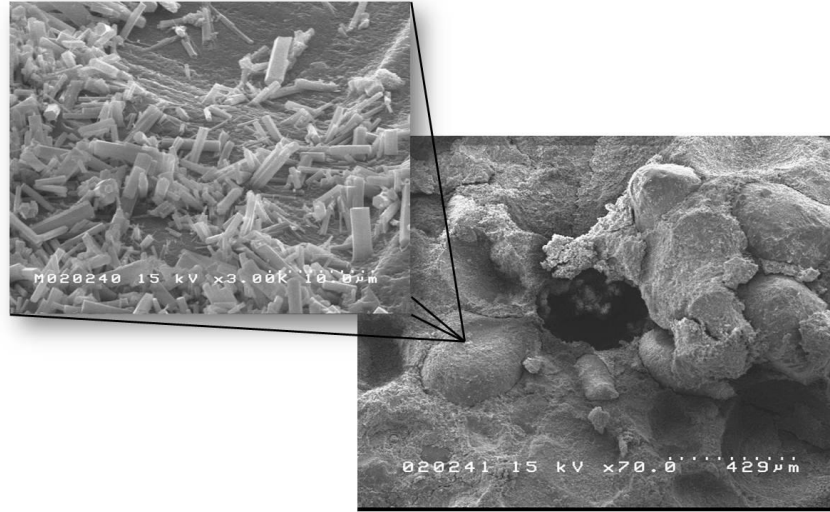


Figure 3-11. SEM image of the CSAB#4 cement used in mortar with sand grains clearly embedded in the paste; with a zoomed view of the sand grain surface.

3.6. Conclusions

The FBC material has potential for use in the production of calcium sulfoaluminate belite cements. The utilization of the FBC spent bed material in CSAB cement shows potential as a large-volume use for the material. Heating FBC bottom ash, PCC fly ash, limestone and bauxite at 1250°C (about 200°C lower than that used for portland cement clinker), produced a large quantity of Klein's compound and belite (Juenger, Winnefeld et al. 2011). The FBC ash provides needed calcium sulfate and, particularly, calcium oxide. The calcium oxide within the ash is an effective substitute for limestone, which is required as a raw material for CSAB cement clinker. In fact, if changes in the FBC combustion process were to result in substantially less lime in the spent bed material, its value as a CSAB clinker raw material would be limited since FGD gypsum would provide a more concentrated and refined source of calcium sulfate.

The synthesized CSAB clinkers were soft and readily milled to cement fineness. Milling the clinker with FGD gypsum was effective in providing the additional calcium and sulfate required to “activate” the clinker to form ettringite. The compressive strength of the commercial and laboratory CSAB cements produced high-early strengths that exceeded those of ordinary portland cement. Additional long-term strength was possibly provided by hydration of dicalcium silicate (C_2S) within the clinker.

Milling the laboratory CSAB clinker with Class F fly ash, in addition to FGD gypsum, appeared to improve the dimensional stability of CSAB mortar. In every cement that contained fly ash addition, destructive expansion did not occur and drying shrinkage improved. However, fly ash addition generally decreased the compressive strength, although the water reduction achieved with the fly ash, helped to offset this. Future work will focus on optimizing the quantity of fly ash addition to provide maximum water reduction benefits and minimize the strength loss.

A major issue regarding the production of CSAB cement is one of cost. Because CSAB clinker production requires substantial quantities of bauxite, the cost of these cements is high. In order to minimize or eliminate bauxite, alternatives to this raw material need to be pursued. The replacement of some bauxite with high-iron raw materials could have the net effect of replacing some of the aluminum with iron, which is considerably less expensive. Thus, future research should focus on the use of high-iron materials, such as certain Class F fly ashes and/or red mud, as partial replacements for bauxite.

CHAPTER 4 : INTERFACIAL BOND BETWEEN REINFORCING FIBERS AND CSA CEMENTS: FIBER PULLOUT CHARACTERISTICS

4.1. Introduction

This chapter presents the results of an experimental investigation on the influence of the interfacial bond of reinforcing fibers embedded in a calcium sulfoaluminate matrix on the fiber-pullout peak load and energy consumption. Bonding at the fiber-matrix interface plays an important role in controlling the mechanical performance of cementitious composites. In particular, composites formed from sulfate-based systems, i.e. calcium sulfoaluminate cements (CSA), as opposed to the silicate systems found in portland cement.

The primary reason for the addition of fibers to cementitious matrices is to delay and contain cracking (Naaman et al., 1991; ACI 5445R-10, 2010). While it is generally believed that the inclusion of fibers enhances the pre-cracking behavior of cement composites by increasing its cracking strength, the effect of fiber addition becomes evident only after cracking (Naaman et al., 1991; Lin and Li, 1997; ACI 5445R-10, 2010). Fibers bridge the cracked parts of the matrix, thus delaying sudden global failure of the composite (Lin and Li 1997). Therefore, in the post-cracking stage the fiber behavior is governed by the interfacial bond stress response as being subjected to pull-out loads (Naaman et al., 1991). The bond between fiber and matrix is important, if fibers have a weak bond with the matrix they can slip out at low loads and do not contribute to preventing the propagation of cracks. However, if the bond is too strong then the fibers may rupture before they can contribute to the post-crack strength of the matrix material.

Fiber-reinforced composites (FRC) resist tensile forces through a composite action, whereby part of the tensile force is resisted by the matrix, while the balance is taken by the fibers (Naaman et al., 1991). The transmission of forces between the fiber and the matrix is achieved through a bond defined as the shearing stress at the interface between the fiber and the surrounding matrix (Naaman et al., 1991). The fiber contribution to increasing the toughness (total energy absorbed with a unit mJ) of the composite is primarily dictated by the mechanisms of fiber pullout (Naaman et al., 1991; Brown et al., 2002). Fiber pull-out tests are often used to study the fiber-matrix bond behavior in fiber reinforced cement composites. This test simulates the fiber bridging-pull-out mechanism during the fracture process of FRC (Wang et al., 1988). In relating pullout test results with the fiber-matrix bond characteristics, numerous studies have been completed to demonstrate the reliability of the data (Bentur et al., 1989; Naaman et al., 1991; Herrera-Franco and Drzal, 1992; Betterman et al., 1995; Mobasher and Cheng, 1996; Zucchini and Hui, 1996; Wille and Naaman, 2012).

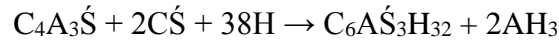
Composites made with brittle fibers, such as steel, and brittle matrices, i.e. calcium sulfoaluminate (CSA) cement, can exhibit high fracture toughness when failure occurs preferentially along the interface before fibers fracture. Most of the important toughening mechanisms are a direct result of the interface-related shear failure which gives rise to an improved energy absorption capability with a sustained crack growth stability through crack surface bridging and crack tip blunting (Li and Stand, 1997). The prevalent type of cracking depends on the properties of the interface relative to the fiber and matrix (Kim and Mai, 1998). According to Kim and Mai (1998), when a crack approaches an isolated fiber, the following failure mechanisms may be expected to take

place: 1) fiber-matrix interface debonding; 2) post-debonding friction; 3) fiber fracture; 4) stress redistribution and 5) fiber pullout.

The cement-fiber interfacial bond results from some combination of mechanical interlocking of cement hydration products with the fiber surface and chemical reaction between fiber and cement paste within the interstitial transition zone (Kim and Mai, 1998; Brown et al., 2002; Chan and Chu, 2004; Markovic, 2006). In FRC materials, the principal factor governing load transfer from the matrix to the fiber is shear strength of the interfacial bond between the two components. Fractured specimens of fiber-reinforced concrete shows that failure takes place primarily due to fiber pullout or debonding. Generally fiber pullout rather than rupture confers a larger ductility to the fiber reinforced composites (Li and Stang, 1997; Lin and Li, 1997). Unlike plain concrete, a fiber-reinforced concrete specimen does not break immediately after initiation of the first crack; thereby increasing the work of fracture, or toughness. Within the cracked section, the matrix does not resist any tension and the fibers carry the entire load applied to the composite. With an increasing load on the composite, fibers will tend to transfer additional stress to the matrix through bond stresses. If these bond stresses do not exceed the bond strength, then there may be additional cracking in the matrix. This process of multiple cracking will continue until either the fibers fail or accumulated local debonding will lead to fiber pullout (Shah, 1991; Mehta and Monteiro, 2006).

The principal phases of CSA clinker are $4\text{CaO}\cdot 3\text{Al}_2\text{O}_3\cdot \text{SO}_3$ ($\text{C}_4\text{A}_3\text{S}$), also called Klein's compound or yeelimite, Ca_2SiO_4 (C_2S) or belite, and C_4AF (or brownmillerite) (Arjunan et al., 1999). Other phases such as calcium aluminates (e.g. C_{12}A_7 or $\text{C}_{11}\text{A}_7\text{CaF}_2$) are sometimes present. Unlike portland cement which gains its strength from the hydration

of calcium silicates, alite (C₃S) and belite (C₂S), CSA cement gains strength from the hydration of Klein's compound with calcium sulfate (such as gypsum C \acute{S} H₂ or anhydrite C \acute{S}) to form ettringite via these reactions (Marroccoli et al., 2007):



These reactions are relatively fast, and are nearly complete within 1 month. When the sulfate anion is depleted, ettringite C₆A \acute{S} ₃H₃₂ (AFt phase) is converted to monosulfate C₄A \acute{S} H₁₂ (AFm phase or "mono" phase) which reduces the strength of the cement (Ikeda, 1980).

4.2. Research Significance – Chapter 4

Calcium sulfoaluminate cements present considerable environmental advantages compared to portland cement because of lower production energy, lower CO₂ emissions and use of coal combustion wastes as raw materials. Although there is sufficient information on the performance of CSA systems; there is a lack of research that characterizes the bond properties of fibers in these cements. Therefore this paper presents the development of CSA-fiber interfacial bond characteristics in the context of material design under the guidance of micro-mechanical tools. Specifically, this study illustrates how the fiber-matrix interface is enhanced by the use of sulfate-based cements when compared to silicate-based systems; providing some guidance in properly selecting a combination of fiber and matrix that provides efficient bond strength.

4.3. Experimental Results and Discussion

4.3.1. Single-Fiber Pullout Test

Tests were performed using single fibers to compare the pullout (direct tension) resistance and energies consumed during debonding and pullout of PVA, PP and steel fibers. Results of the single-fiber pullout test indicated increased peak stress and energy consumption for CSA-based cements than results obtained with an ordinary portland cement, Table 4-1. Load-position curves were very different between the four fiber types as seen in Figure 4-1. The 3-way ANOVA indicated the peak-stress test data varied statistically ($\alpha = 0.05$) according to cement type ($P < 0.01$), fiber type ($P < 0.01$) and days of curing ($P < 0.01$), but that the type of cement and days of curing interaction did not vary statistically. The statistical analysis demonstrated a significant interaction between the fiber type and days of curing; also between cement type and fiber type. Additionally, for the pullout-energy consumption the 3-way ANOVA indicated test data varied statistically according to fiber type ($P < 0.01$), days of curing ($P < 0.01$), but that the type of cement interaction did not vary statistically. The statistical analysis demonstrated a significant interaction between cement type and fiber type; with less significance between fiber type and days of curing. The steel fibers showed overall higher peak load and energy consumption than the polypropylene and PVA fibers ($P < 0.01$) in all three cement types.

Table 4-1. Peak load (N) and energy consumption values (mJ)

Cement	Time (days)	Peak Load, N (lbf)			Energy Consumption mJ (in-lbf)		
		PVA	PP	Steel	PVA	PP	Steel
OPC	1	1.0 (0.2)	6.6 (1.5)	9.9 (2.2)	0.93 (.008)	25.77 (.228)	48.76 (.432)
	7	3.6 (0.8)	11.4 (2.6)	15.7 (3.5)	1.97 (.017)	45.12 (.399)	34.49 (.305)
	21	3.6 (0.7)	10.9 (2.5)	24.6 (5.5)	5.23 (.046)	40.76 (.361)	88.89 (.787)
	28	3.9 (0.9)	4.9 (1.1)	31.0 (7.0)	3.99 (.035)	16.78 (.149)	88.48 (.783)
	56	11.1 (2.5)	9.6 (2.2)	18.5 (4.2)	4.37 (.039)	26.99 (.239)	70.33 (.622)
Comm. CSAB	1	2.0 (0.4)	8.5 (1.9)	11.1 (2.5)	5.53 (.049)	25.28 (.224)	30.64 (.271)
	7	6.2 (1.4)	11.9 (2.7)	56.9 (12.8)	6.68 (.059)	50.19 (.444)	107.39 (.950)
	21	5.1 (1.1)	7.1 (1.6)	61.8 (13.9)	6.30 (.056)	22.59 (.200)	173.98 (1.54)
	28	5.6 (1.3)	9.3 (2.1)	67.7 (15.2)	3.36 (.030)	23.84 (.211)	109.85 (.972)
	56	4.2 (0.9)	11.8 (2.7)	56.6 (12.7)	3.83 (.034)	42.62 (.377)	74.33 (.658)
CAER CSAB	1	1.2 (0.3)	6.1 (1.4)	25.3 (5.7)	0.97 (.009)	22.01 (.195)	99.45 (.880)
	7	1.7 (0.4)	9.8 (2.2)	33.6 (7.6)	3.85 (.034)	33.61 (.297)	115.24 (1.02)
	21	4.6 (1.0)	6.9 (1.6)	46.4 (10.4)	4.72 (.042)	16.71 (.148)	114.28 (1.01)
	28	6.0 (1.3)	5.2 (1.2)	77.4 (17.4)	6.36 (.056)	16.78 (.149)	181.05 (1.60)
	56	4.4 (1.0)	7.8 (1.8)	55.8 (12.5)	7.06 (.062)	21.81 (.193)	126.05 (1.12)

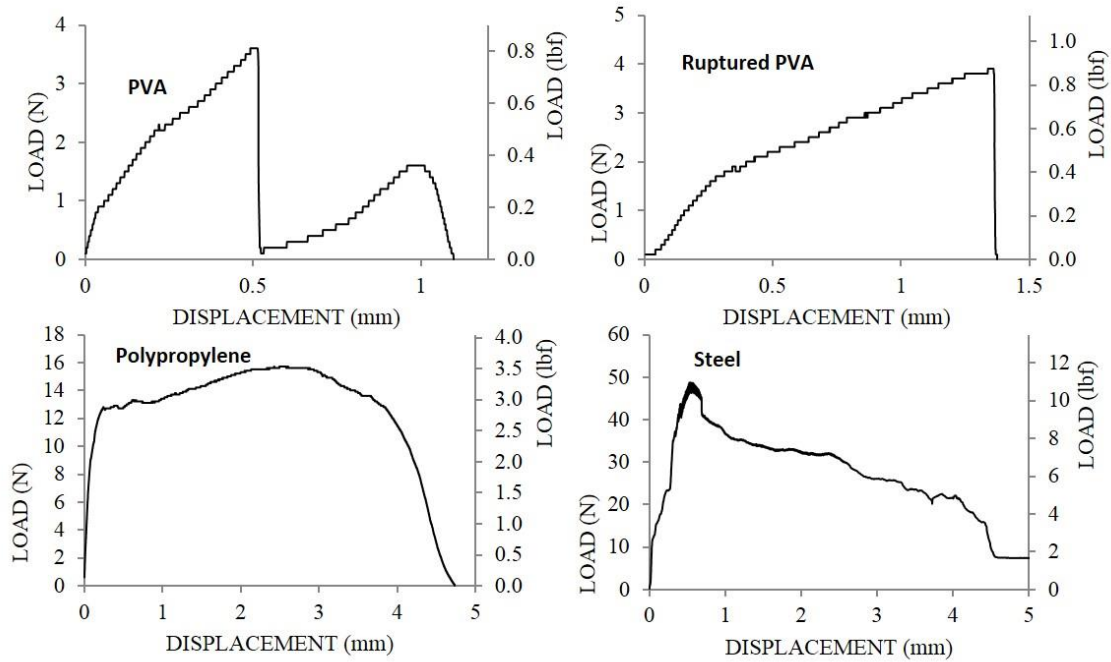


Figure 4-1. Typical load-displacement curves for each fiber type.

4.3.2. PVA Fiber

Breaking of the chemical bond is evident in the first significant load drop, in a typical single PVA-fiber pullout curve. It is hypothesized that the second increase in load with fiber pullout results from a slip hardening affect; this behavior is achieved through multiple cracking of the reinforced matrix (Redon et al., 2001; Wille and Naaman, 2012). However, as the matrix continues to hydrate and chemically bond to the fiber surface, fiber failure is experienced more often and is seen as a truncation in the load curve. This type of failure occurs when the fiber-matrix bond strength is greater than the tensile load capacity of the fiber, thus the fiber ruptures in the fiber-free zone or debonded region of the fiber.

The use of PVA fibers has caused the mechanism of failure to change. The strong bond between the hydrophilic fiber and matrix has caused the failure site to move from the fiber surface to the more porous matrix region, creating multiple cracks (Chu et al., 1994). The porous region is most likely more brittle by comparison with the ductile interfacial layer with steel fibers (Chu et al., 1994). Another possibility is the shear load will focus on the fiber itself causing the fiber to rupture. Fiber surfaces were observed with a scanning electron microscope (SEM) (Hitachi S-4800) to determine mechanical-bond characteristics that can be related to the data collected from the fiber pullout test (Figure 4-2).

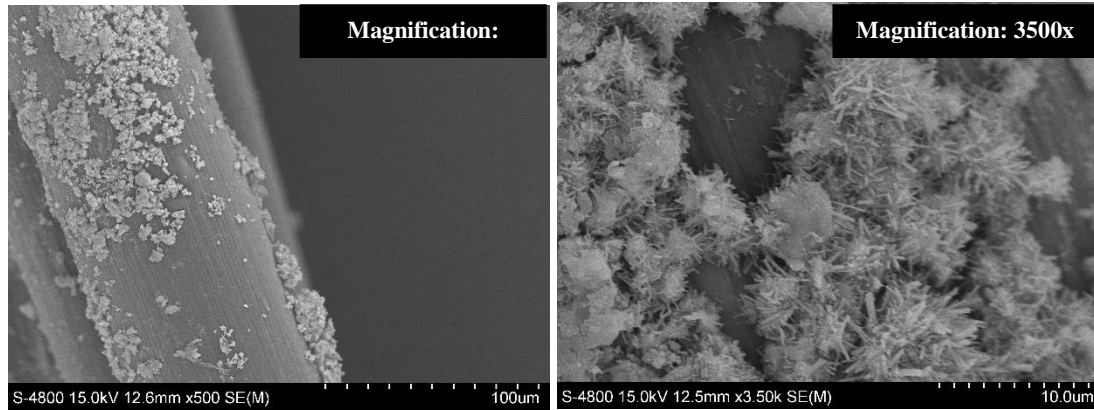


Figure 4-2. Clusters of ettringite crystals adhered to a single PVA fiber after 3-days of curing.

4.3.3. Polypropylene Fiber

A typical single polypropylene-fiber pullout curve shows a broad curve with a large area below the curve, demonstrating the PP fiber's ability to increase the toughness of the composite (Figure 4-1). PP fibers do not chemically bond to the surrounding matrix, they are hydrophobic and non-polar; therefore the fiber separates from the matrix in an adhesive (no matrix phase residue on the fiber) manner (Hertzberg, 1996; Brogren and Karlsson, 1997). The surface morphology of PP fibers allow for surface irregularities ideal for matrix bonding; in addition to the potential for increased frictional loading during fiber pullout, due to the valley-and-ridge structure on the fiber surface (Figure 4-3).

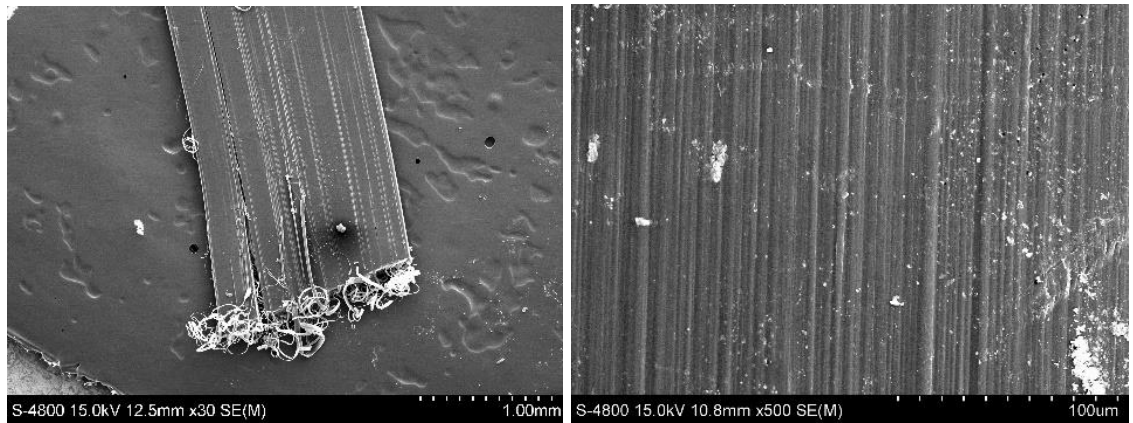


Figure 4-3. *Left*: Polypropylene fiber after the pullout test. *Right*: Surface of fiber with valley-and-ridge structure.

4.3.4. Steel Fibers

A typical single steel fiber pullout curve displays high peak loads, relative to PVA and PP fibers along with a shallow-sloping curve, indicative of slip hardening; and a large energy consumption (Figure 4-1). The coated-steel fibers are coated with copper for corrosion resistance as stated by the manufacturer's product specifications. A SEM analysis of the fiber surface after a pullout test revealed the copper coating provided a preferential bonding surface for hydration products (Figure 4-4). High peak loads with the steel fibers are attributed to the copper coating and surface roughness (Stengel, 2010; Wille and Naaman, 2012). Hydration products likely formed a complex with copper in the surface (as well as copper ions in solution), to form a strong bond (Chu et al., 1994). This bond allowed the interfacial layer of the matrix to remain bonded to the fiber during pullout.

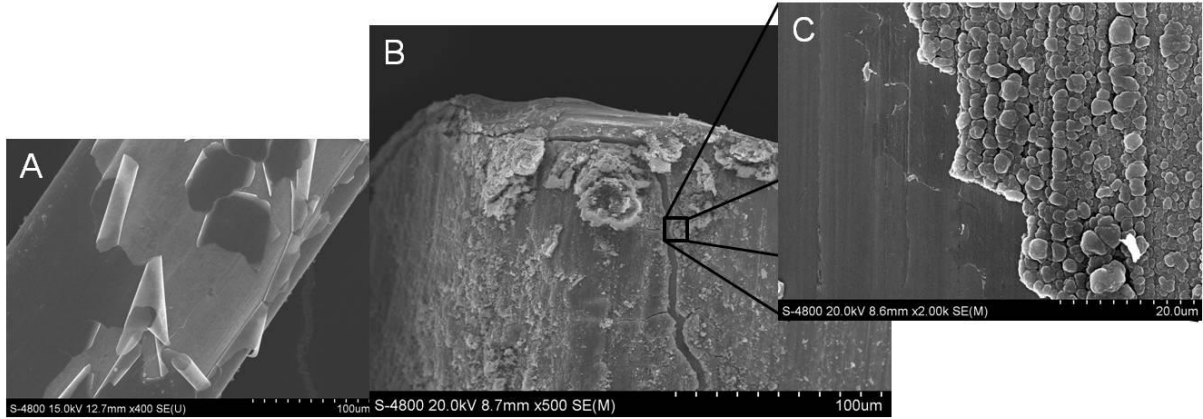


Figure 4-4. SEM images of a copper-coated steel fiber: (A) Copper coating peeled from fiber surface; (B) Fiber end with crack in copper coating; (C) Zoomed image of crack with defined boundary between copper coating and steel surface.

4.4. Peak Load Analysis

4.4.1. Ordinary Portland Cement

The steel fibers demonstrated the highest overall bonding strength from 7 to 56 days of curing, 31.0 N (7.0 lbf); represented by the peak-load data in Figure 4-5. However, the polypropylene fibers exhibited greater bond strength after one day of curing, 6.6 N (1.5 lbf). As the ordinary portland cement (OPC) matrix continued to gain strength it also increased in stiffness; therefore, the fiber that exhibits a similar stiffness, would yield higher peak load. Similar to steel fibers, PVA fibers also have a high modulus of elasticity and show resistance to stretching. The PVA fibers achieved a maximum peak load of 11.1 N (2.5 lbf) at 56 days of curing. After 21-days of curing the fiber-rupture rate increased, as expected, with increasing stiffness of the matrix and fiber-matrix bond. This is a similar trend exhibited by the CSAB cements that will be discussed in the following sections. The SEM images in Figure 4-6 indicate the fibers were completely

pulled from the matrix since there was no indication of failure along the fiber tip. There are particles attached to the fibers which indicate the presence of bonding between fiber and matrix; as compared to the surface of the fiber before they were embedded in the matrix.

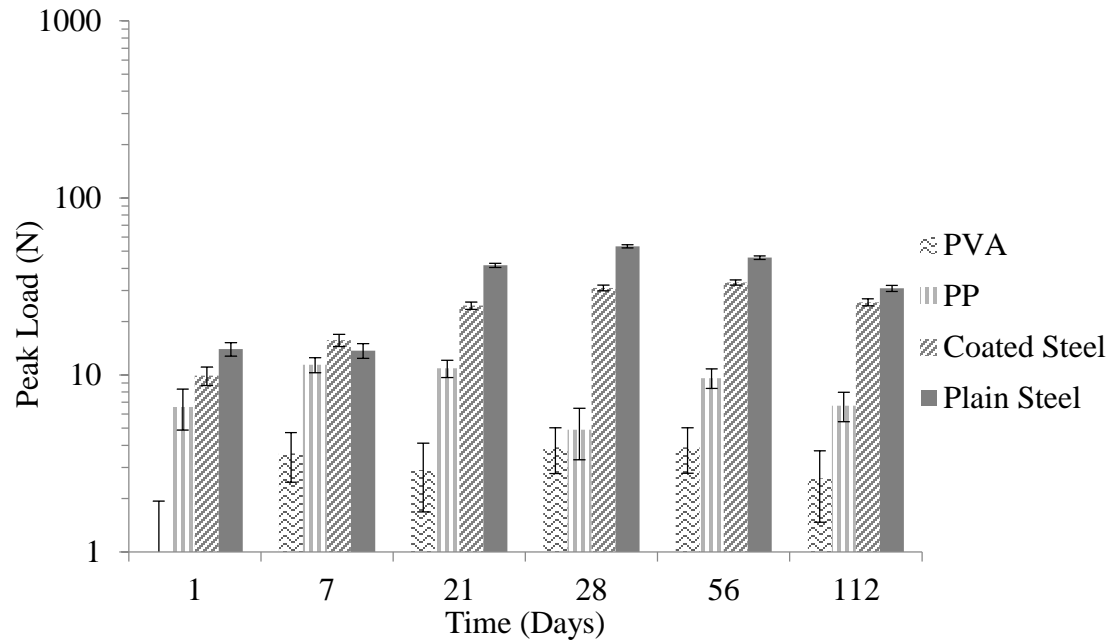


Figure 4-5. Peak load development of PVA, PP and steel fibers embedded in an OPC matrix; standard error of the mean are indicated for each column.

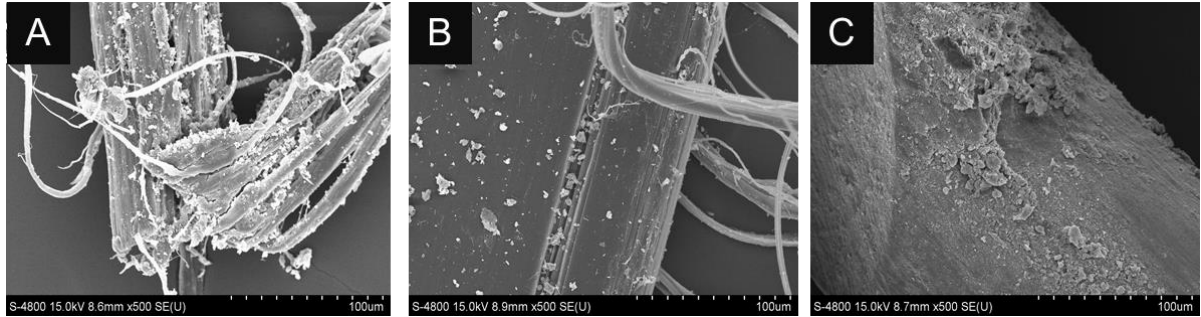


Figure 4-6. SEM images of fibers pulled from the OPC matrix (500x magnification): (A) PVA; (B) PP; (C) Steel.

Calcium silicate hydrate (C-S-H) grains form a fibrous, or fibrillar, morphology within the hardened paste (Neville, 1995; Richardson, 1999). These grains help form the interfacial bond between the fiber and surrounding matrix. However they are thin and do not form an extremely dense structure as seen within an ettringite-based matrix. The PVA fiber in Figure 4-6a demonstrates the preference for bonding to this type of fiber. PVA fibers easily form a complex cluster with available metal hydroxide ions, and in some cases bond to the matrix through the interfacial transition zone by a layer of calcium hydroxide, $\text{Ca}(\text{OH})_2$ (Horikoshi et al., 2008).

4.4.2. Commercial CSAB Cement

The main hydration product of CSA is ettringite, which precipitates together with amorphous $\text{Al}(\text{OH})_3$ until the available calcium sulfate is consumed after 1 – 2 days of hydration. Afterwards, monosulfate is formed. However the microstructure of CSA cement is denser than portland cement even after 16 hours of hydration. The dense structure and acicular nature of ettringite crystals aids the increased bond strength development (Figure 4-7). Whereas, OPC hydration products form layers of C-S-H gel

and calcium hydroxide crystals on the fiber surface; a minor amount of a phase near the composition of ettringite forms during early hydration stages (Taylor, 1997).

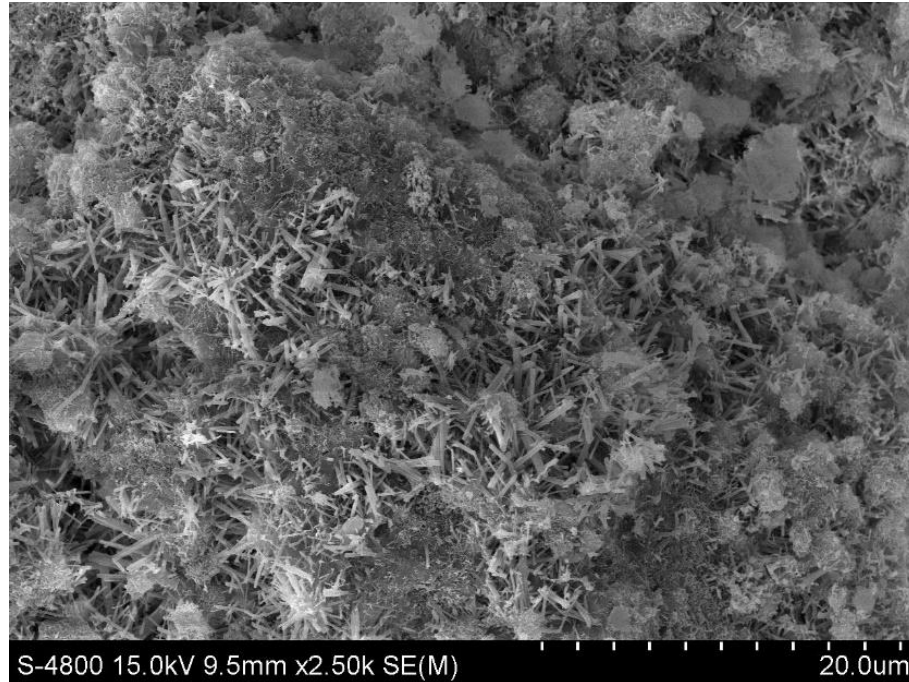


Figure 4-7. SEM image of the matrix morphology for the commercial CSAB cement.

The steel fibers have the highest overall bonding strength from 1 – 56 days of curing, as represented by the peak loads (Figure 4-8). The PP fibers exhibit an increasing peak load from 3 hours to 56 days with a maximum load of 12 N (2.7 lbf) attained at 7 and 28 days of curing. PVA fibers achieved a maximum peak load of 6.2 N (1.4 lbf) at 7 days of curing. One reason for the lower peak loads with PVA fibers is from the crystallization of hydrated phases at nucleation sites on the fiber surface (Cadek et al., 2002; Bin et al., 2006; Naebe et al., 2008). The associated stronger bond moves the failure mode from the cement matrix into the fiber itself, resulting in rupture. Table 4-1 shows a decrease in pullout strength and toughness after 28-days of curing. This is attributed to the hydration mechanics of CSA cement in which the matrix has increased in density and strength to a

point that will not permit dispersion of pullout forces throughout the matrix. Therefore the fiber-matrix interface is the point of failure as the interface bond stress is exceeded by the pullout load. Long-term pullout behavior of fibers in CSA cements should be evaluated for strength-loss trends.

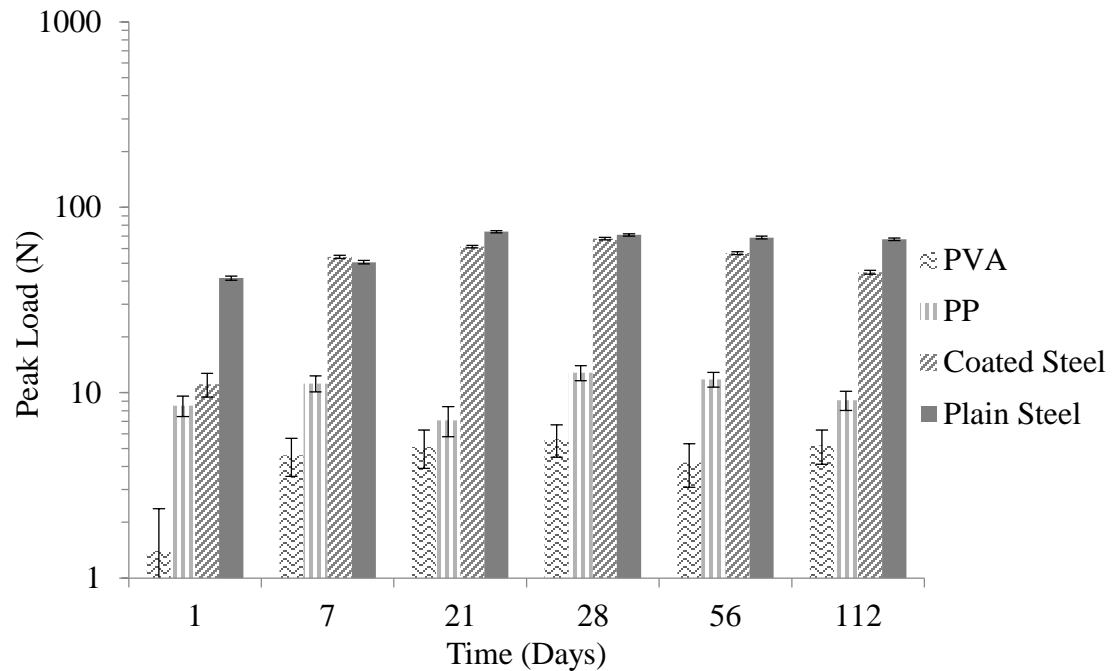


Figure 4-8. Peak load development of PVA, PP and steel fibers in the Commercial CSAB matrix.

The SEM images in Figure 4-9 provide a qualitative comparison of the fiber-matrix bond that occurs during hydration of the cement matrix. The PVA fiber demonstrates some surface deformation due to the interfacial bonding with the CSA matrix; the PP fiber shows less deformation than the OPC and CAER CSAB cement with an increased percentage of the surface coated with hydrated-matrix phases; the steel fiber shows large areas of bonding with the CSA matrix. In Figure 4-9C the copper coating and bare-steel

fiber boundary is shown; the copper coating in the lower half of the image is completed covered with hydrated-matrix phases.

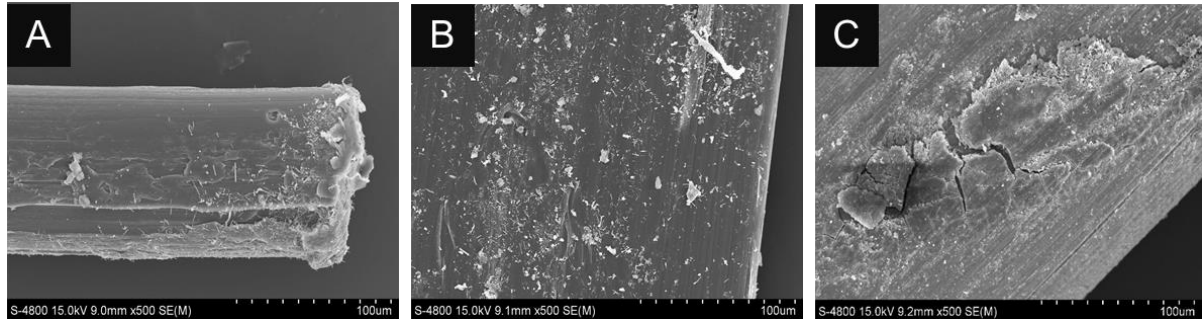


Figure 4-9. SEM images of fibers pulled from the Commercial CSAB matrix (500x magnification): (A) PVA; (B) PP; (C) Steel.

4.4.3. CAER CSAB Cement

The CAER CSAB cement is rich in Klein's compound, which in the presence of flue-gas desulfurization (FGD) gypsum hydrates rapidly to form ettringite. The CAER CSAB cement differs from commercially available CSA cement in that the ettringite crystals formed are longer and more slender; allowing for a tighter-interwoven network of crystals (Figure 4-10). This explains the increased bonding strengths seen in Figure 4-11 as compared to the commercial CSAB cement in Figure 4-5. The steel fibers exhibited higher peak loads as compared to the PP and PVA fibers. As previously mentioned, the increased pull-out load may be attributed to the influence of copper-coating on the bond between steel fibers and cement matrix.

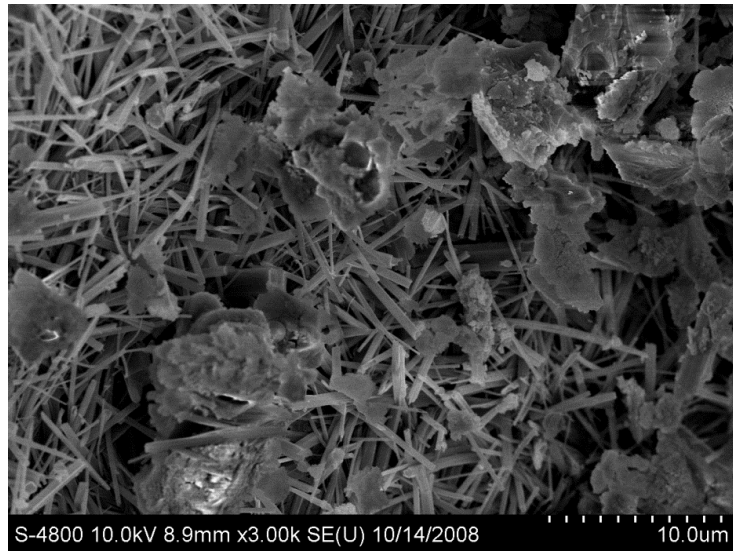


Figure 4-10. SEM image of the CAER CSAB cement with long needle-like ettringite crystals.

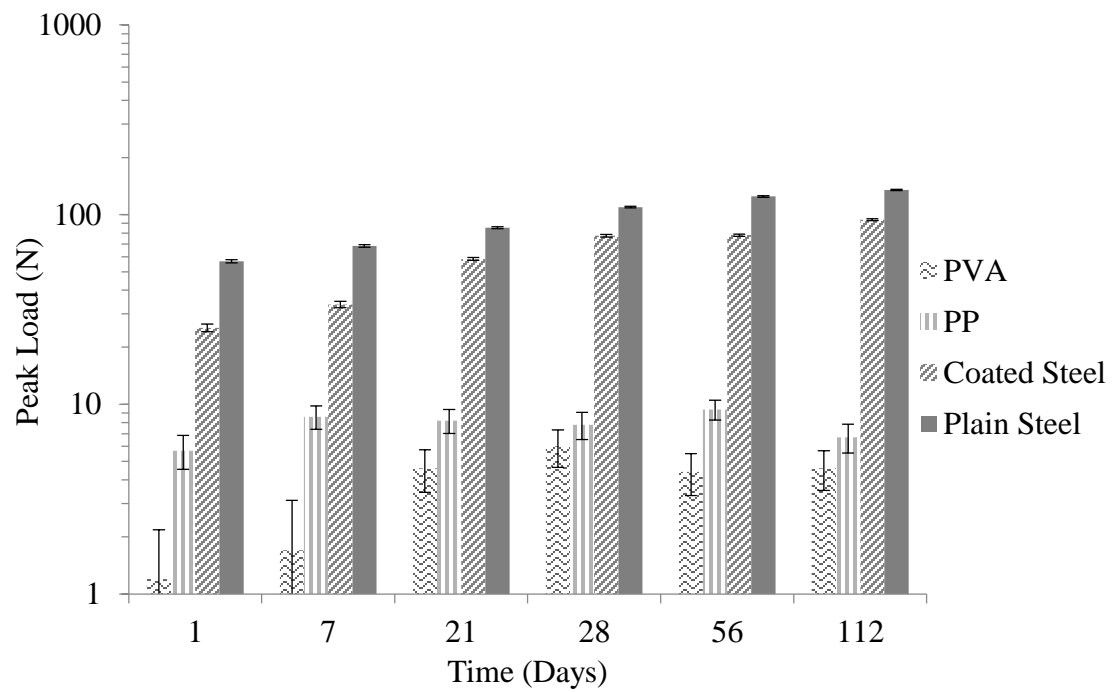


Figure 4-11. Peak load development of PVA, PP and steel fibers in the CAER CSAB cement.

The SEM images in Figure 4-12 demonstrate the increased fiber-matrix bond. The PVA fiber shows a high level of deformity when compared to its original form; sections of fiber have been pulled from the original structure providing evidence of a strong bond between the fiber and surrounding matrix. The PP fiber shows a minor degree of deformity with voids and impressions filled with hydrated-cement phases; the steel fiber was covered by greater than 90% of matrix material bonded to the surface, or copper layer.

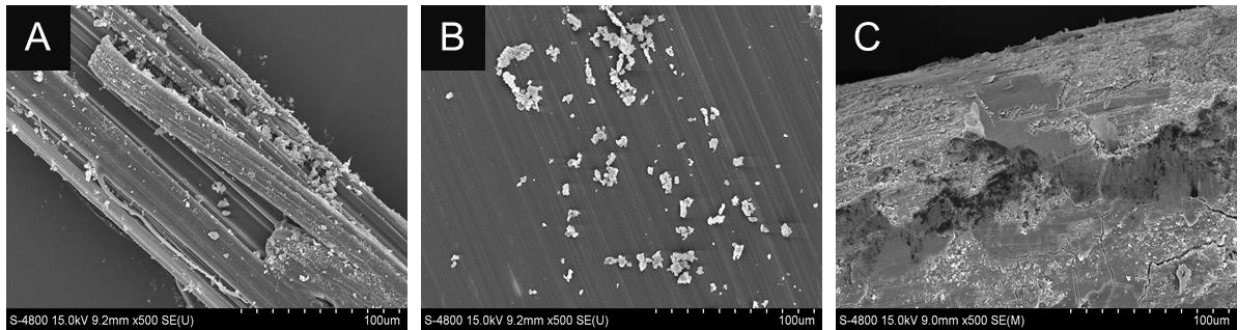


Figure 4-12. SEM images of fibers pulled from the CAER CSAB matrix (500x magnification): (A) PVA; (B) PP; (C) Steel.

4.5. Energy Consumption Analysis

Energy consumption corresponding to the single-fiber pullout test refers to energy absorbed in the debonding process which corresponds to the area under the load-displacement curve (Lin and Li, 1997). The energy consumption was determined with the Instron machine operating software, “Partner”.

4.5.1. Ordinary Portland Cement

The plain-steel fibers obtained the highest overall energy consumption from 1 to 112 days of curing, with a maximum of 172 mJ at 28 days; as seen in Figure 4-13. The

coated-steel fibers did not reach the peak loads of the plain-steel fiber, however the results followed a similar trend. The PP fibers exhibited the highest energy consumption, 45.12 mJ at 7 days of curing. PVA fibers achieved a maximum energy consumption of 5.23 mJ at 21-days. The early-age (1 to 7 days) pullout tests yielded the best results with the softer PP fiber, in which the bond between the fiber and matrix was sufficiently strong enough to transfer the excess energy into the matrix. However as the matrix continued to gain strength at 21 to 56 days of curing the harder steel fibers were able to sustain the increased load for the entire fiber debonding process. After 21 days of curing the fibers with a higher modulus of elasticity have a tendency to exhibit higher energy consumption.

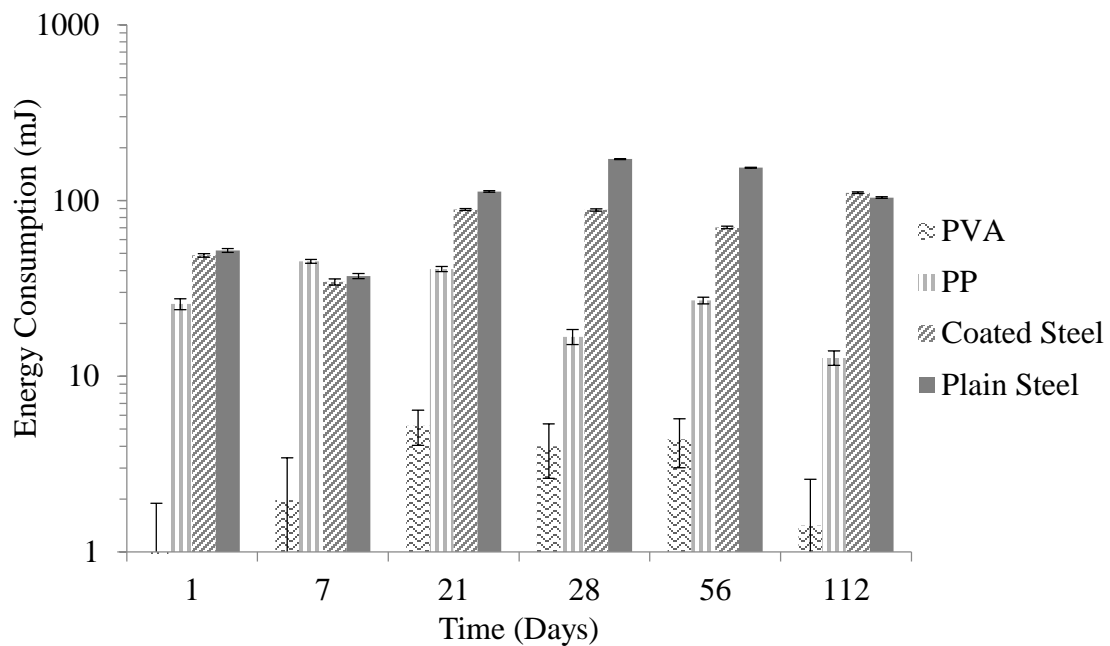


Figure 4-13. Energy consumption development of PVA, PP and steel fibers in the OPC matrix.

Strands of PP fiber that appear to have peeled away from the main fiber body highly influence the large energy consumption exhibited by this type of fiber. In addition to the fiber-matrix bond, which appears minimal when compared to the matrix remnants bonded to the PVA and steel fibers, as the strands of PP are peeled away they add to the energy consumption by enhancing frictional stresses during loading. The plastic nature of the PP fiber prevents catastrophic failure from occurring; alternatively a broad stress-strain curve is produced.

4.5.2. Commercial CSAB Cement

The steel fibers obtained the highest overall energy consumption from 1 to 56 days of curing with a maximum of 173.98 mJ (1.54 in-lbf) attained at 21 days, Figure 4-14. The PVA fibers achieved a maximum energy consumption of 6.68 mJ (0.059 in-lbf) after 7 days of curing. PP fibers attained a maximum energy consumption of 50.19 mJ (0.444 in-lbf) after 7 days of curing. The decrease in energy consumption after 1 and 7 days of curing, for the PP fibers, may be attributed to a decrease in ductility with increasing hydration of Klein's Compound to form ettringite, thereby forming an extremely dense matrix structure.

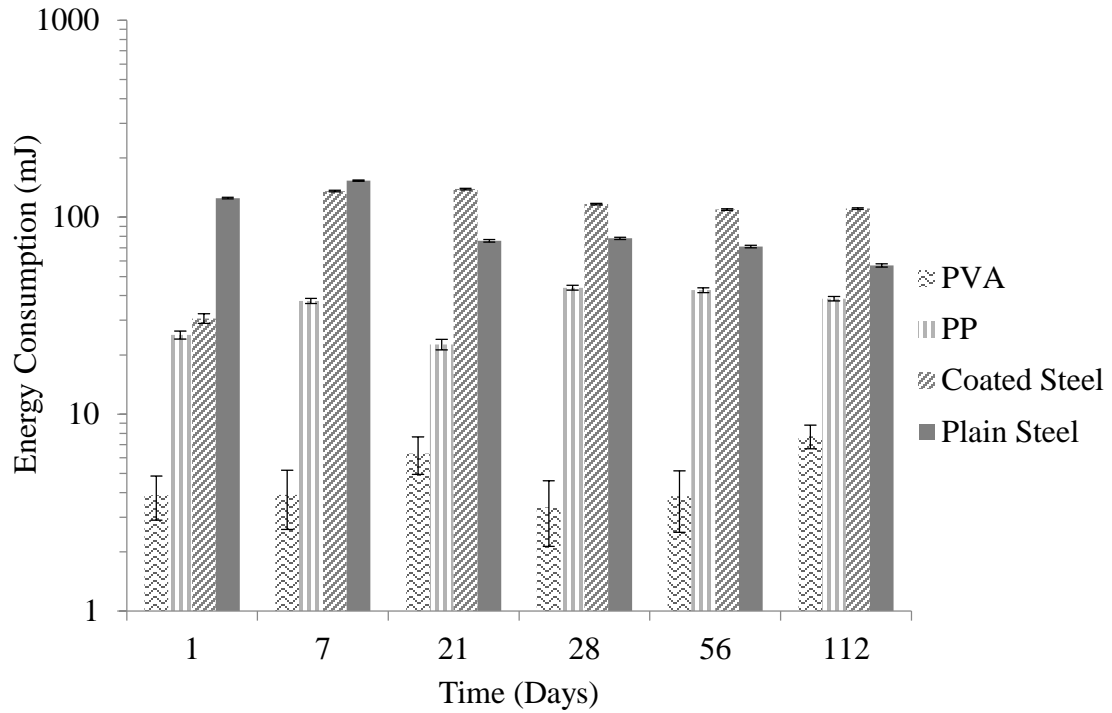


Figure 4-14. Energy consumption development of PVA, PP and steel fibers in the Commercial CSAB cement.

4.5.3. CAER CSAB Cement

Similar to the Commercial CSAB cement the steel fibers exhibited the highest overall energy consumption from 1 to 56 days of curing with the CAER CSAB cement, with a maximum of 181.05 mJ attained at 28 days (Figure 4-15). The PP fiber had a decreasing trend with time, correlating to a decrease in peak load. This may be attributed to an abundance of Klein's compound in the CAER CSAB cement which will hydrate to form a larger volume of ettringite than the Commercial CSAB cement.

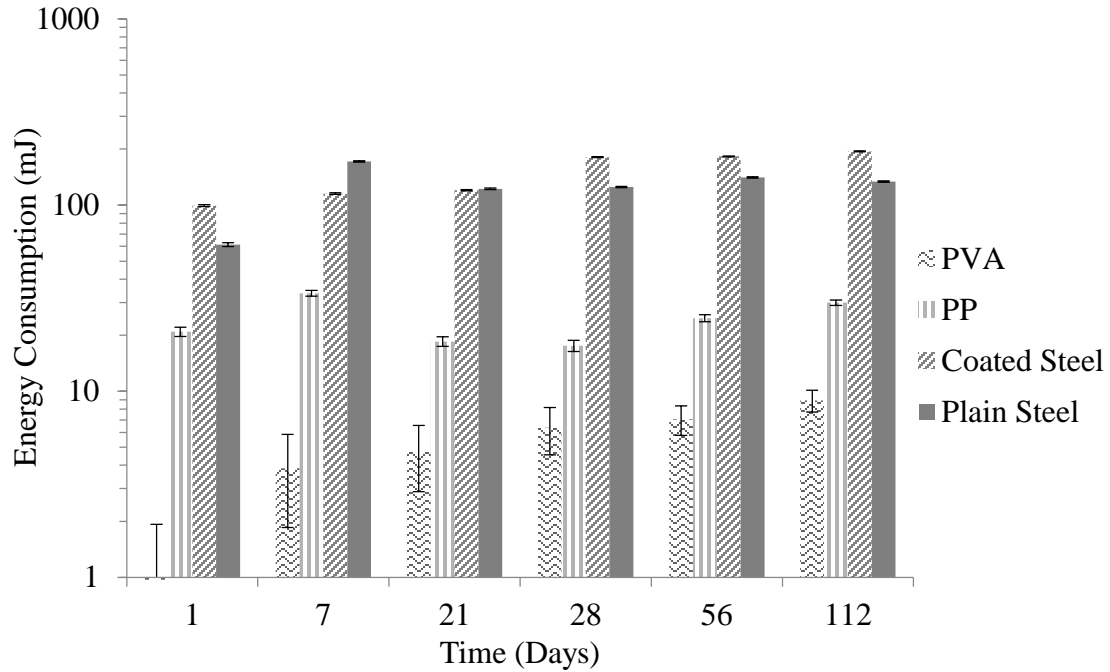


Figure 4-15. Energy consumption development of PVA, PP and steel fibers in the CAER CSAB cement.

Fibers with a high Young's modulus showed an overall increase in energy consumption for each of the pullout test days, including the PVA fiber. Though results were not as high as those attained with steel fibers, the PVA fiber reached a maximum energy of 3.85 mJ at 7 days of curing; and sustained an energy consumption of around 7 mJ out to 56 days of curing. The leveling-off of maximum energy after 7 days for PVA fibers is directly associated with an increased percentage of fibers that ruptured during pullout.

4.6. Statistical Analysis

A statistical analysis was performed to determine any significance of the effects measured for the following experimental responses: the peak load corresponding to the maximum load supported by the fiber at the point before debonding; the total energy consumption during the pullout process that corresponds to the region below the load-

displacement curve (Chanvillard and Aitcin, 1996). Based on the Box-Cox transformation technique, the data was log transformed (Box and Cox, 1964). This reduced variance heterogeneity and made the data more symmetric, thus justifying the use of ANOVA inference methods on the transformed data.

Consistent with the Box Cox log transformation, the summaries of peak load and energy consumption visualized in Figures 4-5, 4-8, 4-11, 4-13, 4-14 and 4-15 are displayed on a logarithmic scale. Specifically, for the transformed data, mean plus/minus standard error of the mean were calculated and transformed back to the original scale. Thus, the original magnitudes can be seen directly from the figures, but at the same time, it is possible to validate the appropriateness of the statistical inference which was based on the transformed data.

4.6.1 Peak Load

Table 4-1 displays the transformed mean-loads obtained for each peak load for each of the 45 studied configurations. Table 4-2 gives the results of the ANOVA of the peak load data. From the table it can be concluded that the cement, fiber, cement-fiber interaction, day and fiber-day interaction have been shown to have a statistically significant effect.

Table 4-2. Analysis of variance on peak load

Source	DF	Type III SS	Mean Square	F Value	Pr > F
Cement	2	8.805	4.402	16.96	<.0001
Fiber	2	200.921	100.461	386.98	<.0001
Cement*Fiber	4	7.644	1.911	7.36	<.0001
Day	4	23.386	5.847	22.52	<.0001
Cement*Day	8	2.398	0.300	1.15	0.3292
Fiber*Day	8	12.609	1.576	6.07	<.0001
Cement*Fiber*Day	16	6.514	0.407	1.57	0.0814

4.6.2. Pullout Energy Consumption

Table 4-1 displays the mean energy consumption during the pullout process for each of the configurations studies, and Table 4-3 gives the results of the ANOVA for the energy consumption. From the table it can be concluded that the fiber, day, cement-fiber interaction and fiber-day interaction variable have been shown to have a statistically significant effect.

Table 4-3. Analysis of variance on energy consumption

Source	DF	Type III SS	Mean Square	F Value	Pr > F
Cement	2	4.099	2.050	3.50	0.0321
Fiber	2	380.025	190.012	324.88	<.0001
Cement*Fiber	4	8.109	2.027	3.47	0.0094
Day	4	12.631	3.158	5.40	0.0004
Cement*Day	8	5.230	0.654	1.12	0.3533
Fiber*Day	8	12.684	1.586	2.71	0.0077
Cement*Fiber*Day	16	14.810	0.926	1.58	0.0773

4.6.3. Synthesis of the Statistical Analysis

To summarize the significant effects for peak load the cement type, fiber type, days of curing and the interaction between cement and fiber type were highly significant. For energy consumption the fiber type, days of curing, interaction between cement and fiber type, and the interaction between fiber type and days of curing were highly significant. The fiber type and days of curing always plays an important role when evaluating behavior of the fiber with respect to all variables. Table 4-4 summarizes the significant effects for each variable under study. The interaction between cement and fiber also plays an important role when evaluating the peak load and energy consumption.

Table 4-4. Synthesis of statistical analysis

Variable	Highly Significant	Less Significant
Peak Load	C; F; D; C x F	C x F x D
Energy Consumption	F; D; C x F, F x D	C x F x D
C = cement type; F = fiber type; D = days of curing		

In comparing the significant variables between peak load and energy consumption the cement played a key role in the peak load; which contributes to the significance of the cement-fiber interaction. The type of cement and cement-fiber interaction played a key role in influencing the peak load analysis of the pullout test. The type of cement was not significant for the energy consumption; instead the type of fiber, days of curing, cement-fiber interaction and fiber-day interaction played a key role in the pullout test. Fiber type was instrumental in sustaining toughness of the composite beyond the peak load of the pullout test. However, the fiber type that achieved the largest toughness was dependent on the right type of cement interaction.

4.7. Conclusions

The bonding characteristics of three fiber types and three different types of cement were examined. The single-fiber pullout test was used to quantify peak load and energy consumption; SEM analysis provided a qualitative comparison of the physical bonding characteristics for the fibers and matrix. As evident from this study the ability to transfer interfacial stress from fiber to matrix is an important factor in bond strength. The more rigid-dense ettringite crystal structure yielded higher peak loads and larger energy consumption. Thin-fibrous C-S-H structures of the OPC matrix provided good bonding properties, which equated to large maximum peak loads. However, unable to resist debonding-shear stresses the thin C-S-H structure resulted in a fiber-matrix bond with small energy consumption. Pull-out test results indicated the following:

- Peak load and pullout-energy consumption differed significantly according to the fiber type, days of curing and the interaction between fiber type and type of cement. The steel fibers showed higher peak load and energy consumption than the PP and PVA.
- High Young's modulus fibers achieved larger failure loads and energy consumption within a CSA-matrix throughout the curing regime. However this result is only true in an ordinary portland cement matrix after 7 days of curing.
- Low modulus fibers, i.e. PP, are best suited to resist pullout forces in an OPC system at early ages of curing < 7 days. This is attributed to the soft-physical nature of the fiber which is susceptible to deformation from delamination; which in turn increases the frictional-shear resistance to pullout loads.

- Evidenced from the pullout test PVA fibers have a significantly lower strain capacity than the PP and steel fibers. Despite complete debonding the decreased strain capacity is attributed to a high-strength chemical-bond to the matrix with failure occurring near the fiber tip, close to the onset of shear-crack propagation.

A statistical analysis of peak load and energy consumption data was performed with the ANOVA test. Results indicated:

- The importance of cement type, fiber type and curing time on the peak load data obtained from the pullout test.
- The interaction between cement and fiber type was highly significant indicating performance will either improve or diminish based on the combination of these two variables.
- Cement type was not highly significant for energy consumption as compared to the significance of fiber type and days of curing.
- Energy consumption was greatly influenced by the cement-fiber interaction. This was demonstrated by comparing the pullout test data between OPC and CSAB cement with fibers of varying elastic moduli.

In summary, the CAER CSAB cement, fabricated from CCBs, demonstrated optimum bonding characteristics with both steel and PVA fibers; optimum with regards to maximum peak load and energy consumption. However, PP fibers demonstrated optimum bonding within the Commercial CSAB cement. Cements that produce rapid-high early strengths, such as CSA cements, are most compatible with fibers that exhibit a high modulus of elasticity. The known performance characteristics of reinforcing fibers

in an OPC system do not reflect the performance of the same fibers in a CSA cement system. This is supported by the results of the ANOVA indicating the cement-fiber interaction is highly significant for both peak load and energy consumption.

CHAPTER 5 : INFLUENCE OF CEMENT TYPE ON MULTIPLE CRACKING BEHAVIOR IN FIBER COMPOSITES

5.1. Introduction

This chapter presents the results of an investigation to examine the effect of the interfacial bond between the fiber and cement matrix on the multiple cracking behavior of the composite by quantifying the debonding-energy density and maximum fiber-bridging stress. This was accomplished by comparing the multiple cracking behavior of reinforcing fibers embedded in composites formed from sulfate-based systems, CSA, as opposed to the silicate systems found in portland cement; utilizing the single-fiber pullout test.

Reinforcing fibers are an essential element in the design of engineered cementitious composites (ECC) and ultrahigh performance concrete (UHPC). These materials are targeted at creating a fiber-reinforced cementitious material that can sustain large compressive and flexural loads and exhibit excellent toughness, specifically by demonstrating pseudo strain-hardening and multiple cracking (Li and Leung, 1992; Lin and Li, 1997; Li and Fischer, 2002; Yang, Wang et al., 2008). As cementitious matrices continue to be engineered to perform at ultrahigh compressive and flexural strengths an underlying need for the characterization of how these enhanced systems interact with reinforcing fibers becomes more prevalent. High-strength cementitious systems are brittle and have low-energy absorption or toughness as a result of their inability to sustain deformation and crack resistance. The following research intends to illustrate how the fiber-matrix composite is influenced from the utilization of calcium sulfoaluminate

cements with a high modulus of elasticity; as compared an ordinary portland cement system, with a lower modulus of elasticity. Moreover, there is a need to better understand the pullout process and the energy absorbing mechanisms associated with engineered cementitious composites. This paper will evaluate the relationship between fiber-matrix crack-bridging stress and debonding-energy density and how these mechanisms contribute to multiple cracking behavior.

The relationship between crack bridging and crack opening when stressed is considered the most important link between the properties of fiber, matrix and fiber-matrix interface and that of a composite. This relation defines the ultimate stress and strain of a uniaxial tensile stress-strain curve and the energy consumption due to fiber bridging, which in turn control the strength, ductility and toughness of an engineered cementitious composite (Lin and Li, 1997). The crack-bridging behavior, a concept first proposed by Marshall and Cox (1988), and associated fiber-matrix debonding stress is used as the linking concept between interfacial bond and composite failure behavior (Marshall et al., 1985; Cox et al., 1985; Marshall and Cox, 1988, Li et al., 1997; Kanda et al., 1997). A fiber-matrix composite is engineered to sustain additional loads after the matrix has been cracked. However, this is only true if the pull-out resistance of the fibers, after the matrix is cracked, is greater than the load when the matrix cracked. When the matrix has been sufficiently cracked and unable to sustain external loading, the fibers take on any additional load experienced by the composite. The zone between the fiber and matrix performs many functions, but it primarily provides a pathway to transfer additional stresses back into the matrix, through bond stresses. If these bond stresses do not exceed the bond strength, multiple cracking may be induced in the matrix. This process of

multiple cracking will continue until either the fibers fail or the accumulated local debonding will lead to fiber pullout (Shah, 1991; Mehta and Monteiro, 2006).

The bond between the fiber and matrix is important, if the bond is weak the fiber can slip out at low loads and do not contribute to crack arresting. However, if the bond is too strong then the fibers will rupture before they can contribute to the post-crack strength of the matrix material and will exhibit a low debonding strength and reduced damage tolerant behavior.

To fully understand the performance of the entire composite, the contribution of each component must be evaluated. Particularly, the pullout behavior of a single fiber embedded in a cementitious matrix. The contribution of the interfacial bond between a single reinforcing fiber and surrounding cement matrix, may seem inconsequential to the overall performance of a fiber-reinforced composite. However, that infinitesimally small transition zone is what governs the ultimate load, toughness and debonding stress of a composite when considering the volume of fibers present. The microstructural development within the transition zone is governed by cement hydration and hardening of the bonding system which defines the mechanical properties of the fiber-matrix composite (Janotka et al., 2003; Krajci et al., 2003).

A popular interface characterization test is the single-fiber pullout test (Nairn et al., 2001; Liu et al., 2001). In the single-fiber pullout test, the end of a fiber is embedded in a cement matrix and pulled out while the matrix is held in place. The peak force, P , required to debond the fiber is typically recorded as a function of time and/or displacement; however, in this study it will be compared to curing time.

Fiber-reinforced composites (FRC) resist tensile forces through a composite action, whereby part of the tensile force is resisted by the matrix, while the balance is taken by the fibers (Naaman, Namur et al. 1991). The transmission of forces between the fiber and the matrix is achieved through bond defined as the shearing stress at the interface between the fiber and the surrounding matrix (Naaman et al., 1991). It is generally agreed that the fiber contribution to increasing the toughness of the composite is primarily dictated by the mechanisms of fiber pullout (Naaman et al., 1991). The term toughness refers to the work dissipated, or the total energy absorbed prior to complete failure; or the critical potential energy release rate of a composite specimen with a unit mJ (Brown et al., 2002). As a precursor to toughness a composite must be able to withstand brittle failure through multiple cracking. The ability for a fiber-matrix combination to dissipate a large volume of cracking energy may be determined by quantifying the debonding-energy density.

The cement-fiber interfacial bond results from some combination of mechanical interlocking of cement hydration products with the fiber surface and chemical reaction between fiber and cement paste within the interstitial transition zone (Kim and Mai, 1998; Brown et al., 2002). In fiber reinforced composite materials, the principal factor governing load transfer from the matrix to the fiber is the shear strength of the interfacial bond between the two components. Without the benefit of a mechanism, i.e. fibers, to dilute crack-induced energy within the matrix the result is sudden failure as demonstrated by plain concrete. Fibers have the effect of increasing the work of fracture by absorbing the energy of a single crack and redistributing it by creating multiple cracks. Fractured specimens of fiber-reinforced concrete shows that failure takes place primarily due to

fiber pullout or debonding. Debonding of the fiber-matrix interface generally initiates before the ultimate load is reached. Regarding engineered cementitious composites it is generally fiber pullout rather than rupture that enables a larger ductility to the fiber reinforced composites (Li and Stang 1997, Lin and Li 1997). The development of multiple cracking from the redistribution of cracking energy is reminiscent to strain-hardening behavior.

5.2. Research Significance – Chapter 5

The increasing interest in researching and utilizing UHPC as a means to lessen or eliminate the need for reinforcing steel in the construction process. As cementitious matrices continue to be engineered to perform at ultrahigh compressive and flexural strengths there is an underlying need for the characterization of how these enhanced systems interact with reinforcing fibers. High-strength cementitious systems are brittle and exhibit low-energy absorption or toughness as a result of their inability to sustain deformation and crack resistance. This study intends to illustrate how the fiber-matrix composite is influenced from the utilization of high-strength cementitious systems, specifically calcium sulfoaluminate cements. As compared to lower-strength systems, like that of an ordinary portland cement. Moreover, there is a need to understand better the pullout process and the energy absorbing mechanisms associated with increased toughness in composites.

The bond between the fiber and matrix is important, if the fibers have a weak bond with the matrix they can slip out at low loads and do not contribute to preventing the propagation of cracks. However, if the bond is too strong then the fibers will rupture

before they can contribute to the post-crack strength of the matrix material. Ideally the debonding stress will be such that external loads are successfully transferred from the matrix to the fiber and back into the matrix multiple times, over the entire length of the embedded fiber as it's pulled completely free from the surrounding matrix. Determining the fiber-matrix pairing that will provide the most efficient bond to allow for the development of multiple cracking will in turn control the strength, ductility and toughness of a structural member.

Therefore this paper presents the development of the CSA cement-fiber interfacial performance in the context of material design under the guidance of micro-mechanical tools. Specifically this study illustrates how the fiber-matrix interface is enhanced by the use of sulfate-based cements when compared to silicate-based cements, in regards to debonding stress and multiple cracking. The overarching goal is to provide some guidance in properly selecting a combination of fiber and matrix that provides efficient damage tolerant behavior.

5.3. Experimental Program

The single-fiber pullout test was conducted to investigate the evolution of debonding-energy density and fiber-bridging stress over time. The major parameters investigated were cement type and fiber type and their effect on the ability for a cementitious composite to dissipate deleterious external loads. The fiber-matrix debonding-energy density and fiber-bridging stress was determined for each fiber-cement combination; these composite properties were used to evaluate the multiple cracking behavior differences in CSA and ordinary portland cements.

5.4. Experimental Results and Discussion

The influence of fiber and cement type on the fiber pullout energy and associated multiple cracking was determined from the analysis of load-deflection curves. The primary binder in CSA-cement systems differ greatly from that in OPC systems, both chemically and physically. To evaluate the influence of these different binders on the bond between cement and fiber the stress associated with multiple cracking was quantified and analyzed for statistically significant interactions with fiber type, cement type and days of curing. The effect of cement and fiber type on the ability for a composite to induce multiple cracking was evaluated by quantifying the fiber bridging load versus displacement.

5.4.1. Fiber/Matrix Debond-Energy Density

The primary behavior defining a tough material is the formation of multiple cracking (i.e. microcracks) at increasing composite tensile stress (Mobasher et al., 1990). This behavior hinges on two complementary requirements; first, the peak interfacial bond strength between the fiber and matrix must exceed the first cracking strength of the matrix. This condition is necessary so that the load, prior to matrix cracking, can be supported by the fiber after matrix cracking. Second, according to Li and Leung (1992), propagation of a matrix crack must occur at a constant stress and constant crack opening in a flat configuration (Li and Leung, 1992; Li and Fischer, 2002). These requirements are necessary in the development of multiple cracking in fiber reinforced brittle matrix composites. Which has been extensively studied, starting with the investigation of fiber reinforced cement by Aveston et al. (1971). Mobasher et al. (1990) evaluated the

micromechanics of matrix fracture in portland cement-based fiber composites using an acoustic emission technique in combination with optical microscopy; which were used to identify and confirm microcracking (Mobasher et al., 1990). The study found the maximum acoustic emission to occur at the point where the stress-strain relationship reached a maximum on the linear portion of the curve (Mobasher et al., 1990). The study detected microcracks prior to the directional change of the stress-strain curve; with a majority of the cracks located within the interfacial zone between the fiber and matrix (Mobasher et al., 1990; Brandt, 2008). Therefore the debonding-energy density was used to quantify the energy absorption capacity, through microcracking, up to peak loading. In regards to the single-fiber pullout test peak loading represents the point in which the microcracks within the interfacial zone have initiated the transition from fiber-matrix debonding to fiber pullout. This is analogous to the coalescence of microcracks described by Mobasher et al. (1990) at which point the first microcrack band was developed (Mobasher et al., 1990).

To quantify the energy associated with multiple cracking, Equation 5-1, can be interpreted as follows: the cumulative energy consumed from the onset of loading to maximum fiber bridging stress $\sigma_{B,peak}$ and corresponding crack opening δ_{peak} ; (i.e. the energy consumed from fiber-matrix debonding). Graphically, the debonding energy density is the area to the right of the $\sigma - \delta$ curve up to the peak stress.

$$\text{Debonding Energy Density} = \int_0^{\delta_{peak}} \sigma_B(\delta) d\delta. \quad (5-1)$$

With initiation of the first crack, the linear stress-strain relationship comes to an end.

After this point more cracks continue to form at higher deformation levels. Eventually

the crack resistance will be reduced when the crack bridging capacity is exceeded at a particular crack location, deformation of the composite will localize at this site (van Zijl, 2011). The inclusion of reinforcing fibers provides the catalyst to deformation resistance by increasing the stress over a larger strain by retarding the localization of deformation.

Pseudo strain-hardening in fiber reinforced composites is associated with the multiple cracking phenomenon of the brittle matrix (Li and Wu, 1992). If crack spreading is unstable, then a first macroscopic crack is formed in the composite. A load applied to a fiber-reinforced composite will be shared by the bridging fibers. These fibers then transfer the load through their interface back into the matrix. If enough load is transferred, the matrix may crack again and the process repeats until the matrix is broken by a series of sub-parallel cracks of approximately equal crack spacing (Li and Wu, 1992). Straining of the bridging fibers across the matrix cracks and within the matrix zones give rise to a composite strain that can be substantially higher than the matrix failure strain alone (Li and Wu, 1992).

Figure 5-1 shows the debonded-energy density as determined from equation 4-1 for the coated steel and plain steel fibers embedded in the OPC, Commercial CSA cement and CSAB#4 cement. The plain-steel fibers attained the highest debonding-energy density at 1 day (33.49 mJ/mm^3) in the Commercial CSA cement paste. A positive increasing trend in debonding-energy density was exhibited in both the OPC and CSAB#4 cement, increasing from 18.65 mJ/mm^3 (1 day) to 28.18 mJ/mm^3 (112 days) in the OPC paste, increasing from 11.30 mJ/mm^3 (1 day) to 24.89 mJ/mm^3 (56 days) in the CSAB#4 paste before decreasing to 19.75 mJ/mm^3 at 112 days. An increased debonding-energy density suggests plain-steel fibers in the OPC matrix is the best combination for maximum

energy absorption through multiple cracking of the cementitious matrix. Countering the trend of the OPC and CSAB#4 matrix the Commercial CSA cement had a decreasing trend from 1 day (33.49 mJ/mm^3) to 112 days (1.03 mJ/mm^3). The rapid-hardening nature of the Commercial CSA cement has attributed to the reduction of energy density in the fiber-matrix debonding zone of the stress-strain curve. The increasing elastic modulus of the CSA cement made it more difficult to induce multiple cracking, thereby creating a more brittle composite with the plain-steel fibers. However the CSAB#4 cement showed an increasing debonding-energy density with time which is surprising considering the similarity in chemistry and mineral phases present in both the Commercial CSA and CSAB#4. The answer may reside in the microscopic differences in the morphology of the ettringite crystals themselves; these differences will be discussed in the following section on hydrated cement morphology.

The coated-steel fibers demonstrated a decreasing trend in debonding-energy density from 1 to 112 days in all three cements tested (Figure 5-1). The range in debonding-energy densities from 1 day to 112 days in OPC was 16.16 mJ/mm^3 to 0.49 mJ/mm^3 ; in the Commercial CSA, 29.21 mJ/mm^3 to 4.74 mJ/mm^3 ; and in the CSAB#4, 22.85 mJ/mm^3 to 9.79 mJ/mm^3 . The coated-steel fiber has a similar elastic modulus as the plain-steel fiber; however, the coating added for corrosion control (Figure 2-1), appears to have modified the fiber surface thereby reducing the effectiveness of the fiber-matrix bond which is demonstrated by the reduction in debonding-energy density in each cement. The cementitious matrix creates a strong bond with the coating, which readily breaks free from the fiber surface reducing the level of stress/energy present through the

debonding zone of the stress-strain curve. The corrosion-control coating works as a lubricant or a bond release agent.

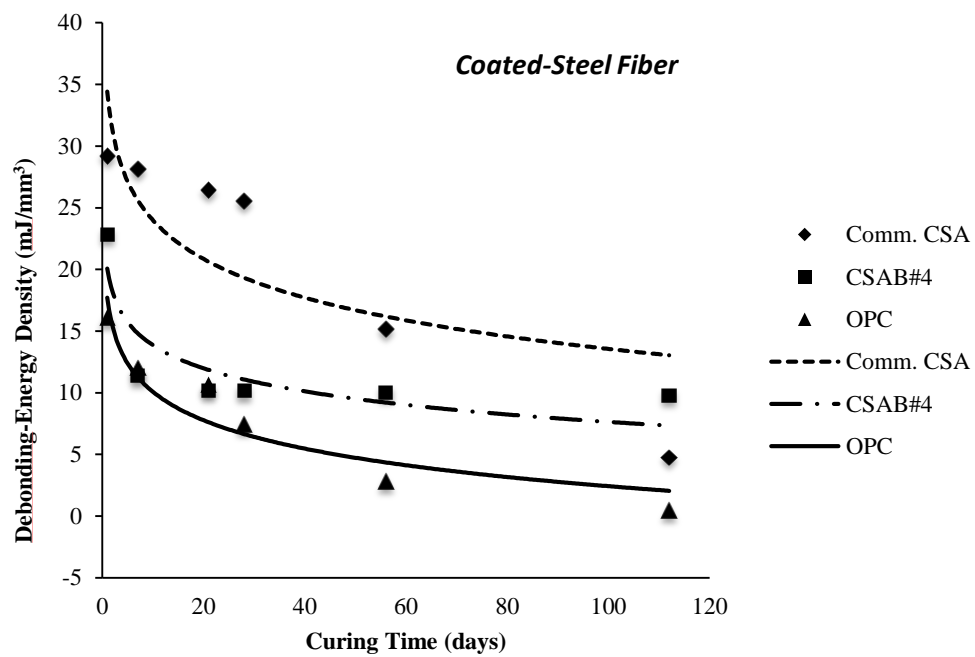
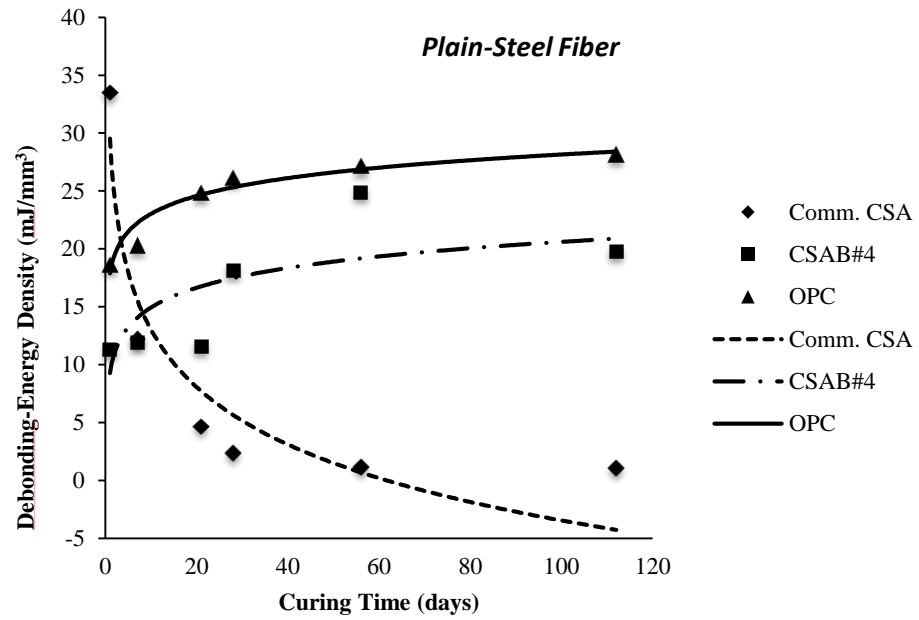


Figure 5-1. Fiber-matrix debond-energy density as a function of curing time for the steel fibers.

Figure 5-2 shows the debonding-energy density as determined from equation 1 for the polyvinyl-alcohol and polypropylene fibers embedded in the OPC, Commercial CSA cement and CSAB#4 cement. The PVA fiber showed an increasing debonding-energy density with time from 1 to 112 days of curing in the cementitious composite. The greatest energy density range was exhibited in the CSAB#4 paste (0.17 mJ/mm³ to 7.82 mJ/mm³), followed by the Commercial CSA paste (1.26 mJ/mm³ to 4.85 mJ/mm³), and the lowest energy density range was demonstrated in the OPC paste (0.45 mJ/mm³ to 1.58 mJ/mm³).

The polypropylene fibers produced the most consistent ability to form multiple cracking in the ordinary portland cement over the full range of curing time; with a debonding-energy density range of 2.83 mJ/mm³ to 4.98 mJ/mm³. However with the PP fiber embedded in the Commercial CSA cement there was an increasing debonding-energy density from 1 to 112 days. Whereas the energy density decreased in both the CSAB#4 and ordinary portland cement matrixes, over the range of curing.

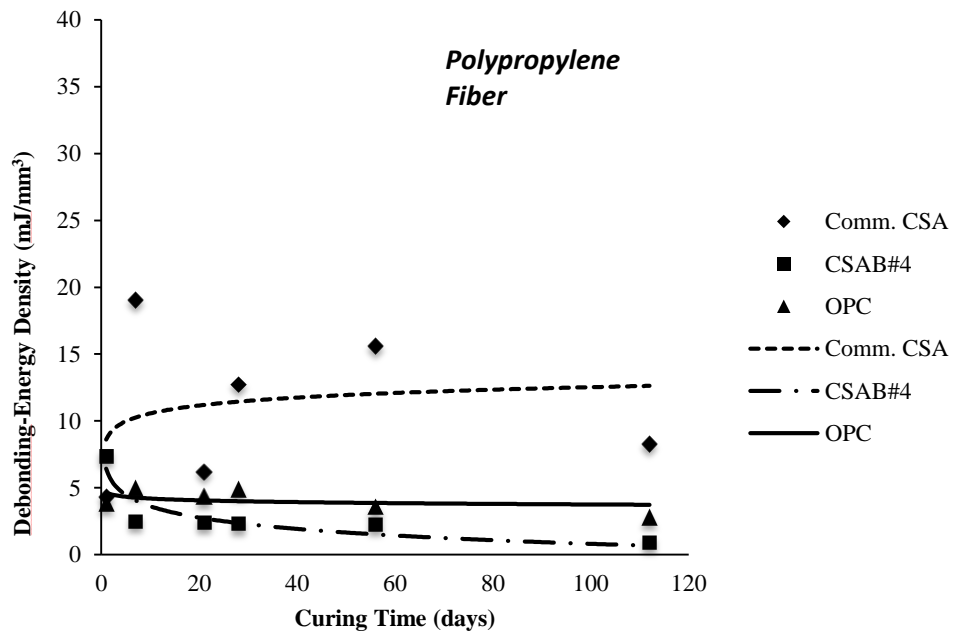
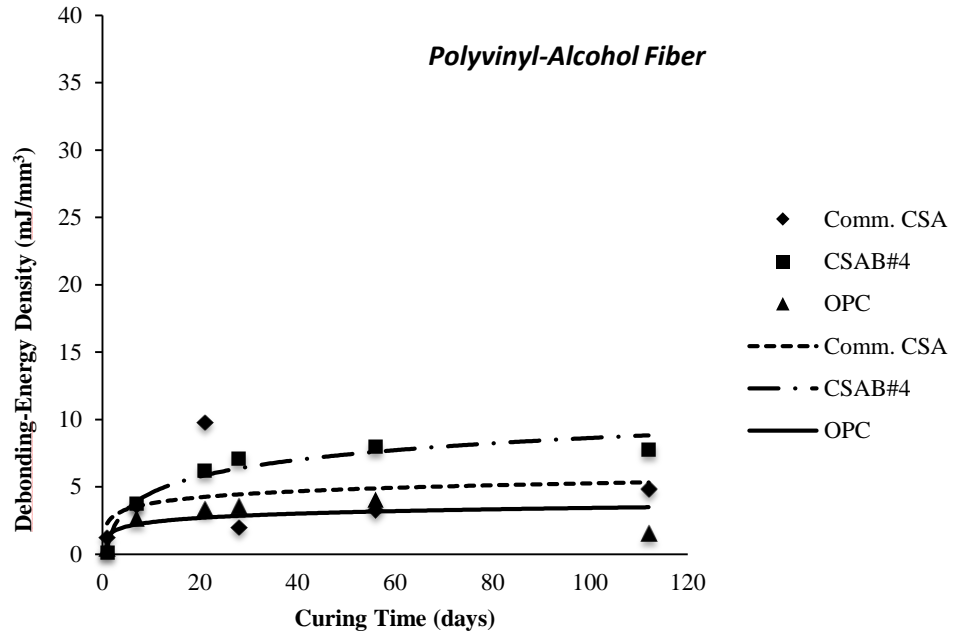


Figure 5-2. Fiber-matrix debond-energy density as a function of curing time for the synthetic fibers.

5.4.2. Influence of Hydrated Cement Morphology

The transition zone (TZ) between the cement matrix and fiber plays a crucial role in governing the performance of the fiber-matrix composite. The bond developed in the TZ between the fiber and matrix is strongly influenced on the nanostructure and microstructure of the hydrated cement; which is analogous to the inter- and intramolecular interactions of every amorphous and crystalline solid (Fahlman, 2011). The cement paste structure depends on the composition of the original cement grains, the starting water:cement ratio, the temperature of hydration, and the presence of chemical admixtures at the time of hydration (Hannant, 2000). Considering the entire paste structure, there is a wide range of particle sizes and void spaces making each fiber-matrix bond unique. Each fiber-matrix TZ may be composed of unhydrated cement grains of irregular shape of approximately 10 – 20 μm in size, the space between them filled with less than 1 μm calcium silicate hydrates of complex forms including partly crystalline fibers and sheet-like networks in which other phases are present like plates of calcium hydroxide, Figure 5-3 (Hannant, 2000).

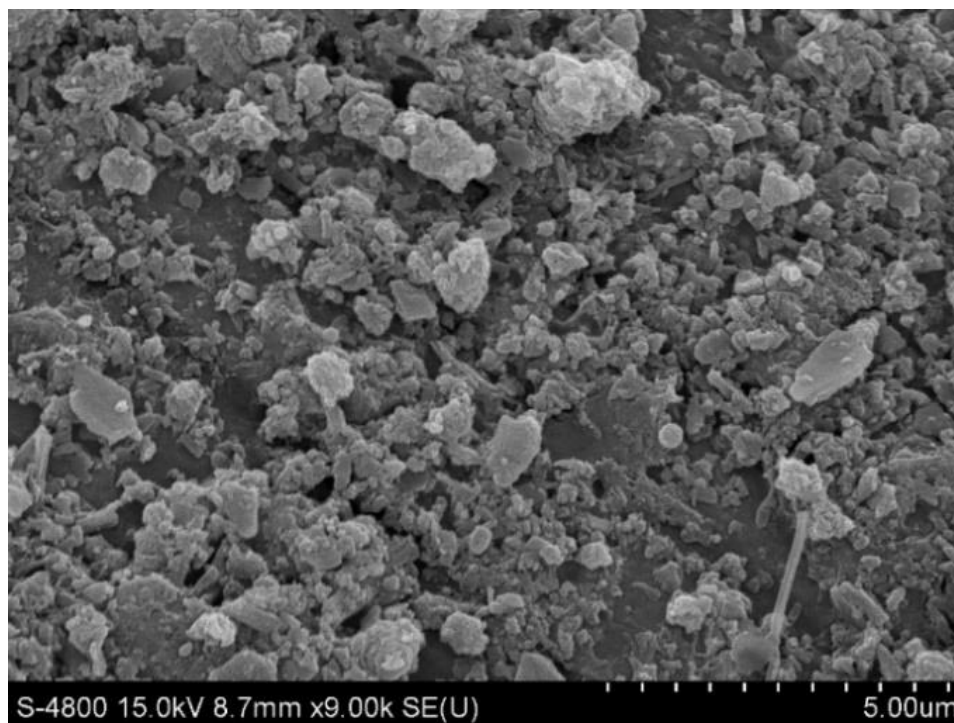


Figure 5-3. SEM image of OPC paste showing irregular structure of C-S-H phases; 9000x magnification.

Whereas the CSA fiber-matrix transition zone is composed primarily of ettringite crystals, an acicular crystal with a large aspect ratio, Figure 5-4(Taylor 1997, Stark and Bollmann 2000, Komatsu, Mizukoshi et al. 2009). In fact the variation in strength between the Commercial and CSAB#4 cements may be attributed to the morphology of the ettringite crystal in addition to the availability of ettringite-forming phases. The ettringite crystals formed within the Commercial CSA matrix are primarily less than 4 microns in length, Figure 5-4. Whereas the CSAB#4 developed ettringite crystals that are primarily less than 10 microns in length, Figure 5-4. The longer crystals of the CSAB#4 may be more brittle and are unable to form a dense of a network as the shorter crystals in the Commercial CSA.

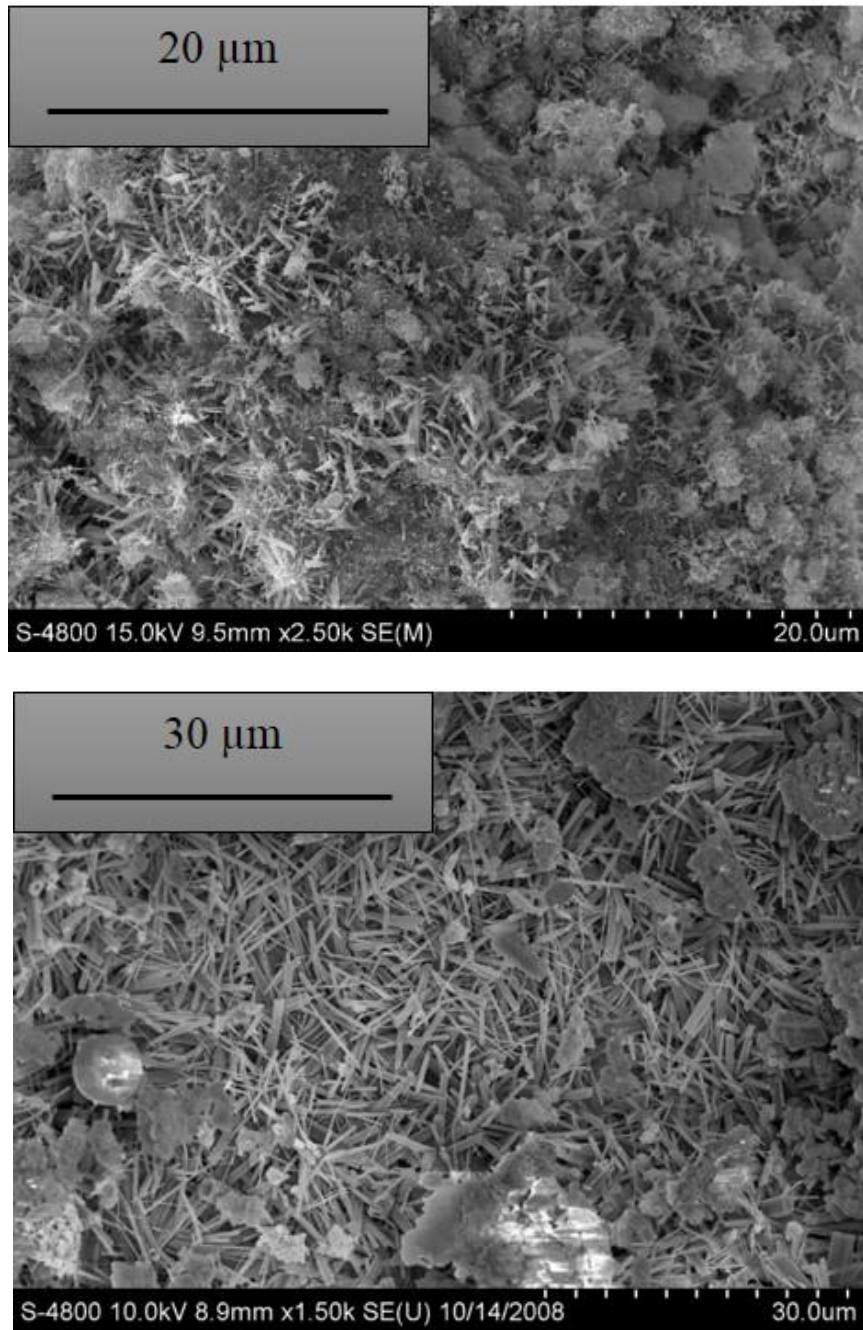


Figure 5-4. SEM images of hydrated CSA cement: *Top*: Commercial CSA, 2500x magnification; *Bottom*) CSAB#4, 1500x magnification.

The variation in debonding-energy density between OPC and CSA cement is likely attributed to the difference in the morphological assemblage of hydrated cement phases within the transition zone. The resistance to uniaxial pullout forces are focused on these assemblages that populate the TZ.

Many toughness theories of composite materials have been developed mainly for those with unidirectional fibers. Kim and Mai (Kim and Mai 1998) emphasized the various origins of toughness in composites may be characterized by considering the sequence of microscopic fracture events that lead to crack propagation macroscopically under monotonic increasing loads, such as the single-fiber pullout test. The cracks in a cement matrix can propagate along the fiber-matrix, referred to as longitudinal cracking; or transversely through the fiber and matrix, referred to as transverse cracking. The longitudinal cracking relies heavily on the physical and chemical adhesion between the fiber and matrix; with an additional bond component related to frictional stresses (Najm et al., 1994). The prevalent type of cracking depends on the properties of the interface relative to the fiber and matrix (Kim and Mai, 1998). According to Kim and Mai (1998), when a crack present in the matrix approaches an isolated fiber, the following failure mechanisms may be expected to take place: 1) fiber-matrix interface debonding; 2) post-debonding friction; 3) fiber fracture; 4) stress redistribution and 5) fiber pullout.

5.4.3. Fiber Bridging Stress

As a matrix cracks under an applied load the newly formed cracks will encounter an embedded fiber which will either fracture or bridge the crack, the prevailing mode depends on the interface properties. Fiber-crack deflection, deformation and pullout

within the bridging zone contribute to the overall toughness of the fiber-paste composite. Toughness encompasses the energy absorbed by the composite, the inflicted energy results from the opening of matrix cracks which causes an increasing stress on the fiber; which corresponds to the fiber-bridging stress. Therefore researchers have focused on improving the strength and toughness of discontinuous fiber composites by optimizing fiber-matrix response to applied loads (Shah, 1991; Beyerlein et al., 2001). To achieve a high composite strength the fiber-matrix bond needs to be strong; a strong interface provides an effective stress transfer medium (Beyerlein et al., 2001; Jewell et al., 2015). The fiber-bridging stress can be described by an equation modified from Li and Leung (1992):

$$P(\delta) = \frac{\pi}{2} \sqrt{(1 + \eta)E_f d_f^3 \tau \delta} \quad (5-2)$$

With fiber diameter of d_f , fiber elastic modulus E_f , shear strength τ , fiber displacement corresponding to peak load δ , and $\eta = (V_f E_f)/(V_m E_m)$; where V_f and V_m are the fiber and matrix volume fractions, and E_f and E_m are the fiber and matrix elastic modulus (Li and Leung, 1992). The equation presented by Li and Leung (1992) accounted for the snubbing effect, originally reported by (Li et al., 1990), which accounts for increased bridging forces due to an inclined fiber angle with respect to pullout direction. The snubbing effect was not considered as the applied load is parallel to the length of the fiber for the single-fiber pullout test.

Figure 5-5 shows the fiber bridging stress as determined from equation 5-2 for the coated steel, plain steel, polypropylene and polyvinyl alcohol fibers, with respect to curing time, embedded in an OPC matrix. The top portion of the figure illustrates the corresponding

fiber-matrix strain. The plain- and coated-steel fibers had a similar bridging stress at 1 day of approximately 100 MPa. However from 7 to 112 days of curing there was an increase in bridging stress for the plain-steel fibers that paralleled the increasing matrix strength; while the coated-steel fibers decreased in bridging stress over the same time. An increasing fiber-bridging stress with decreasing fiber displacement, over time, suggests the increasing matrix strength is more resistant to creating new fracture surfaces and additional loading is focused on the fiber-matrix interface. The polyvinyl-alcohol fibers increased in bridging stress from 1 day (4 MPa) to 56 days (16 MPa), and were able to withstand larger strains before fiber pullout was initiated. The larger strains may be attributed to a combination of the chemical bond and low elastic modulus allowing the fiber to readily deform; absorbing additional energy over a greater distance. The plain-steel fibers achieved a fiber-bridging stress of 107 MPa at 1 day and increasing to 151 MPa at 28 days before decreasing to 130 MPa at 112 days. The coated-steel fibers demonstrated a decreasing trend in bridging stress from 1 day (106 MPa) to 112 days (127 MPa). The bridging stress was reduced by approximately 50% during the 112 days. The coated-steel fiber has a similar elastic modulus as the plain-steel fiber however the coating, added for corrosion control, modifies the fiber surface thereby reducing the effectiveness of the fiber-matrix bond which is demonstrated by the reduction in bridging stress. The PP fibers maintained a fairly constant bridging stress through the 112 days of curing; which may indicate a threshold to the bridging stress. Figure 5-5 highlights the performance differences between the steel and synthetic fibers in the OPC matrix. Both of the steel fibers show a decreasing trend, with time, in the strain capacity of the single-fiber composite; however, the synthetic fibers did not exhibit a decreasing trend. The PP

fibers maintained consistent strain capacity, while the PVA fibers were able to sustain greater strains with increasing time. Compared to the PP fiber the modulus of elasticity of the PVA fiber increased from 5,000 MPa to 30,000 MPa and the tensile strength increased from 600 MPa to 1200 MPa; the increased strength and stiffness in combination with the strong hydrophilic bond that these fibers exhibit, allowed PVA fibers to attain greater strains with increasing time. Polypropylene fibers are designed to defibrillate, through this deformation mechanism the pullout resistance is fortified as the fiber is gradually pulled into segments; lending to the consistent strain capacity.

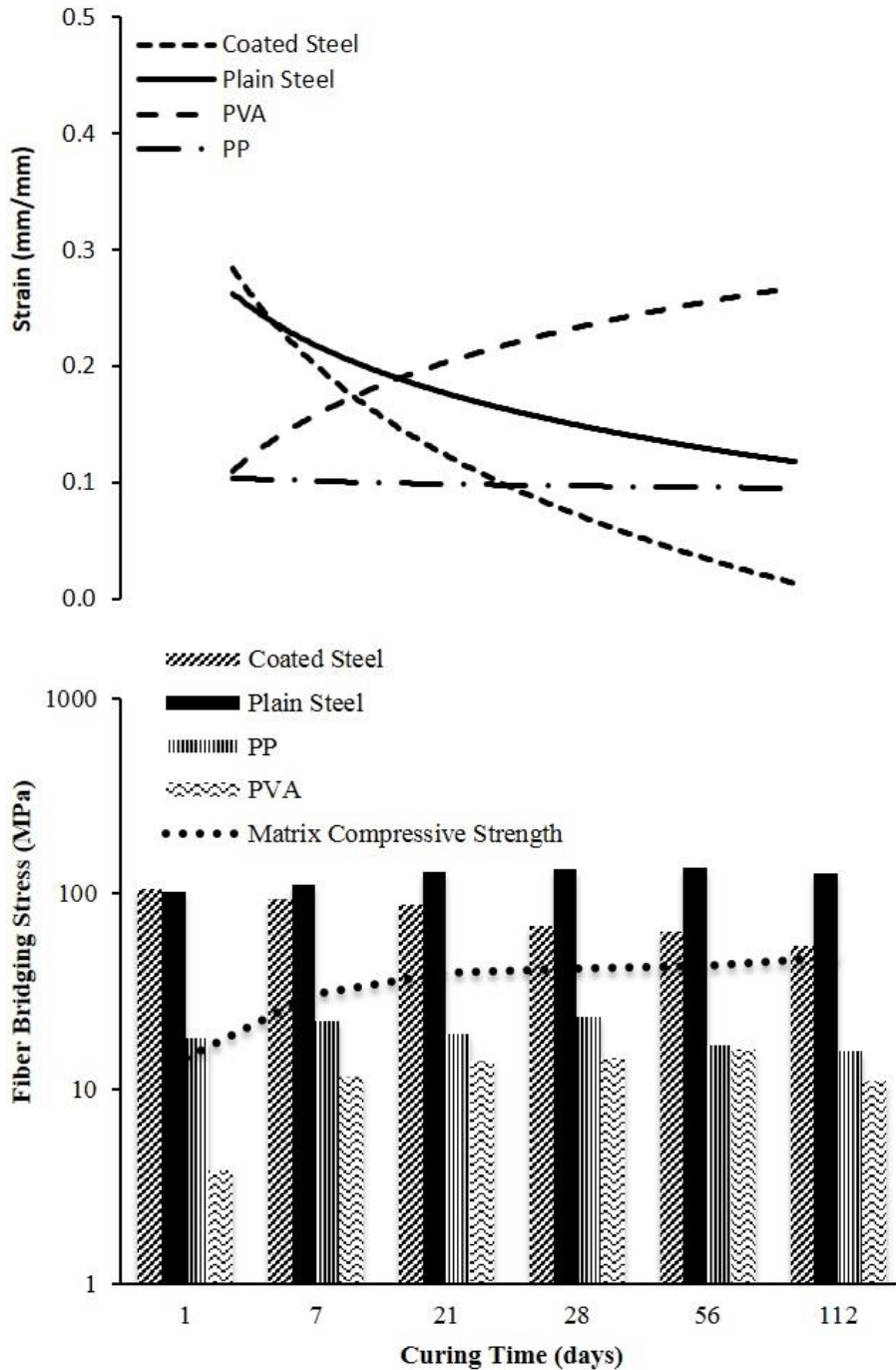


Figure 5-5. Fiber bridging stress as a function of curing time in the OPC paste.

Figure 5-6 shows the fiber-bridging stress as determined from equation 2 for the coated steel, plain steel, polypropylene and polyvinyl alcohol fibers, with respect to curing time,

embedded in the Commercial CSA cement matrix. The top portion of the figure illustrates the corresponding fiber-matrix strain. Again the steel fibers demonstrated the highest fiber-bridging stress from 1 to 112 days of curing. However, unlike the OPC matrix where the plain-steel fibers achieved the highest bridging stress the coated-steel fibers had the best ability to sustain additional fiber-bridging stresses from 1 to 112 days of curing; decreasing from 178 MPa at 1 day to 122 MPa at 112 days. Additionally the fiber-bridging stress increased by approximately 68% by embedding the fibers in the Commercial CSA cement matrix, instead of the OPC matrix. The plain-steel fibers had a similar decreasing trend as the coated-steel fibers; decreasing from 135 MPa (1 day) to 75 MPa (112 days). Polypropylene fibers experienced a positive increasing trend in bridging stress from 1 to 112 days; 19 MPa to 28 MPa, respectively. Comparable to the PP fibers, PVA fibers demonstrated an increasing trend to sustain bridging stresses from 1 day (7 MPa) to 21 days (17 MPa). The bridging stress then levelled off through 112 days of curing, ranging from 16 MPa to 17 MPa. Figure 5-6 shows similar strain profiles for each fiber as was illustrated in Figure 5-5 for the OPC matrix; with the strain increasing with time for the synthetic fibers, while the strain for the steel fibers decreases with time. As the cementitious matrix increases in strength and stiffness over time greater loads are required to create new fracture surfaces. The steel fibers contributed to greater peak loads more than the synthetic fibers due to their higher elastic modulus, see Table 4-1 and Jewell et al. (2015). However the increased stiffness of the steel fibers lead to fiber pullout at lower strains than the flexible synthetic fibers that would more readily deform and achieve greater strains. However, the polypropylene fiber was able to sustain greater strains in the Commercial CSA matrix. This may be explained by taking

into account the low elastic modulus (5000 MPa) and high fiber elongation (25%) this monofilament fiber was able to transfer loads, that would otherwise focus on the fiber-matrix bond, to the fiber itself which was able to withstand damage (by delamination of the fiber surface) and yet maintain a sufficient bridging stress to allow for increased strains. The PVA fibers increased the strain capacity in all three cements, this is attributed to the fiber-matrix bonding behavior. As previously mentioned PVA fibers chemical bond with the surrounding matrix, this bonding behavior is a unique property of reinforcing fibers. The fiber-matrix bond provides a strong interface for transferring loads to the fiber, thereby preserving the matrix. In regards to the increased strain capacity seen in Figure 5-5, Figure 5-6 and Figure 5-7, the low elastic modulus of PVA fibers (30,000 MPa) combined with the high tensile strength (1,200 MPa) provided an excellent substrate to absorb the additional load over the greater strains. However, this bonding behavior that is beneficial to increasing the fiber-bridging stress and strain capacity is known to increase the frequency of fiber rupture; resulting from the coalescence of applied stresses within the fiber and not within the fiber-matrix interface.

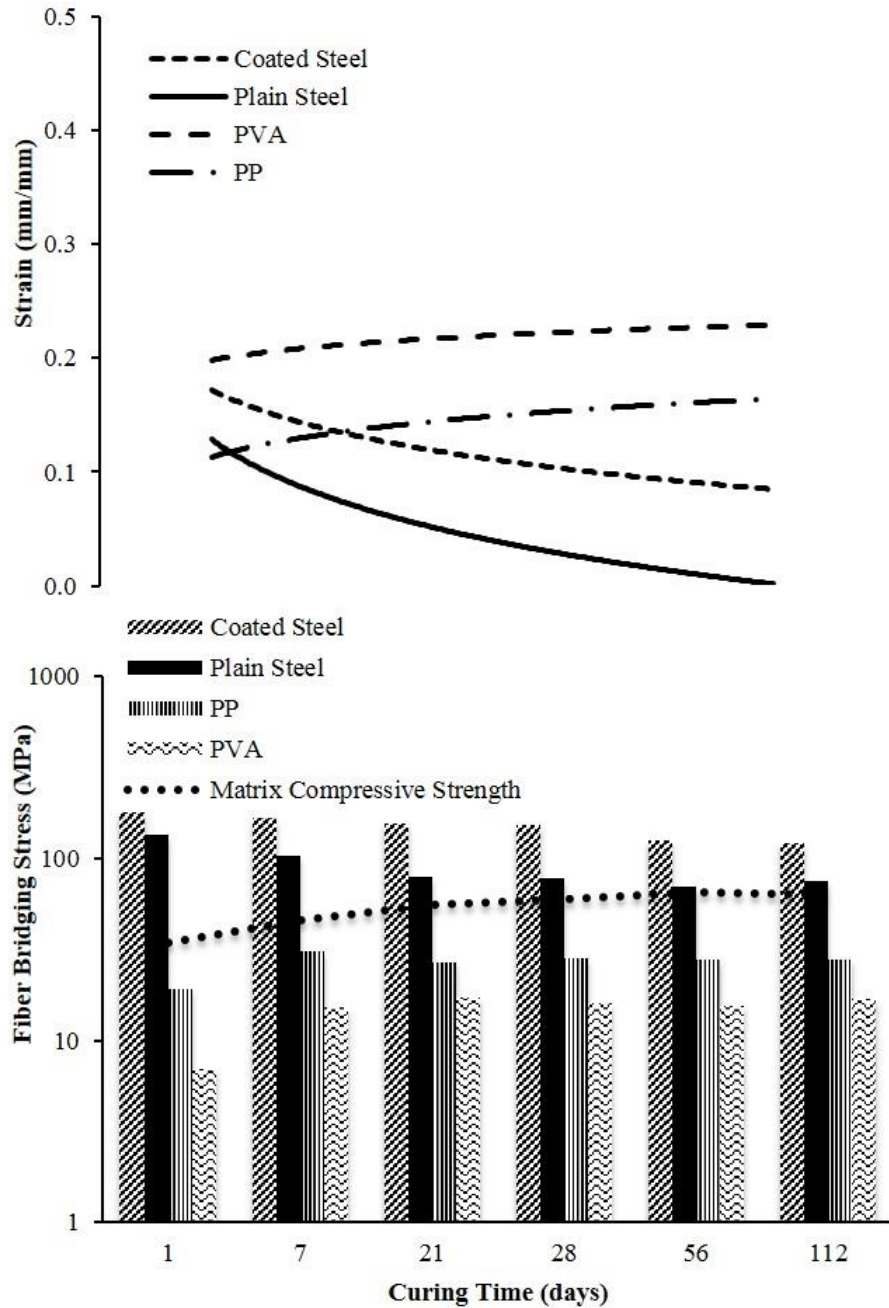


Figure 5-6. Fiber bridging stress as a function of curing time in the Commercial CSA cement paste.

Figure 5-7 shows the fiber bridging stress as determined from equation 5-2 for the coated steel, plain steel, polypropylene and polyvinyl alcohol fibers, with respect to curing time,

embedded in the CSAB#4 cement matrix, which was fabricated from coal combustion byproducts (Chapter 3 and Jewell et al., 2015). The plain-steel and coated-steel fibers maintained similar bridging stresses 1 to 112 days. However the coated-steel fibers decreased from 1 day (144 MPa) to 112 days (87 MPa); while the plain-steel fibers increased from 104 MPa to 148 MPa over the same time period. The polypropylene fibers exhibited a decreasing trend in bridging stress 1 day (21 MPa) to 112 days (12 MPa); differs from the increasing trends seen in the OPC and Commercial CSA cement matrix. The sudden change in bridging stress from one CSA cement to another is likely explained by the morphology of the ettringite crystals. As was discussed in the hydrated cement morphology section the Commercial CSA cement is comprised of short ettringite crystals, while the CSAB#4 cement is comprised of long ettringite crystals. The PVA fibers exhibited a preference for the long crystal structure with an increasing strain capacity over time, which is reflected by the increasing bridging stress from 1 day (3 MPa) to 112 days (24 MPa).

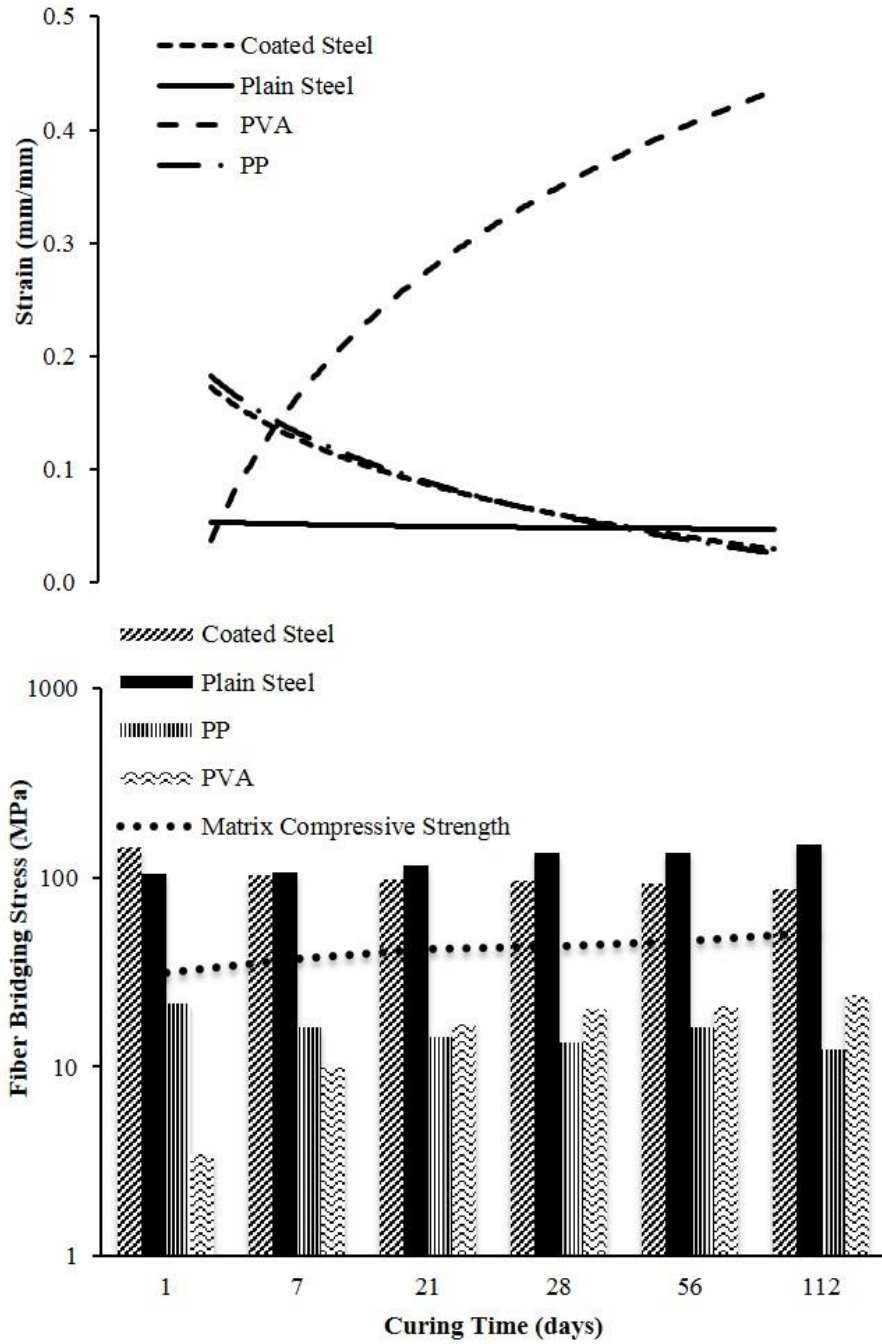


Figure 5-7. Fiber bridging stress as a function of curing time in the CSAB#4 cement paste.

5.4.4. Toughening Mechanisms

Composite toughness is expected to increase with crack-induced deformation attributed to the breakdown of the fiber-matrix bond. However, the major toughening mechanism is believed to result from fiber pullout (Kim and Mai, 1998). To influence the toughness of a composite, fibers must effectively bridge and stop matrix cracks. Kim and Mai (1998) described four primary factors that influence fracture toughness of composites which include: 1) matrix deformation; 2) fiber rupture; 3) fiber-matrix debonding and multiple cracking; and 4) fiber pullout.

Matrix deformation more commonly relates to ductile matrices and is considered negligible for brittle OPC and CSA-cement matrices. Fiber rupture provides little toughness to the system by means of plastic deformation of the fiber; however every fiber contains flaws of varying sizes which develop into fracture planes leading to fiber rupture. Fiber-matrix debonding and crack-induced deformation is governed by a composite's ability to promote multiple cracking. If the fiber-matrix bond is sufficiently strong enough to resist fracture, the load path will redirect back to the matrix. This process will continue until either fiber pullout or rupture occurs. Fiber pullout is the primary toughening mechanism in composites. Complete pullout enables the full energy-absorbing capacity of the embedded-fiber length. If the fiber-matrix bond is strong enough to resist fracture normal to the pullout load, then multiple cracking is likely to occur. Assuming that the fiber-matrix bond is not greater than the ultimate strength of the fiber.

Composites made with brittle, high elastic modulus, fibers and matrices, i.e. steel and CSA cement, can exhibit high composite toughness when failure occurs preferentially along the fiber-matrix interface before fibers fracture (Chapter 4 and Jewell et al., 2015). Most important toughening mechanisms are a direct result of the interface-related shear failure which gives rise to an improved energy absorption (Li and Stang, 1997). Three distinct groups were identified in Figure 5-8 based on the relationship between fiber strain and fiber-bridging stress; the regions are identified as PVA, PP and Steel (both coated and plain) fibers. Composites made with the high elastic modulus fibers exhibited an increased capacity to dissipate damage from loading in the form of multiple cracking before the onset of fiber pullout at early ages. However this behavior decreased with increasing age of the fiber-matrix composite for the steel fibers. For the synthetic fibers, both PP and PVA, there is an associated increase in fiber bridging stress and fiber strain with increasing time.

Compared to the high elastic modulus of the steel fibers the low elastic modulus of the polyvinyl-alcohol fibers sustained lower fiber-bridging stresses in conjunction with higher fiber strains; particularly in the CSA cement pastes. The soft nature of polypropylene fibers allow them to readily deform, particularly by delamination, which provides a mechanism to absorb the energy emitted from matrix fractures. This allows for greater fiber-bridging stresses than the PVA fibers; at the cost of lower strains.

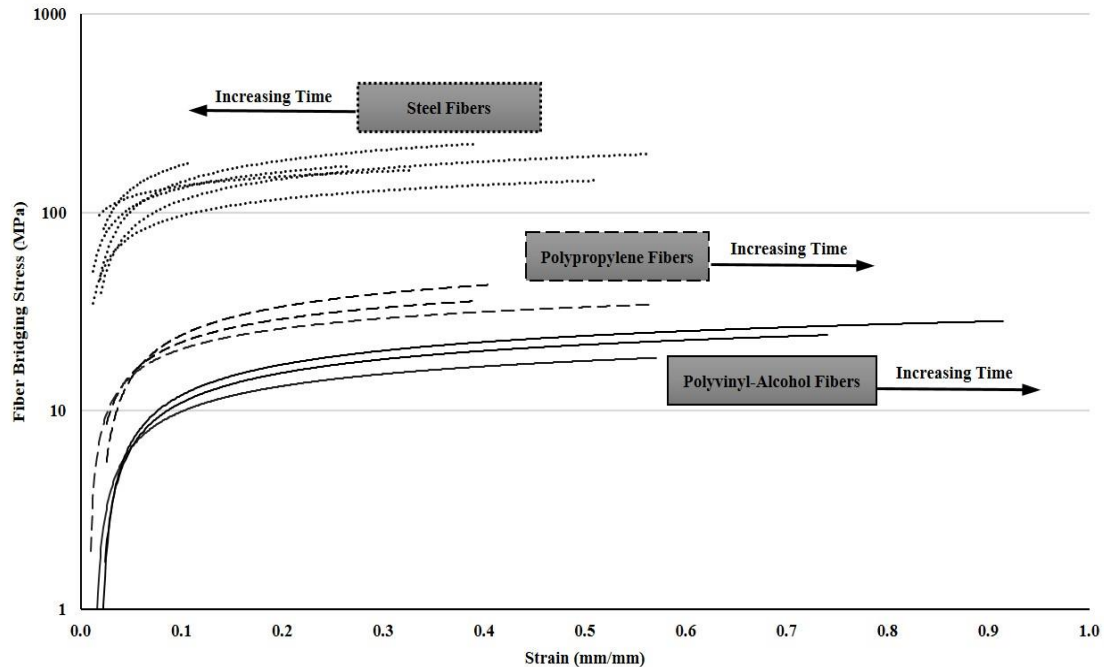


Figure 5-8. Chart illustrating relationship between fiber strain and fiber-bridging stress.

5.5. Statistical Analysis

Each type of cement was analyzed statistically using a two-way general linear model analysis of variance (GLM/ANOVA) (Cox and McCullagh, 1982; Silknitter et al., 1999; Vano et al., 2006; McDonald, 2009). Factorial analysis of variance is a useful tool to assess the effects of cement type and curing time for each fiber type. Specifically, polynomial response curves were fit for each cement which related the dependent variable, debonding-energy density, to curing time. Higher order terms were tested and removed using backward elimination. The resulting model was tested for lack of fit. The test for interaction of cement type and fiber type was used to determine whether there was any significant differences in the relationship of fiber-matrix debonding-energy density and curing time between cement types, including OPC and CSA cement

(Yamazaki et al., 2006). A significance level of $\alpha = 0.05$ was used throughout for statistical analyses. To reduce variance heterogeneity and to make the data more symmetric a log transformation was performed in SAS 9.4 (Box and Cox, 1964). The log-log transformation increased the R-squared value for each of the fiber types with respect to the dependent variable, debonding-energy density, Table 5-1. This provided greater support for the use of ANOVA inference methods on the transformed data.

Table 5-1. Coefficient of determination before and after log transformation

Fiber Type	R ² Before Transformation	R ² After Transformation
Coated Steel	0.4754	0.6600
Plain Steel	0.3631	0.6468
PVA	0.3590	0.5554
PP	0.2331	0.2712

As evidence to the significance difference between the OPC trends and the CSA trends, ANOVA was used to test if separate linear and quadratic were required. The results of this test were not significant (Plain Steel, P=0.219; Coated Steel, P=0.841; PVA, P=0.218; PP, P=0.593) and therefore separate quadratic and cubic interactions were not required, and indeed there does exist significant difference between the trends of the OPC and CSA cements over time.

Mean values of the debonding-energy densities for the fibers in each cement type are shown in Figure 5-1 and Figure 5-2. The results of the respective ANOVA analyses are shown in Tables 5-2 through 5-4; the four fiber types were placed into more generalized groups, steel fiber and synthetic fiber. There were differences in the days of curing dependence based on the type of cement and fiber type. However there was no overarching significant difference in the debonding-energy density for all cement types and fiber types.

5.5.1. Steel Fiber Results

Steel fibers achieved a higher debonding-energy density than the synthetic fibers in both the CSA and portland cements, Figures 5-9 and 5-10. Figure 5-11 shows the plot of the ANOVA procedure for debonding-energy density with respect to plain-steel fibers. The plot shows a positive-trending regression profile for the OPC matrix. There is interaction between the two CSA cements and between the OPC and CSA cements. The nearly linear, to positive-trending quadratic profile of the CSAB#4 and the positive-trending profile of the Commercial CSA cements show interaction with the positive-trending portland cement quadratic profile. This highlights statistical significance exists in support of the hypothesis that fibers perform differently in CSA cements than they do in portland cement, particularly based on a linear relationship ($P < 0.0001$). Particularly, statistical significance exists in the interaction between curing time, $\text{Log}(\text{Day})$, and Cement Type ($P < 0.0001$) for debonding-energy density, Table 5-2. Disregarding cement type there exists significance between the day of curing and debonding-energy density ($P = 0.0039$).

Table 5-2. ANOVA results for effect of cement type and levels of days of curing on debonding-energy density for the plain-steel fiber

Source	DF	Type I SS	Mean Square	F Value	Pr > F
c1 (contrast) OPC:CSAB#4	1	1.11008015	1.11008015	1.58	0.2125
Cement	1	49.01451910	49.01451910	65.72	<.0001
Log(Day)	1	6.19069431	6.19069431	8.81	0.0039
Log(Day)*Log(Day)	1	0.06232385	0.06232385	0.09	0.7667
c1*Log(Day)	1	0.40483858	0.40483858	0.58	0.4501
Log(Day)*Cement	1	47.59506216	23.79753108	67.13	<.0001
c1*Log(Day)*Log(Day)	1	0.22811706	0.22811706	0.32	0.5705
Log(Day)*Log(Day)*Cement	1	0.08425079	0.08425079	0.12	0.7301

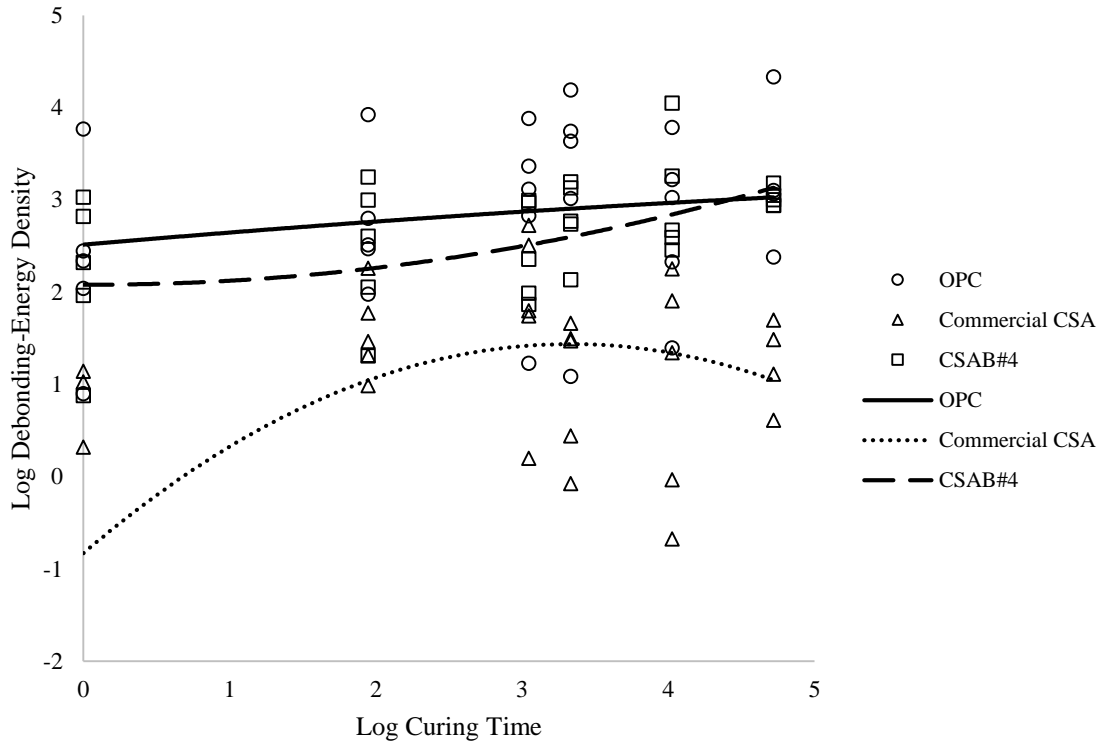


Figure 5-9. Analysis of variance for debonding-energy density for the plain-steel fiber.

Figure 5-10 is a plot of the ANOVA model for coated-steel fibers with debonding-energy density as the dependent variable. The Commercial CSA and CSAB#4 show differing trending quadratic lines with interaction throughout the curing period. The CSAB#4 cement has a negative-trending quadratic line from 1 to 28 days of curing then becoming positive trending out to 112 days of curing. The Commercial CSA and OPC have similar positive-trending profiles from 1 to 56 days of curing before becoming negative trending to 112 days. The trend of the CSAB#4 cement and the opposing trend of the portland cement suggests cement type does have an effect on the debonding-energy density of the coated-steel fiber-matrix system ($P = 0.0253$). Statistical significance exists between linear coefficients with interaction between curing time and cement type ($P = 0.0048$).

Table 5-3. ANOVA results for effect of cement type and levels of days of curing on debonding-energy density for the coated-steel fiber

Source	DF	Type I SS	Mean Square	F Value	Pr > F
c1 (contrast) OPC:CommCSA	1	29.98190363	29.98190363	51.09	<.0001
Cement	1	3.04597086	3.04597086	5.19	0.0253
Log(Day)	1	33.86704118	33.86704118	57.71	<.0001
Log(Day)*Log(Day)	1	7.32800511	7.32800511	12.49	0.0007
c1*Log(Day)	1	3.97697714	3.97697714	6.78	0.0110
Log(Day)*Cement	1	4.92657863	4.92657863	8.39	0.0048
c1*Log(Day)*Log(Day)	1	0.81217665	0.81217665	1.38	0.2429
Log(Day)*Log(Day)*Cement	1	8.34311459	8.34311459	14.22	0.0003

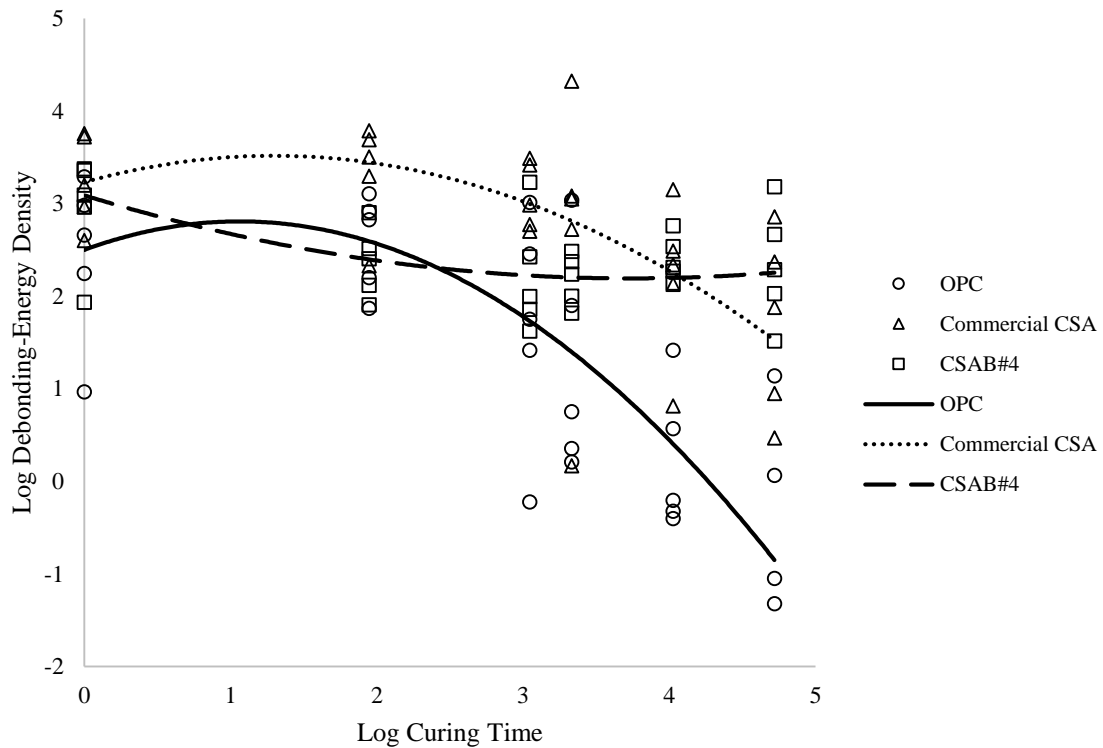


Figure 5-10. Analysis of variance for debonding-energy density for the coated-steel fiber.

5.5.2. Synthetic Fiber Results

The ANOVA test demonstrated statistical difference ($P < 0.0001$) in the debonding-energy density of polypropylene fiber embedded in CSA cements as compared to portland cement, Table 5-4. Figure 5-11 shows a similar decreasing trend in the dependent variable for the CSAB#4 cement and the ordinary portland cement with interaction existing after 1 day of curing. In contrast to the CSAB#4 cement and OPC, the Commercial CSA cement showed significant interaction with OPC by having a positive-trending quadratic profile from 1 to 56 days of curing; before turning negative to 112 days of curing. To examine the statistical significance ($P = 0.0002$) that exists for debonding-energy density in relationship to cement type, disregarding curing time a contrast was set up within the GLM statement between OPC and CSA cements. Contrast variables may be used to analyze trends over time and to make comparisons between times in repeated measures data; for this study between OPC and CSA cements (Littelle et al., 1998). The results of the contrast may be seen in Table 5, which shows significance ($P = 0.0146$); so the debonding-energy density shows significant difference based on cement type.

Table 5-4. ANOVA results for effect of cement type and levels of days of curing on debonding-energy density for the polypropylene fiber

Source	DF	Type I SS	Mean Square	F Value	Pr > F
c1 (contrast) OPC:CommCSA	1	11.06456813	11.06456813	6.22	0.0146
Cement	1	27.64209779	27.64209779	15.54	0.0002
Log(Day)	1	2.70307289	2.70307289	1.52	0.2212
Log(Day)*Log(Day)	1	4.59251827	4.59251827	2.58	0.1119
c1*Log(Day)	1	3.87909427	3.87909427	2.18	0.1436
Log(Day)*Cement	1	0.7223435	0.72234359	0.41	0.5257
c1*Log(Day)*Log(Day)	1	1.59682577	1.59682577	0.90	0.3461
Log(Day)*Log(Day)*Cement	1	1.40701304	1.40701304	0.79	0.3764

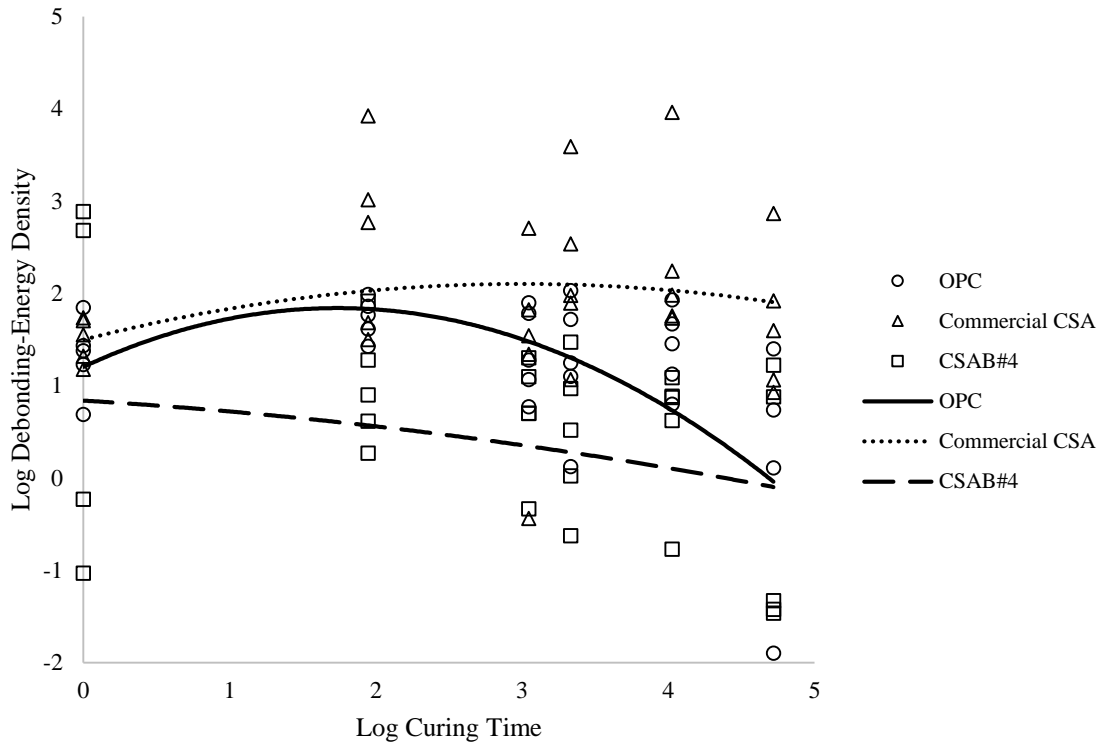


Figure 5-11. Analysis of variance for debonding-energy density for the polypropylene fiber.

The trends of the debonding-energy density of the PVA fiber shows different sloping regression trends up to 21 days of curing (Figure 5-12). The quadratic regression lines for OPC and the Commercial CSA appear similar while the regression line for CSAB#4 has a more linear trend. However significance does exist between the quadratic regression lines ($P = 0.0570$), suggesting the PVA fiber does perform differently in each cement type and demonstrates dependence on the day of curing (Table 5-5). Regardless of cement type the day of curing is significant ($P < 0.0001$) on the debonding-energy

density. Cement type is also statistically significant ($P < 0.0001$), disregarding days of curing.

Table 5-5. ANOVA results for effect of cement type and levels of days of curing on debonding-energy density for the polyvinyl-alcohol fiber

Source	DF	Type I SS	Mean Square	F Value	Pr > F
c1 (contrast) OPC:CommCSA	1	5.67705488	5.67705488	4.37	0.0398
Cement	1	0.39519155	0.39519155	0.30	0.5829
Log(Day)	1	89.10047515	89.10047515	68.56	<.0001
Log(Day)*Log(Day)	1	18.83660142	18.83660142	14.49	0.0003
c1*Log(Day)	1	0.68542558	0.68542558	0.53	0.4698
Log(Day)*Cement	1	10.43431886	10.43431886	8.03	0.0058
c1*Log(Day)*Log(Day)	1	1.55494458	1.55494458	1.20	0.2773
Log(Day)*Log(Day)*Cement	1	4.84663172	4.84663172	3.73	0.0570

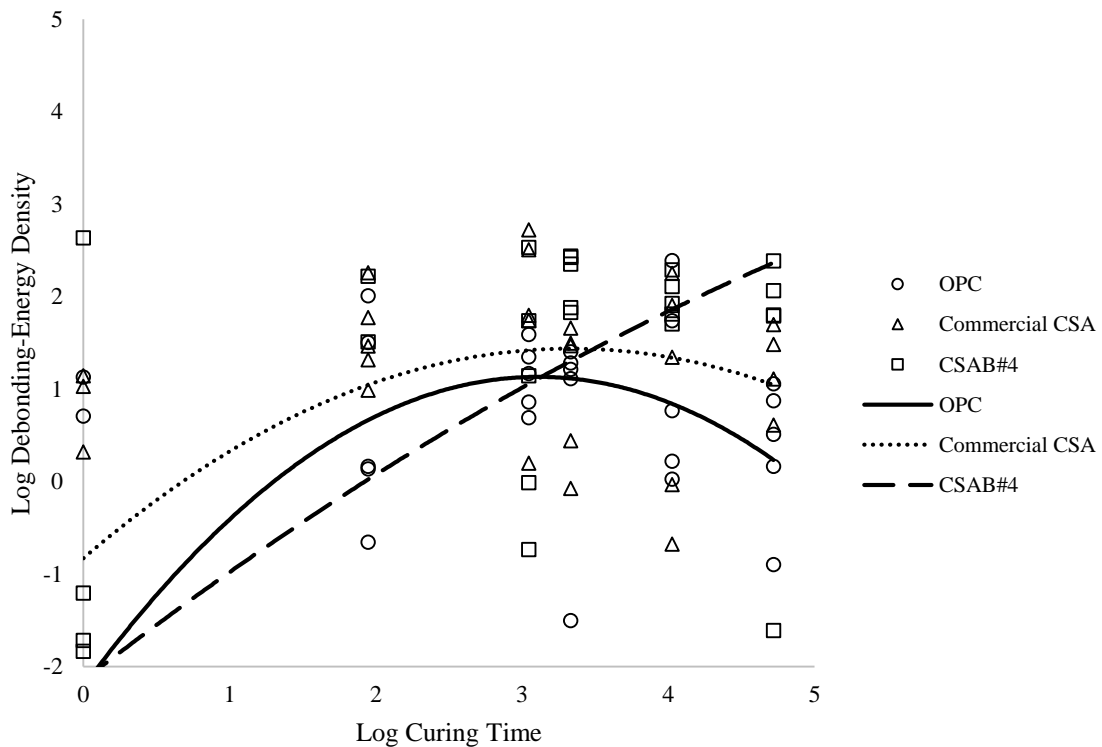


Figure 5-12. Analysis of variance for debonding-energy density for the polyvinyl-alcohol fiber.

5.6. Conclusion

ANOVA results for debonding-energy density shows statistical significance in support of the hypothesis that fibers perform differently in calcium sulfoaluminate cement as compared to ordinary portland cement.

In this paper, the interfacial parameters of three fiber types and three different types of cement were examined. The fiber-matrix bond performance was evaluated by analysis of the debonding-energy density and fiber-bridging stress utilizing the single-fiber pullout test to quantify peak load and corresponding displacement.

An important factor contributing to the bond strength between fiber and matrix was the ability to transfer interfacial stress from fiber to matrix. The more rigid-dense morphology of the CSA cement paste due to the ettringite crystal structure yielded higher debonding-energy densities and fiber-bridging stresses for both steel and synthetic fibers; with the exception of plain-steel fibers in the commercially available CSA cement, in which there was a reduction in the debonding-energy density (Montgomery 1998). The morphology of the C-S-H in the OPC matrix provided good bonding, though lacked the strength and dense-structure found with ettringite in the CSA matrixes.

In summary, fibers embedded in CSA cement show a higher debonding-energy density than fibers embedded in OPC. The increase in debonding-energy density is attributed to the strength of ettringite and the associated morphology from the growth of the acicular crystals. Therefore the combination of a stiffer matrix and the crack arresting ability of fibers, the energy required for crack propagation was increased, as seen by the increase in debonding-energy density. Steel fibers more readily attained debonding-energy density

energy than synthetic fibers in both CSA cement and OPC; due to the high modulus of the fiber which is able to withstand multiple fiber-matrix deformations by redirecting the stresses back into the matrix. The synthetic fibers achieved good debonding-energy densities. Steel fibers are better suited to improve the debonding-energy density at higher peak loads, while the synthetic fibers are best suited to improve debonding-energy density at low peak load events.

CHAPTER 6 : INFLUENCE OF CEMENT TYPE ON FIBER-MATRIX INTERFACE BOND STRENGTH

6.1. Introduction

This chapter presents the results of the interfacial bond strength developed at the interface between reinforcing fibers embedded in a calcium sulfoaluminate (CSA) cement matrix, utilizing the single-fiber pullout.

The stress transfer between fiber and matrix across the interface, under various loading conditions, is a primary factor characterizing fiber composites (Kim and Mai, 1998). The fiber matrix interface, though infinitesimally small, plays a major role in the overall performance of the bulk composite (Li and Grubb, 1994). The properties of the interface are controlled mainly by the chemical and morphological development between fiber and matrix; which determines the overall compatibility, and mechanical behavior, of the two materials (Stang et al., 1990; Kim and Mai, 1998). Fiber composites are targeted at creating a reinforced cementitious material that can sustain large compressive and flexural loads and exhibit increased toughness. The load-bearing capability of a cementitious-fiber composite depends on how well the stress is transferred, which is primarily controlled by the bonding characteristics at the interfacial transition zone (Kim and Mai, 1998). As cementitious matrices continue to be engineered to perform at ultrahigh compressive and flexural strengths an underlying need for the characterization of how these enhanced systems interact with reinforcing fibers becomes more prevalent. High-strength cementitious systems are brittle and exhibit low-energy absorption or toughness as a result of their inability to sustain deformation and crack resistance. The

following research intends to illustrate how the fiber-matrix composite is influenced from the utilization of high-strength cementitious systems, specifically calcium sulfoaluminate cements; as compared to lower-strength portland cement systems. Moreover, there is a need to better understand the pullout process and the energy absorbing mechanisms associated with increased toughness in composites. This paper will evaluate the contribution of the interface bond strength on the fiber pullout resistance.

The mechanical properties of a composite are defined by several parameters including the fiber and matrix elastic modulus and tensile strength, fiber embedment length, aspect ratio, volume fraction, fiber orientation, the surface roughness of the fiber (which influences the interface with the matrix) and the interfacial bond strength. In addition to strength another important factor is the ability for a fiber composite to dissipate fracture-induced energy. A measure of this energy is referred to as the work of fracture, also known as fracture toughness, and can be defined as the energy necessary to create new fractured surface area (Kim and Mai, 1991). Generally, fiber composites will take on additional loads after the first cracking of the matrix if the pull-out resistance of the fibers, at the first crack, is greater than the load at first cracking. This concept of crack-bridging, was first proposed by Marshall and Cox (1988) and is used to link the interfacial bond and composite failure behavior (Marshall et al., 1985; Marshall and Cox, 1988; Li et al., 1997). Resistance to fiber debonding and pullout is primarily a function of the fiber-matrix interface bond shear strength and the interface bond area (Gray, 1984).

To fully understand the performance of the entire composite, the contribution of each component must be evaluated. This may be accomplished by analyzing the pullout behavior of a single fiber embedded in a cementitious matrix. The contribution of the interfacial bond between a single-reinforcing fiber and surrounding cement matrix, may seem inconsequential to the overall performance of a fiber-reinforced composite. However, that infinitesimally small transition zone is what governs the ultimate stress and toughness of a composite when considering the volume of fibers present. The microstructural development within the interfacial transition zone (ITZ) is governed by cement hydration and hardening of the bonding system which defines the mechanical properties of the fiber-matrix composite (Janotka et al., 2003).

A popular interface characterization test is the single-fiber pullout test (Takaku and Arridge, 1973; Gray, 1984; Li and Grubb, 1994; Nairn et al., 2001). In the single-fiber pullout test, an elastic fiber is embedded in an elastic cementitious matrix and pulled out while the matrix is held in place (Figure 6-1). The maximum applied force, P_{max} , required to debond the fiber is typically recorded as a function of time and displacement; additionally, in this study it will also be related to curing time.

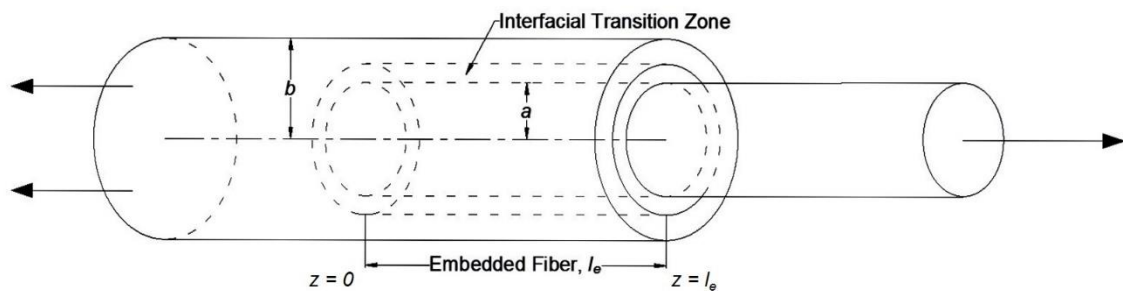


Figure 6-1. Fiber pullout specimen.

Fiber-reinforced composites (FRC) resist tensile forces through a composite action, whereby part of the tensile force is resisted by the matrix, while the balance is taken by the fibers (Naaman et al., 1991). The transmission of forces between the fiber and the matrix is achieved through bond defined as the shearing stress at the interface between the fiber and the surrounding matrix (Naaman et al., 1991; Subramani and Gaurav, 2012). It is generally agreed that the fiber contribution to increasing the toughness of the composite is primarily dictated by the mechanisms of fiber pullout (Naaman et al., 1991). Toughness of a fiber-matrix composite refers to the work dissipated, or the total energy absorbed prior to complete failure; or the critical potential energy release rate of a composite specimen with a unit mJ (Brown et al., 2002).

The cement-fiber interfacial bond results from some combination of mechanical interlocking of cement hydration products with the fiber surface and chemical reaction between fiber and cement paste within the interstitial transition zone (Kim and Mai, 1998; Brown et al., 2002). In fiber reinforced composite materials, the principal factor governing load transfer from the matrix to the fiber is the shear strength of the interfacial bond between the two components (Naaman et al., 1991). Fractured specimens of fiber-reinforced concrete shows that failure takes place primarily due to fiber pullout or debonding. Generally fiber pullout rather than rupture confers a larger ductility to the fiber reinforced composites (Li and Stang, 1997; Lin and Li, 1997). Ideally composites will exhibit strain-hardening behavior achieved through multiple cracking of the reinforced matrix. Unlike plain concrete, a fiber-reinforced concrete specimen does not break immediately after initiation of the first crack. This has the effect of increasing the work of fracture, or toughness.

The length and volume of fibers present in a concrete mix are critical in controlling the flexural strength and toughness of the hardened concrete, including the prevention of crack propagation. If the pullout resistance of the fibers is great enough when a crack develops in the matrix, the composite will sustain greater external loading. Within the cracked section, the matrix does not resist any tension and the fibers carry the entire load taken by the composite. Bond stresses between the fiber and matrix provide a pathway for additional stresses, from increasing loads on the composite, to pass from the fiber back to the matrix. If these bond stresses do not exceed the bond strength, then the developing energy may be released through additional matrix cracking. This process of multiple cracking will continue until either the fibers fail or the accumulated local debonding will lead to fiber pullout (Shah, 1991; Mehta and Monteiro, 2006).

6.2. Research Significance – Chapter 6

There is increasing interest in researching and utilizing UHPC as a means to lessen or eliminate the need for reinforcing steel in the construction process. As cementitious matrices continue to be engineered to perform at ultrahigh compressive and flexural strengths there is an underlying need for the characterization of how these enhanced systems interact with reinforcing fibers. High-strength cementitious systems are brittle and exhibit low-energy absorption or toughness as a result of their inability to sustain deformation and crack resistance. This study intends to illustrate how the fiber-matrix composite is influenced from the utilization of high-strength cementitious systems, specifically calcium sulfoaluminate cements. As compared to lower-strength systems, like that of an ordinary portland cement. Moreover, there is a need to understand better

the pullout process and the energy absorbing mechanisms associated with increased toughness in composites.

The most crucial link between the properties of fiber, matrix and fiber-matrix interface and that of a composite is the crack bridging stress-crack opening relation. This relation defines the ultimate stress and strain of a uniaxial tensile stress-strain curve and the energy consumption due to fiber bridging, which in turn control the strength, ductility and fracture toughness of a structural member (Lin and Li, 1997).

Therefore this paper presents the evaluation of the fiber-matrix interface by quantifying the bond stress and thereby determining the toughness based on the strength and energy criterion. Experimentally this was accomplished by fiber pullout in a CSA cement, and portland cement matrix in context of material design under the guidance of micro-mechanical tools. Specifically this study illustrates how the bond within the fiber-matrix interface is governed by the use of material selection particularly the use of sulfate-based cements when compared to silicate-based cements. The overarching goal is to provide some guidance in properly selecting a combination of fiber and matrix to achieve an effective interface in controlling damage in composites and enhancing the tolerance prior to failure.

6.3. Experimental Program

The single-fiber pullout test was conducted to investigate the fiber-matrix bond stress with respect to curing time. The major parameter investigated was the cement type and if there was any significant influence on pullout resistance with varying types of reinforcing

fiber. The significance of cement-fiber combinations was determined with an analysis of variance using SAS 9.4.

6.4. Experimental Results and Discussion

The influence of fiber and cement type on the interfacial shear stress was determined from the analysis of load-deflection curves. The primary binder in CSA-cement systems differ greatly from that in OPC systems, both chemically and physically. To evaluate the influence of these different binders on the bond between cement and fiber the shear stress was quantified and analyzed for statistically significant interactions with fiber type, cement type and days of curing. The effect of cement and fiber type on the ability to achieve maximum toughness a composite must exhibit high strength and ductility.

6.4.1. Influence of Hydrated Cement Morphology

The interfacial transition zone (ITZ) between the cement matrix and fiber plays a crucial role in governing the performance of the fiber-matrix composite. The bond developed in the ITZ between the fiber and matrix is strongly influenced on the nanostructure and microstructure of the hydrated cement (Janotka et al., 2003). The cement paste structure depends on the composition of the original cement grains, the starting water:cement ratio, the temperature of hydration, and the presence of chemical admixtures at the time of hydration (Hannant, 2000). Considering the entire paste structure, there is a wide range of particle sizes and void spaces making each fiber-matrix bond unique. Each fiber-matrix ITZ may be composed of unhydrated cement grains of irregular shape of approximately 10 – 20 μm in size, the space between them filled with less than 1 μm calcium silicate hydrates of complex forms including partly crystalline fibers and sheet-

like networks in which other phases are present like plates of calcium hydroxide, Figure 6-2 (Hannant, 2000).

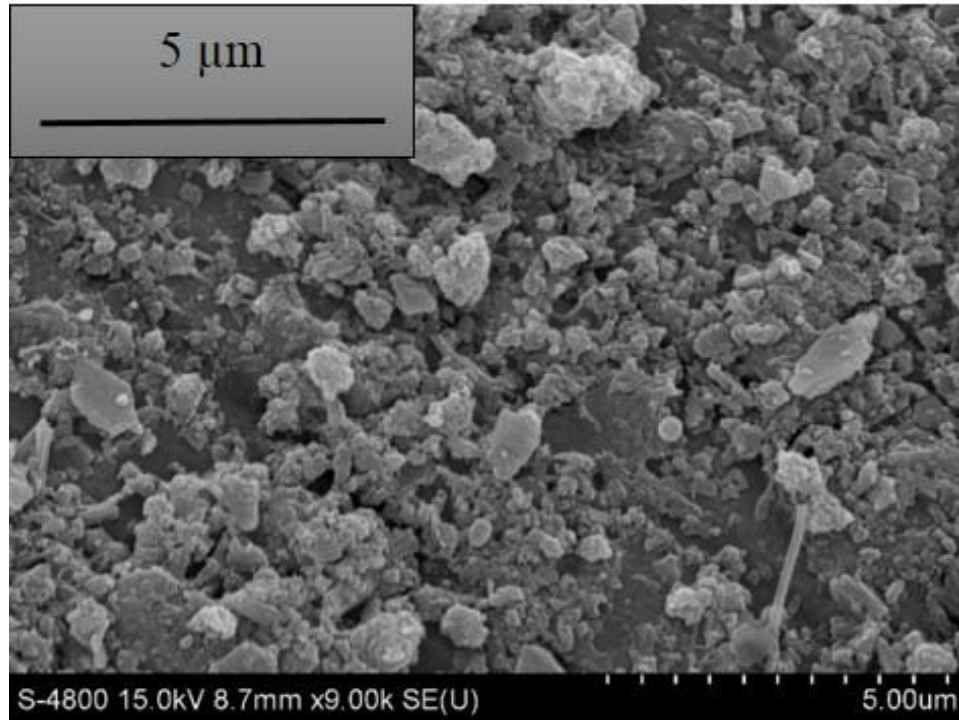


Figure 6-2. SEM image of OPC paste showing irregular structure of CSH phases, magnification is 9000x.

Whereas the CSA fiber-matrix transition zone is composed primarily of ettringite crystals, an acicular crystal with a large aspect ratio, Figure 6-3 (Komatsu et al., 2009). The variation in strength between the Commercial CSA and CSAB#4 cements is likely attributed to the morphology of the ettringite crystal. The ettringite formed within the Commercial CSA matrix are primarily less than 4 microns in length. Whereas the CSAB#4 CSA developed ettringite crystals that are primarily less than 10 microns in length. The larger aspect ratio of the ettringite produced by the CSAB#4 CSA may lead to more brittle crystals and are unable to form as dense of a network as the shorter

crystals in the Commercial CSA. However, improved fiber-matrix bonding was exhibited by the CSAB#4 CSA matrix, as discussed in the next section. A possibility for the increased bond with PVA fibers is attributed to the fiber providing nucleation sites for the crystallization of hydrated cement phases (Cadek et al., 2002; Bin et al., 2006; Naebe et al., 2008).

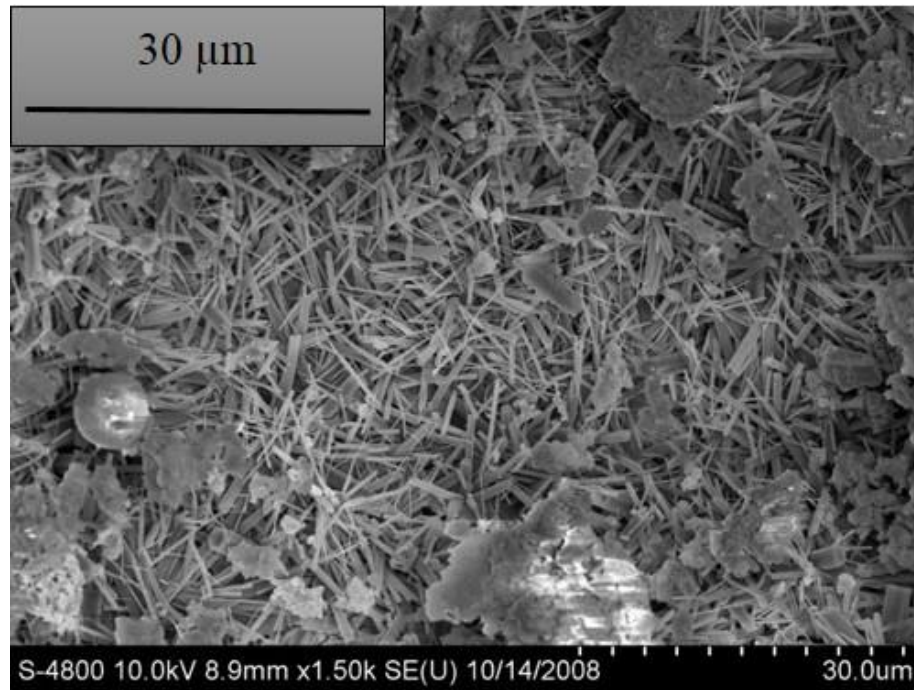


Figure 6-3. SEM image of CSA cement paste showing acicular ettringite structure, magnification is 1500x.

The differences in fiber-matrix bond strength between OPC and CSA cement is likely attributed to the difference in the morphological assemblage of hydrated cement phases within the interfacial transition zone. The resistance to uniaxial pullout forces are focused on these assemblages that populate the ITZ.

6.4.2. Interface Shear Strength

The cement-fiber interfacial bond results from some combination of mechanical interlocking of cement hydration products with the fiber surface and chemical reaction between fiber and cement paste within the interfacial transition zone (Kim and Mai, 1998; Brown et al., 2002). In fiber reinforced composite materials, the principal factor governing load transfer from the matrix to the fiber is the shear strength of the interfacial bond between the two components. Broken specimens of fiber-reinforced concrete shows that failure takes place primarily due to fiber pullout or debonding. Generally fiber pullout rather than rupture suggests a larger ductility to the fiber reinforced composites, which translates to greater toughness (Li and Stang, 1997; Lin and Li, 1997).

Uniform shear bond strength between the fiber and surrounding matrix is often assumed in FRC models and the bond strength from pullout tests is frequently reported in terms of the average value over the embedded fiber surface area (Pan, 1993; Kim and Mai, 1998; Johnston, 2001; Nairn et al., 2001; Mehta and Monteiro, 2006; Subramani and Gaurav, 2012). Additionally many researchers, including Greszczuk (1969), have developed models on the relationship between fiber-matrix interfacial shear stress and embedded fiber length using the assumptions of the shear-lag theory, i.e. assuming that the axial stresses in the matrix are negligible relative to those in the fiber and that the shear stresses in the fiber are small compared to those in the matrix (Greszczuk, 1969). One conclusion from these models allows for the assumption that complete fiber-matrix debonding takes place when the maximum interfacial shear stress is equal to the maximum interfacial bond shear strength. The interfacial shear strength, τ_f , can be calculated from fiber pullout experiments using:

$$(6-1) \quad \tau_f = \frac{P_{max}}{2\pi r_f l_e}$$

Where r_f is the fiber radius and l_e is the embedded fiber length. Physically this term is the average interfacial shear stress at the time of failure (Gray, 1984; Kim et al., 2007). By utilizing the shear-lag theory an analysis of the stress transfer from the fiber to the matrix may be used to evaluate the toughening due to fiber bridging during fiber pullout (Hsueh, 1988; Kim and Mai, 1998). The shear-lag model was first considered by Cox (1952) where an elastic fiber is embedded in an elastic matrix which is subjected to uniaxial tension (Cox, 1952). However early models assumed perfect bonding at the interface between the fiber and matrix, of a fully embedded fiber in a matrix, and the Poisson contraction in the lateral direction is the same in the fiber and matrix. More recent variations of Cox's shear-lag model (Kim and Mai, 1991; Naaman et al., 1991; Zhou et al., 1993) are similar however they take into account the fiber end, which is exposed and is subjected to external tensile stress in the fiber pullout test (Kim and Mai, 1991; Naaman et al., 1991; Zhou et al., 1993). Newer models consider the effect of fiber-axial stress and interface shear stress throughout the length of the embedded fiber, which takes into account the effects of differing Poisson ratios between fiber and matrix. While the bridging stress in the fibers contribute to the toughening of the composite, it's the relative displacements in the loading direction of the fiber-matrix interface that are necessary for the crack-opening displacement. Therefore debonding at the fiber-matrix interface during fiber pullout and additionally frictional sliding between the fiber and matrix are essential to characterizing the toughness of the composite.

When an axial load is placed on the fiber the induced stress is transferred from the fiber to the adjacent matrix by means of the interfacial shear stress. As described by Hsueh

(1990), the load-displacement curve initially shows a linear relationship corresponding to the elastic loading of the composite with a bonded interface (Hsueh, 1990). The linear relationship terminates where an initial debonding stress at the fiber-matrix interface occurs. After this point the interface stress increases with increasing debond length. The debond stress reaches a maximum where complete debonding occurs along the full length of the embedded fiber. After the maximum stress is reached fiber pullout initiates with the stress continuously decreasing to zero until the fiber is completely pulled from the matrix. An example load-displacement curve, from the single-fiber pullout test, is shown in Figure 6-4.

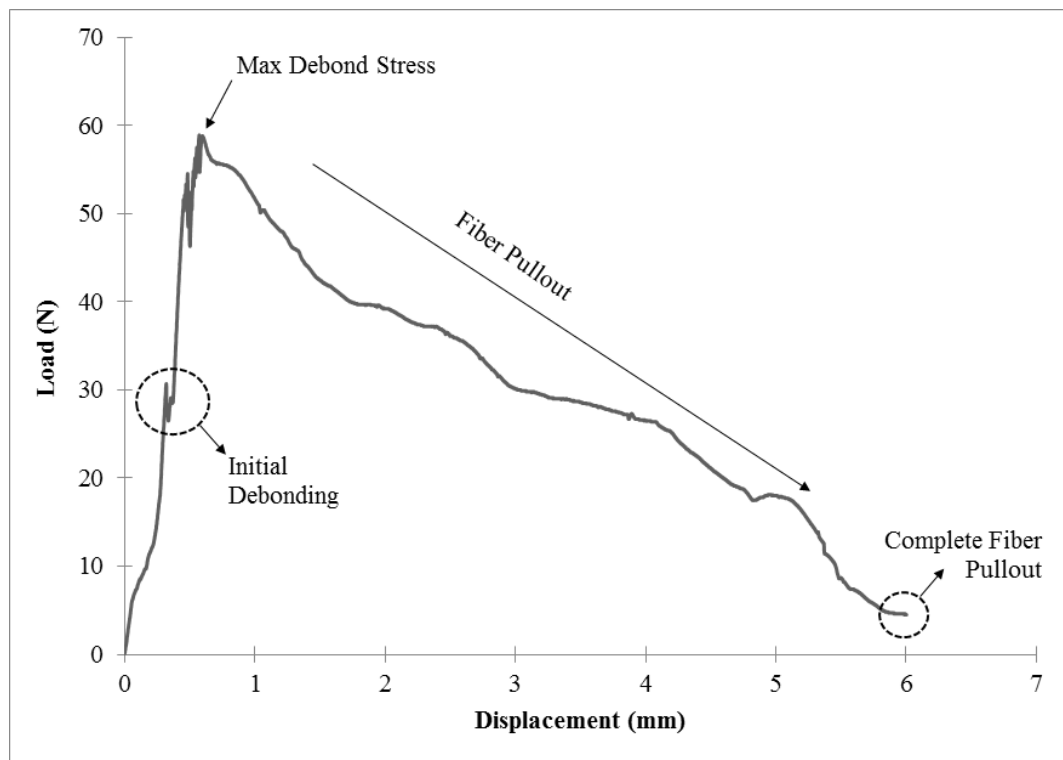


Figure 6-4. Representative load-displacement highlighting key points in the fiber pullout process.

6.4.3. Shear-Bond Stress

Composites made with brittle fibers, i.e. steel, and brittle matrices, i.e. CSA cement, can exhibit high toughness when failure occurs preferentially along the fiber-matrix interface before fibers fracture. Important toughening mechanisms are a direct result of the interface-related shear failure which gives rise to an improved energy absorption through fiber pullout (Stang et al., 1990; Li and Stang, 1997; Hsueh and Becher, 1998). A good shear bond will contribute to direct cracks longitudinally along the fiber maximizing the contribution of the fiber to preventing further crack propagation; thus promoting improved energy toughness. Fiber pullout relies on mode II (i.e. shear) debonding at the fiber-matrix interface which can be analyzed using a strength-based approach, or stress criterion (Stang et al., 1990; Hsueh and Becher, 1998). This approach occurs when the maximum interface shear stress from loading equals the interface shear strength, τ_f ; which assumes that debonding will initiate at this stress level. A review of fiber pullout theories, by Gray (1984) identified that the majority of papers concerning fiber pullout in cementitious systems used the stress criterion theory (Gray, 1984). The alternative approach is to use an energy-based approach through fracture mechanics.

On each of the testing days (1, 7, 21, 28, 56 and 112) there was a relationship between the E_f/E_m ratio and shear bond stress Figures 6-5, 6-6, 6-7 and 6-8. A decrease in E_f/E_m ratio was associated with an increase in shear-bond stress. The shear stresses in the fiber increase with the decrease in the E_f/E_m ratio over time. As the elastic modulus of the matrix increases with curing time the E_f/E_m ratio decreases Table 6-1. Therefore as the matrix strengthens over time the composite becomes more effective in load transfer from

the fiber to the matrix when the fiber is stressed. The Commercial CSA and CSAB#4 CSA matrices followed a similar trend in each figure. However there was a distinguishable difference in trends between the OPC matrix and CSA matrices, for both the E_f/E_m ratio and shear bond strength. The steel fibers achieved much greater shear bond strengths than the synthetic fibers, throughout the range of curing time. After 112 days of curing the steel fibers reached approximately 25 – 35 MPa in the CSA cement and 12 – 19 MPa in OPC (Figure 6-5 and Figure 6-6). While the synthetic fibers reached approximately 1.5 – 3.0 MPa in the CSA cement and 1.2 – 2.0 MPa in OPC (Figure 6-7 and Figure 6-8).

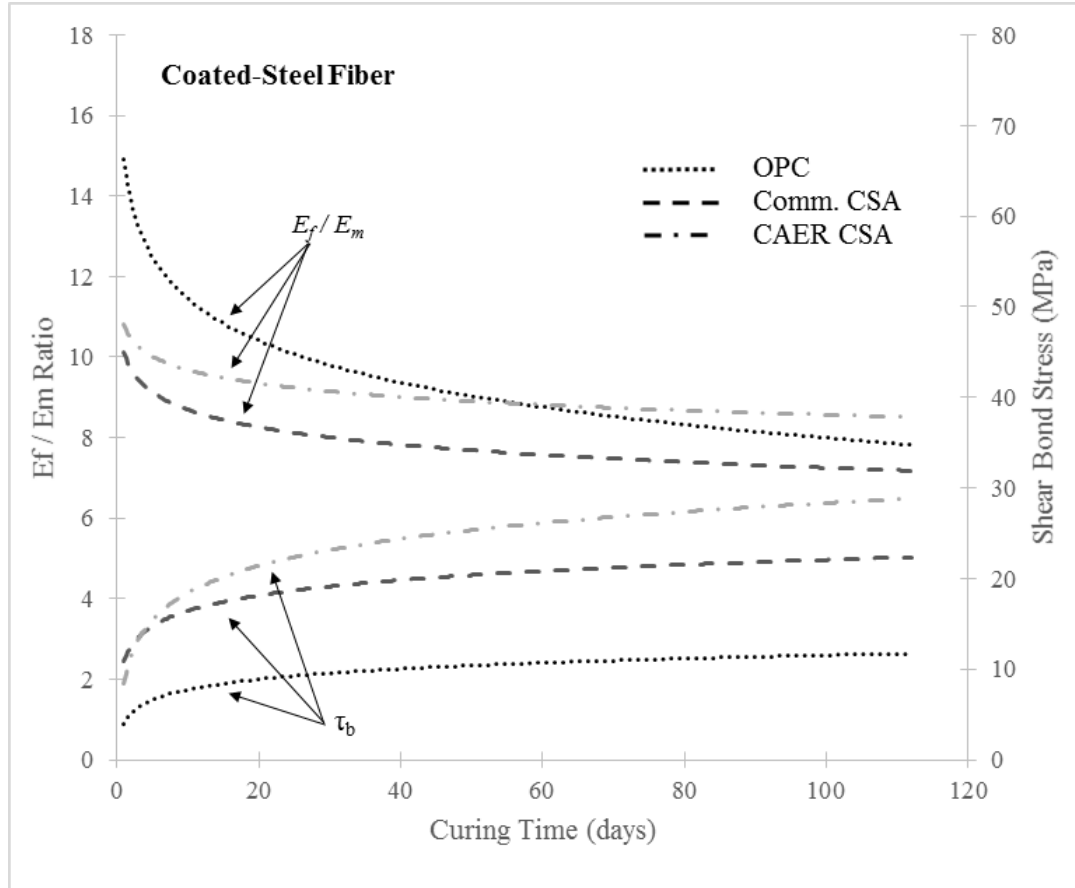


Figure 6-5. Relationship between E_f / E_m ratio and shear-bond stress of coated-steel fibers.

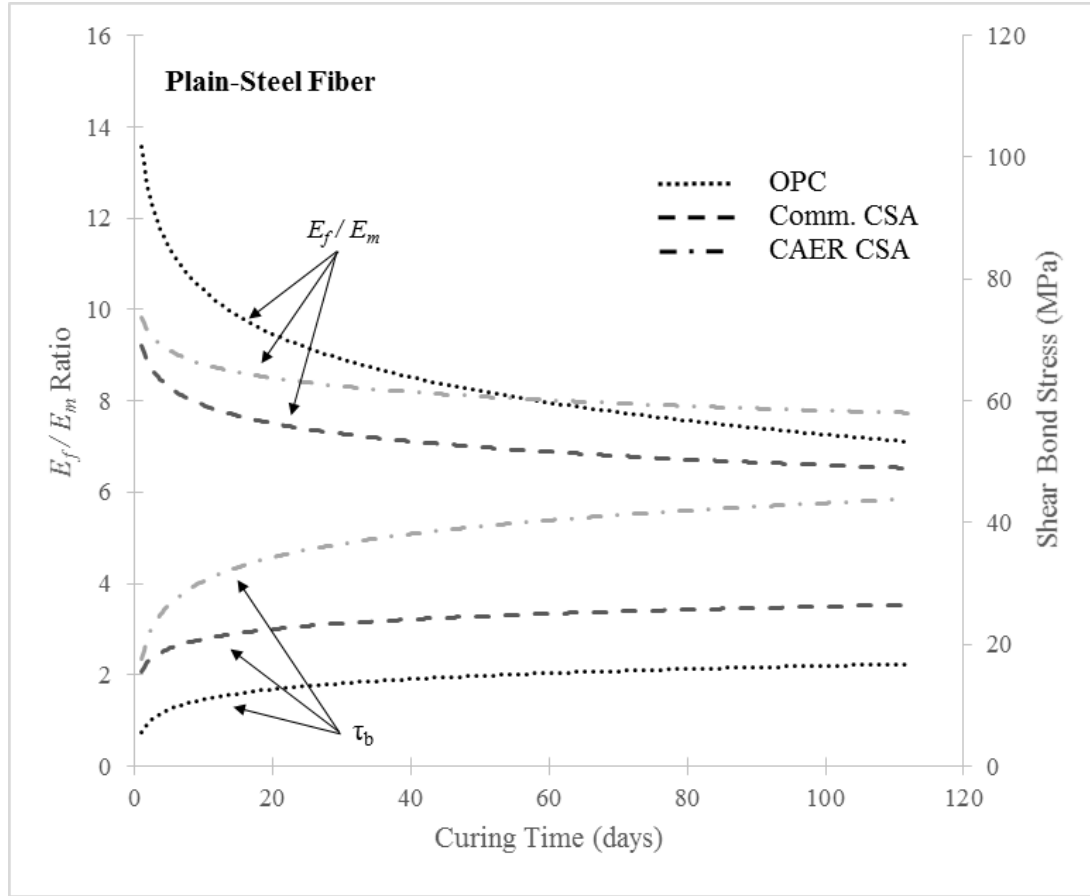


Figure 6-6. Relationship between E_f/E_m ratio and shear-bond stress of plain-steel fibers.

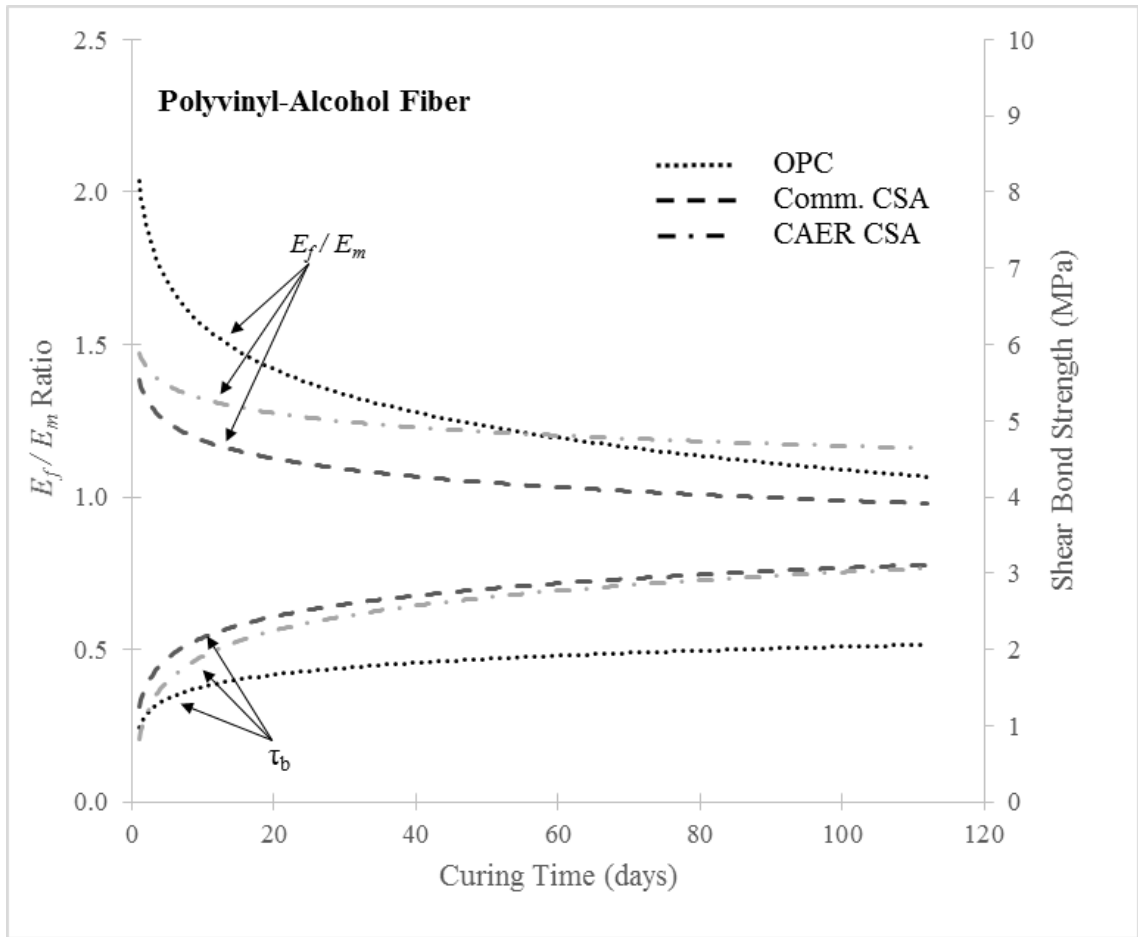


Figure 6-7. Relationship between E_f/E_m ratio and shear-bond stress of PVA fibers.

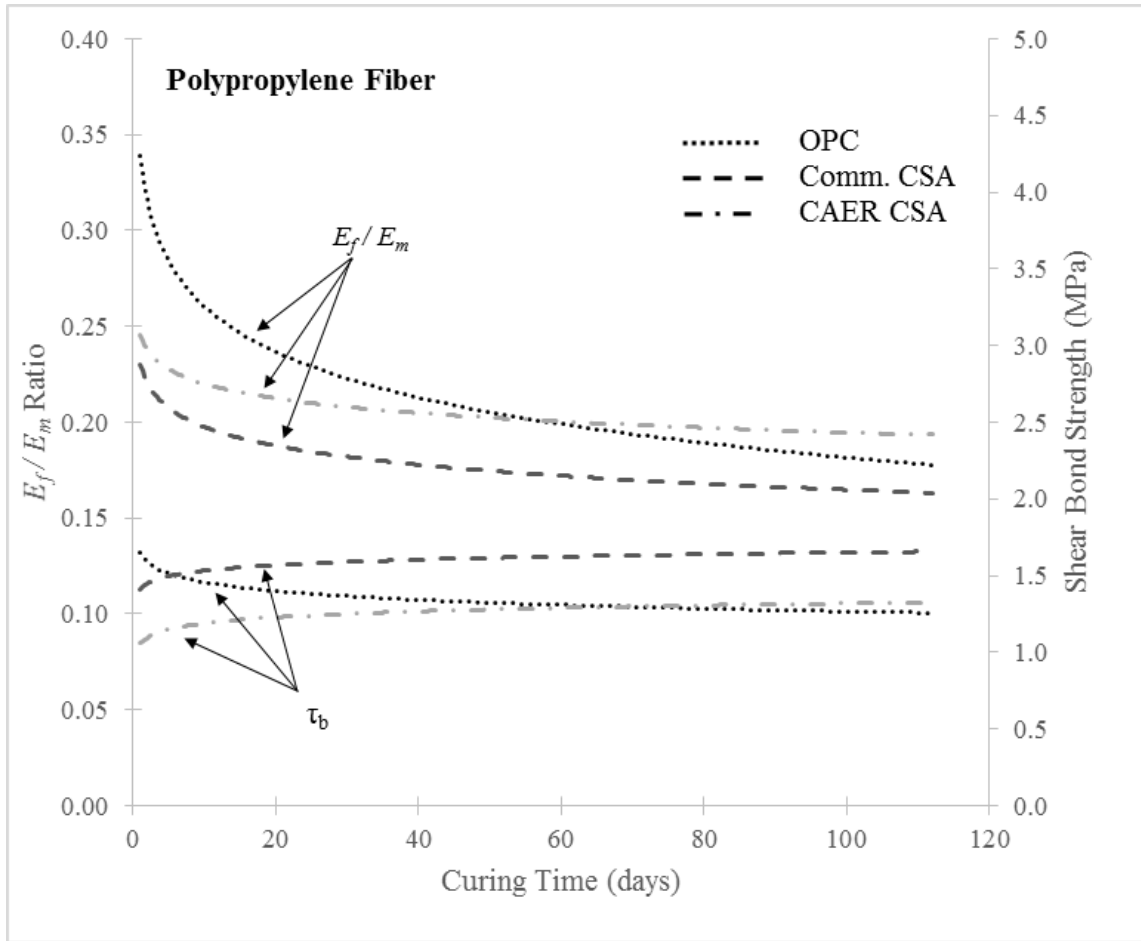


Figure 6-8. Relationship between E_f/E_m ratio and shear-bond stress of PP fibers.

Table 6-1. Matrix strength and elastic modulus results

Days	OPC		Commercial CSA		CAER CSA	
	Strength (MPa)	Modulus (GPa)	Strength (MPa)	Modulus (GPa)	Strength (MPa)	Modulus (GPa)
1	14.33	13.82	34.26	21.36	31.36	20.44
7	30.64	20.20	46.04	24.77	37.05	22.22
21	39.10	22.82	55.70	27.24	41.62	23.55
28	41.54	23.53	59.18	28.08	43.04	23.95
56	42.56	23.81	65.28	29.49	45.94	24.74
112	46.94	25.01	63.30	29.04	50.99	26.06
224	48.00	25.29	67.63	30.02	52.00	26.32

6.4.4. Axial-Bond Stresses

Researchers evaluating the mechanical behavior of fiber-reinforced composites have concluded that the optimal conditions for toughening of composites require debonding at the fiber-matrix interfaces during fiber pullout, and frictional sliding between the fibers and the matrix (Evans and McMeeking, 1986; Becher et al., 1988; Hsueh, 1990). During fiber pullout, interfacial debonding begins at the intersection of the fiber and matrix, where the interfacial shear stress is a maximum (Hsueh, 1990). To determine the effect of bond forces between the fiber and matrix, in addition to the bond stress related to the pullout force, the axial stress distribution σ_f in the fiber and the related interfacial shear stress distribution τ_i are evaluated. The model equations for the axial stress distributions were obtained from Hsueh (1990).

$$(6-2) \quad \sigma_f = \frac{a^2 E_f \sigma_0}{a^2 E_f + (b^2 - a^2) E_m} \left[1 + \left(\frac{b^2}{a^2} - 1 \right) \frac{E_m}{E_f} \frac{\exp(\alpha z) - \exp(-\alpha z)}{\exp(\alpha l_e) - \exp(-\alpha l_e)} + \frac{\exp\{-\alpha(l_e - z)\} - \exp\{\alpha(l_e - z)\}}{\exp(\alpha l_e) - \exp(-\alpha l_e)} \right]$$

$$(6-3) \quad \tau_i = -\sigma_0 \left(\frac{\left[\left(\frac{b^2}{a^2} - 1 \right) \frac{E_m}{E_f} \frac{\exp(\alpha z) - \exp(-\alpha z)}{\exp(\alpha l_e) - \exp(-\alpha l_e)} + \frac{\exp\{-\alpha(l_e - z)\} - \exp\{\alpha(l_e - z)\}}{\exp(\alpha l_e) - \exp(-\alpha l_e)} \right]}{\frac{2}{a} \left[(1 + \nu_m) \left\{ 1 + \left(\frac{b^2}{a^2} - 1 \right) \frac{E_m}{E_f} \right\} \left\{ b^2 \ln\left(\frac{b}{a}\right) - \frac{b^2 - a^2}{2} \right\} \right]^{1/2}} \right)$$

σ_0 is the stress related to the maximum load applied at the surface ($z = l_e$), E and ν are Young's modulus and Poisson's ratio respectively and the subscripts f and m are for the fiber and matrix respectively. The coefficient α is defined in the following equation:

$$(6-4) \quad \alpha = \frac{1}{a} \left[\frac{a^2 E_f + (b^2 - a^2) E_m}{E_f (1 + \nu_m) \left\{ b^2 \ln(b/a) - (b^2 - a^2)/2 \right\}} \right]^{1/2}$$

The normalized axial stresses along the fiber are shown in Figure 6-9 and Figure 6-10 at different ratios of E_f/E_m , see Table 6-2, for coated-steel fibers embedded in an OPC paste. Both Figure 6-9 and Figure 6-10 contain a smaller embedded chart representing a highlighted section of the larger chart; providing greater detail. The axial bond and shear stresses in the fiber decrease with the decrease in the E_f/E_m ratio. This indicates that low ratios of E_f/E_m are more effective in load transfer from the fiber to the matrix when the fiber is loaded; which is agreement with the findings of Hsueh (1988 and 1990). The same trend was demonstrated by the higher elastic modulus CSA cement matrixes. A maximum value for the interfacial shear stress is at the surface, $z = l_e$, where the fiber enters the matrix. As can be seen in Figure 6-10, the intersection between the fiber and surface of the paste plug is indicated on the normalized x-axis as $z/a = 10$. Figure 6-11 demonstrates the axial-stress trends demonstrated in Figures 6-9 and 6-10 (for coated-steel fibers in OPC); however, additionally, the scope was expanded to include plain-steel, PVA and PP fibers in OPC and CSA cement.

After initial debonding (Figure 6-4) frictional sliding occurs at the debonded interface. On the assumption of Coulomb friction at the debonded interface, the interfacial frictional stress results from the radial compressive stress at the interface (Hsueh, 1990). Researchers have identified two sources of the radial stress at the fiber-matrix interface; a net residual compressive stress as a result of differential shrinkage between the fiber and surrounding composite and the stress due to Poisson's contraction of the fiber in the radial direction when the fiber is subjected to an axial tensile stress (Hsueh, 1990; Subramani and Gaurav, 2012).

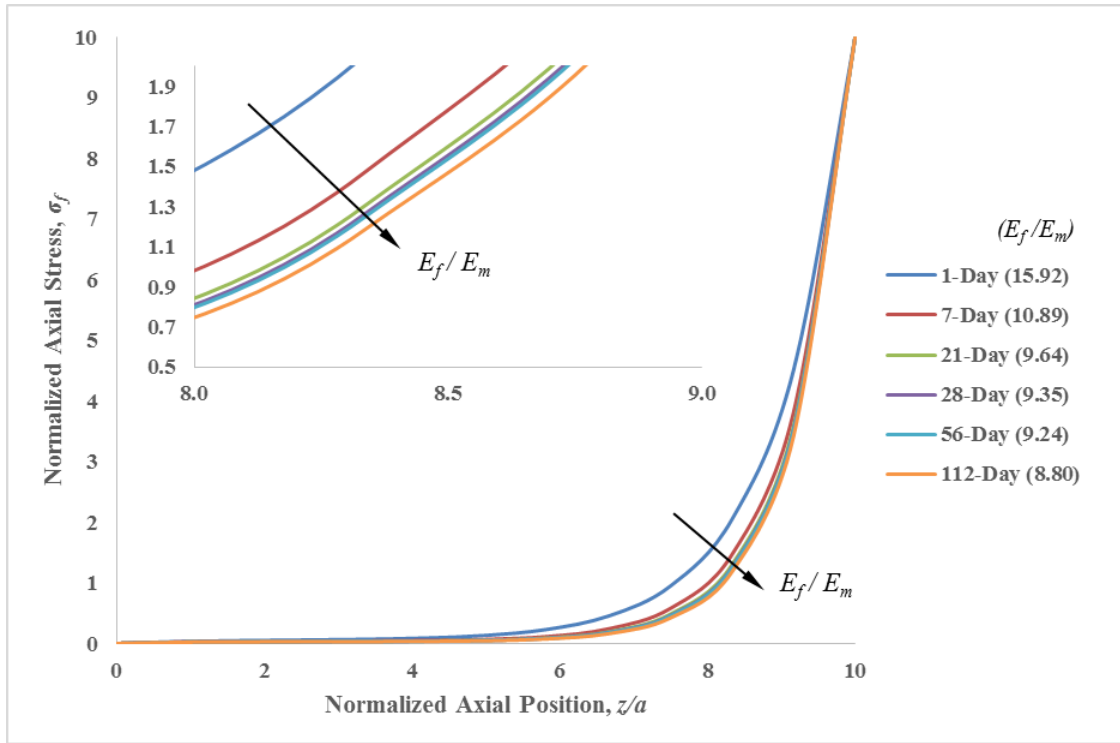


Figure 6-9. Normalized axial stress as a function of normalized axial position for the Coated-Steel Fiber in OPC at different E_f/E_m ratios.

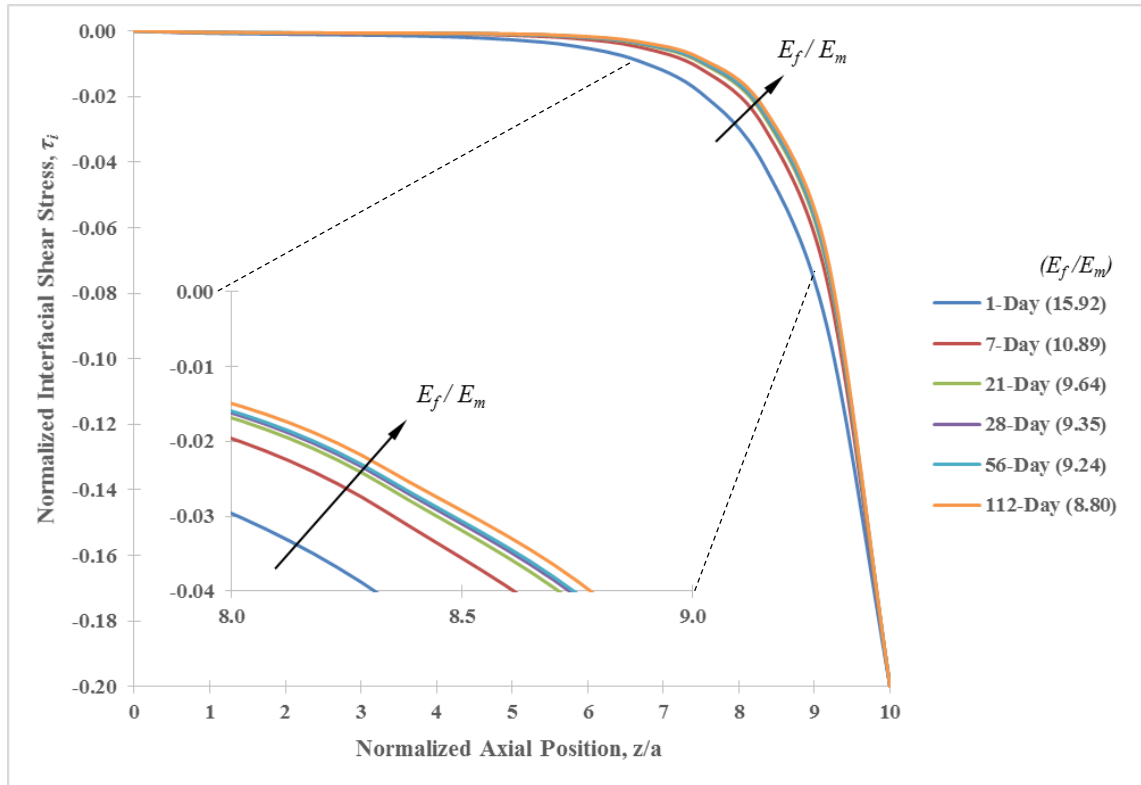


Figure 6-10. Normalized interfacial shear stress as a function of normalized axial position for the Coated-Steel Fiber in OPC at different E_f/E_m ratios.

Table 6-2. E_f/E_m ratios

Day	OPC				Commercial CSA				CAER CSA			
	Coated Steel	Plain Steel	PVA	PP	Coated Steel	Plain Steel	PVA	PP	Coated Steel	Plain Steel	PVA	PP
1	15.92	14.47	2.17	0.36	10.30	9.36	1.40	0.23	10.76	9.78	1.47	0.24
7	10.89	9.90	1.48	0.25	8.88	8.08	1.21	0.20	9.90	9.00	1.35	0.23
21	9.64	8.76	1.31	0.22	8.08	7.34	1.10	0.18	9.34	8.49	1.27	0.21
28	9.35	8.50	1.28	0.21	7.84	7.12	1.07	0.18	9.19	8.35	1.25	0.20
56	9.24	8.40	1.26	0.21	7.46	6.78	1.02	0.17	8.89	8.08	1.21	0.20
112	8.80	8.00	1.20	0.20	7.58	6.89	1.03	0.17	8.44	7.67	1.15	0.19

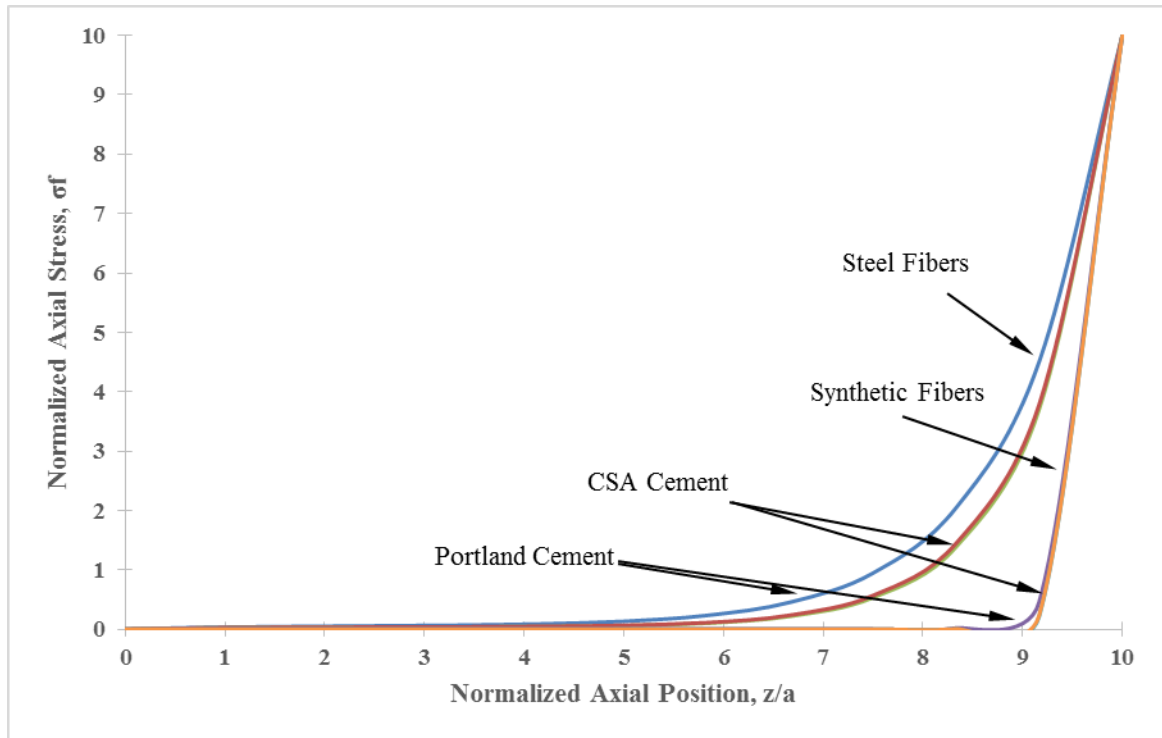


Figure 6-11. Influence of cement and fiber type on fiber-matrix axial stresses.

6.4.5. Influence of Interface Stresses on Composite Toughness

The toughness of a fiber-reinforced composite is influenced by the mechanical properties of the fiber-matrix interface. For example, toughening of a composite is significantly related to the ability of fibers to resist crack growth; thereby absorbing load-related energy and redistributing that energy back into the matrix in the form of newly formed cracks. The resulting interface stresses reflect the necessity for displacements in the loading direction between the fiber and matrix. The displacements are necessary to counteract the crack-opening displacement in the composite.

The shear-bond stresses discussed in the previous two sections directly influence the overall toughness of the fiber-matrix composite. There is good agreement between the shear-bond stress illustrated in Figures 6-5, 6-6, 6-7 and 6-8 with the toughness data

previously reported in Chapter 4 and by Jewell et al. (2015). The fiber pullout toughness (i.e. energy consumption) increased with increasing curing time and increased shear-bond strength (Figure 6-12). The one variation from this pattern exists with the polypropylene fiber in OPC from 1 to 112 days of curing; any other combination of cement and fiber shows an increase in shear-bond strength with time. Polypropylene fiber has the lowest elastic modulus of 5.0 GPa, combined with OPC which has a lower elastic modulus than CSA cement yields increased shear strengths. However the low elastic modulus allows the fiber to readily deform by peeling away segments of the fiber surface, see Chapter 4 and Jewell et al., (2015).

The toughness of a composite increases as a function of the shear-bond strength, Figure 6-12. Figure 6-12 shows an inverse relationship between the energy consumption (toughness) and the total fracture toughness of the composite. The energy absorbed through fracturing of new surfaces reduces with increasing time and increasing shear-bond strength. However the overall toughness of the composite increases with the same increasing shear-bond strength suggesting the energy absorbed through fiber pullout, at the fiber-matrix interface, is more dependent on frictional axial forces in addition to deformation of the fiber itself.

Figure 6-12 also indicates a large difference in performance of steel fiber and synthetic fibers with respect to energy consumption from fiber pullout. Synthetic fibers absorbed between 1.0 and 10.0 mJ/mm³ from 1 to 112 days of curing, respectively; while the steel fibers absorbed between 40.0 and 140.0 mJ/mm³ from 1 to 112 days, respectively.

However when considering fiber performance with respect to total fracture toughness there exists a little difference between the steel and synthetic fibers; both fiber types

resulted in a total fracture toughness range within 8.0 to 16.0 MPa. The primary difference resides in the shear-bond strength where synthetic fibers achieved fracture toughness values at lower shear-bond strengths (1.0 – 3.0 MPa) and a tighter range. As compared to the steel fibers with shear-bond strengths ranging from 3.0 to 25.0 MPa.

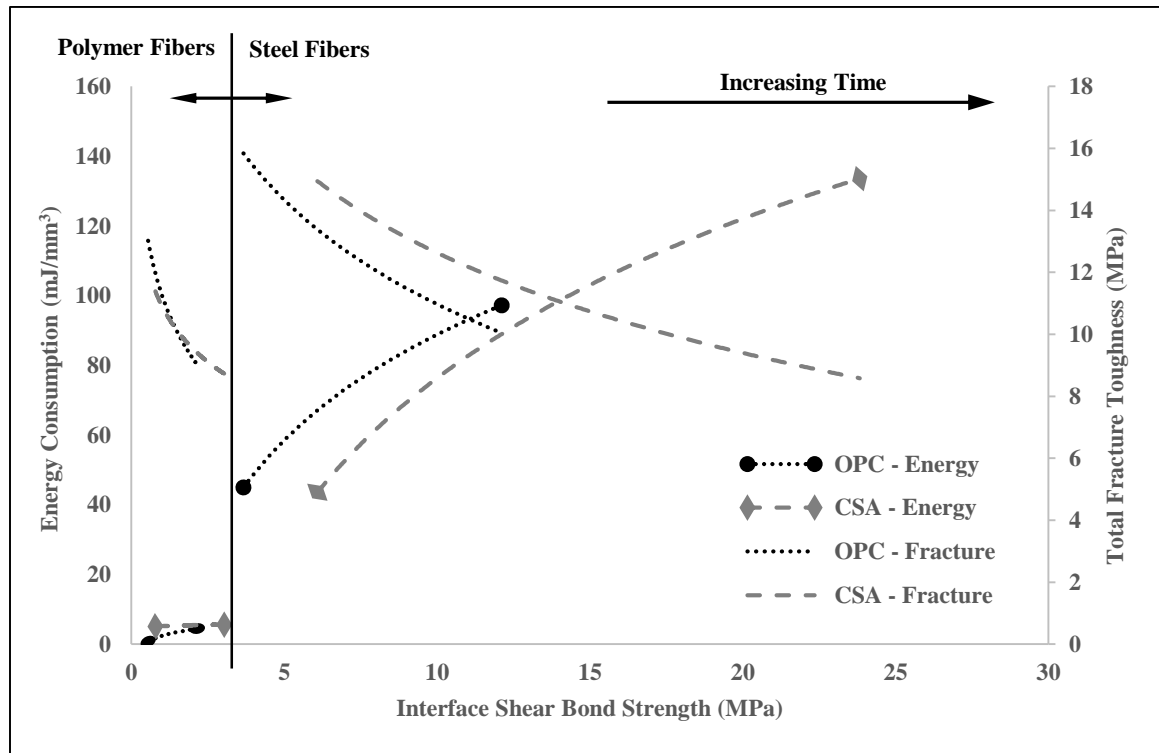


Figure 6-12. Comparing the relationship between energy consumption from total fiber pullout to total fracture toughness as a function of interface shear bond strength.

Composite toughness and fracture toughness both infer the dissipation of work through the creation of new surfaces. Many toughness theories of composite materials have been developed mainly for those with unidirectional fibers. Kim and Mai (1998) emphasized the various origins of toughness in composites may be characterized by considering the sequence of microscopic fracture events that lead to crack propagation macroscopically under monotonic increasing loads, such as the single-fiber pullout test. The prevalent

type of cracking depends on the properties of the interface relative to the fiber and matrix (Kim and Mai, 1998).

The research of Marston et al. (1974) and Atkins (1975) identified the contribution of three major sources of fracture toughness, stress redistribution (F_r), fiber pullout (F_p) and the generation of new surfaces (F_s) (Kim and Mai, 1998). The contribution of each energy consuming component may be summed into the total fracture toughness (F_{tot}), of the single-fiber-matrix composite.

$$(6-5) \quad F_{tot} = F_r + F_p + F_s$$

$$(6-6) \quad F_{tot} = \frac{V_f \sigma_f}{\tau_f} \left[\frac{\sigma_f d}{6} \left(\frac{1}{4} + \frac{\sigma_f}{E_f} \right) + \frac{R_m}{2} \right] + (1 - V_f) R_m$$

V_f is the fiber volume fraction; σ_f is the ultimate strength of the fiber; τ_f is the shear bond strength of the fiber and matrix.

6.5. Statistical Analysis

Each type of cement was analyzed statistically using a two-way general linear model analysis of variance (GLM/ANOVA) (Cox and McCullagh, 1982; Silknitter et al., 1999; Vano et al., 2006; McDonald, 2009). Factorial analysis of variance is a useful tool to assess the effects of cement type and curing time for each fiber type. Specifically, polynomial response curves were fit for each cement which related the dependent variable, interface-shear strength, to curing time. Higher order terms were tested and removed using backward elimination. The resulting model was tested for lack of fit. The test for interaction of cement type and fiber type was used to determine whether there was any significant differences in the relationship of fiber-matrix interface-shear strength

density and curing time between cement types, including OPC and CSA cement (Yamazaki et al., 2006). A significance level of $\alpha = 0.05$ was used throughout for statistical analyses. To reduce variance heterogeneity and to make the data more symmetric a log transformation was performed in SAS 9.4 (Box and Cox, 1964). The log transformation increased the R-squared value for each of the fiber types with respect to the dependent variable, interface-shear strength, Table 6-3. This provided greater support for the use of ANOVA inference methods on the transformed data.

Table 6-3. Coefficient of determination before and after log transformation

Fiber Type	R² Before Transformation	R² After Transformation
Coated Steel	0.4856	0.7912
Plain Steel	0.3772	0.8683
PVA	0.4914	0.7220
PP	0.3145	0.3575

As evidence to the significance difference between the OPC trends and the CSA trends, ANOVA was used to test if separate linear and quadratic were required. The results of this test were not significant (Plain Steel, P=0.191; Coated Steel, P=0.117; PVA, P=0.118; PP, P=0.140) and therefore separate quadratic and cubic interactions were not required, and indeed there does exist significant difference between the trends of the OPC and CSA cements over time.

Mean values of the interface-shear strength for the fibers in each cement type are shown in Figures 6-5, 6-6, 6-7 and 6-8. The results of the respective ANOVA analyses are shown in Tables 6-4 through 6-7; the four fiber types were placed into more generalized groups, steel fiber and synthetic fiber. There were differences in the days of curing dependence based on the type of cement and fiber type. However there was no

overarching significant difference in the interface-shear strength for all cement types and fiber types.

6.5.1. Steel Fiber Results

Steel fibers achieved a higher shear-bond strength than the synthetic fibers in both the OPC and CSA cement matrices. Figure 6-13 shows the log plot of the ANOVA procedure for shear strength with respect to plain-steel fibers. The plot shows similar, positive, trending regression profiles for both types of CSA cement. However the ordinary portland cement regression profile shows interaction over the entire curing time. The similar trends of the CSA cements along with the interaction of the OPC trend reinforces that statistical significance exists between cements regardless of the curing time ($P < 0.0001$) and in regards to curing time between linear coefficients ($P < 0.0001$). This significance supports the hypothesis that a reinforcing fiber performs differently in CSA cements than in ordinary portland cement. There is agreement with this finding for each fiber type evaluated.

Table 6-4. Type I ANOVA for effect of cement type and levels of days of curing on shear strength for the plain-steel fiber

Source	DF	Type I SS	Mean Square	F Value	Pr > F
Cement	2	6726.453232	3363.226616	170.29	<.0001
Day	1	1256.426524	1256.426524	63.62	<.0001
Day*Day	1	1487.607937	1487.607937	75.32	<.0001
Day*Cement	2	621.286952	310.643476	15.73	<.0001
Day*Day*Cement	2	71.461673	35.730836	1.81	0.1704

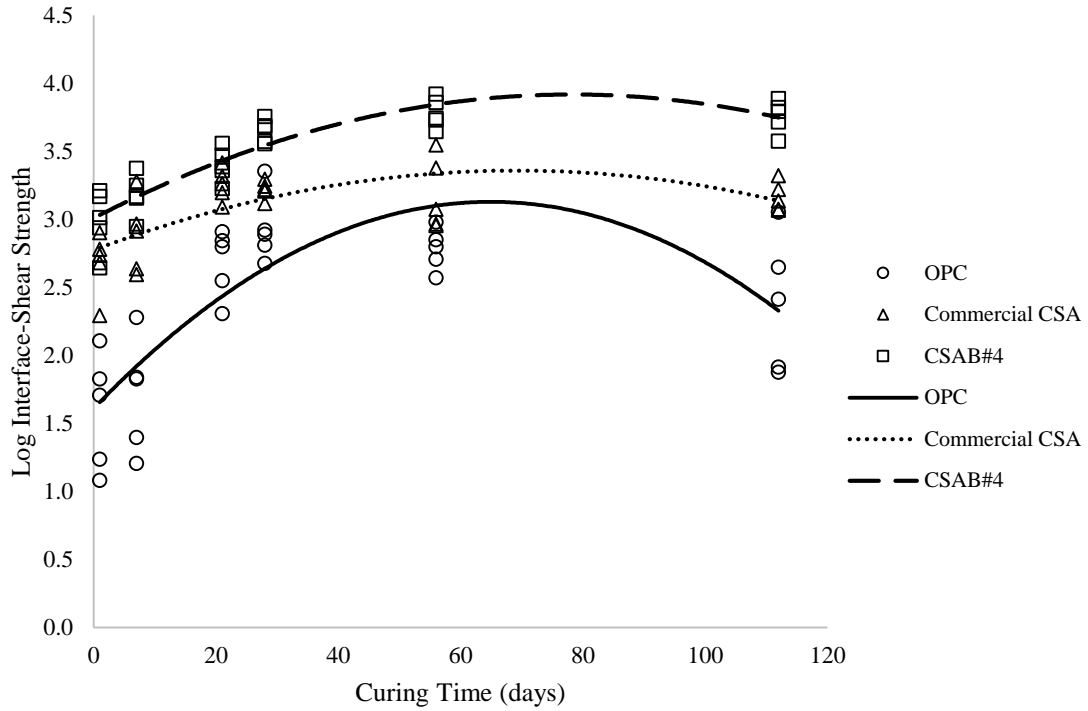


Figure 6-13. Analysis of variance response curves of shear strength for the plain-steel fiber.

Figure 6-14 shows a plot of the ANOVA model for coated-steel fibers with shear strength as the dependent variable. The Commercial and CSAB#4 CSA cements show similar positive-trending quadratic lines with increasing interaction associated with increasing curing time. More importantly there is a large difference between the linear coefficients of the CSA cements and the ordinary portland cement ($P=0.0007$). The similar trend of the CSA cements and the opposing trend of the portland cement, again, suggests statistical significance ($P<0.0001$) that cement type does effect the shear strength of the fiber-matrix composite.

Table 6-5. Type I ANOVA for effect of cement type and levels of days of curing on shear strength for the coated-steel fiber

Source	DF	Type I SS	Mean Square	F Value	Pr > F
Cement	2	2394.279332	1197.139666	63.66	<.0001
Day	1	506.225230	506.225230	26.92	<.0001
Day*Day	1	1266.966800	1266.966800	67.37	<.0001
Day*Cement	2	297.468273	148.734136	7.91	0.0007
Day*Day*Cement	2	96.322678	48.161339	2.56	0.0835

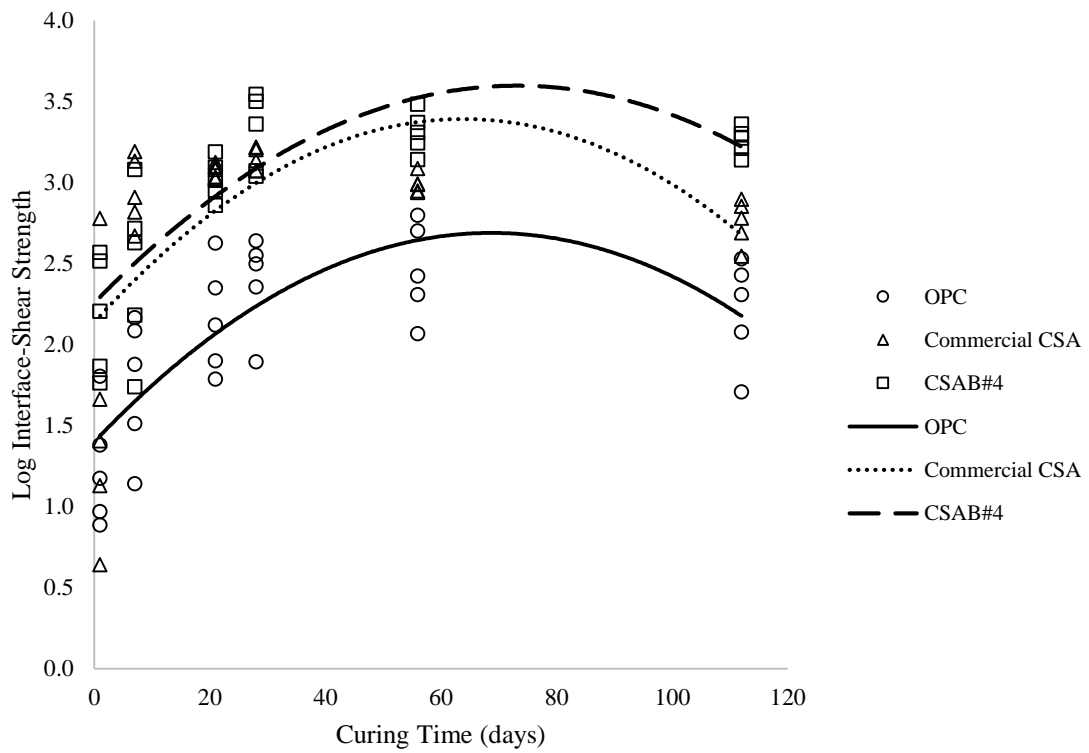


Figure 6-14. Analysis of variance response curves of shear stress for the coated-steel fiber.

6.5.2. Synthetic Fiber Results

The ANOVA test demonstrated statistically significant difference ($P=0.0055$) between the shear strength of polypropylene fibers embedded in CSA cements as compared to the same fiber embedded in ordinary portland cement, no accounting for curing time. Figure 15 depicts an increasing trend for the CSA cements to 56 days of curing after which each cement type shows a decreasing trend. Interaction exists between each cement type of 1 day of curing, particularly between the CSA cements and OPC ($P=0.0055$). However as compared to Figures 6-13 and 6-14 there is less statistical difference between CSA cement and OPC for the polypropylene fiber with respect to curing time for both the linear and quadratic coefficients ($P=0.4003$ and $P=0.2237$, respectively). However, without consideration of cement type there is days of curing is significant with respect to the dependent variable ($P=0.0267$).

Table 6-6. Type I ANOVA for effect of cement type and levels of days of curing on shear stress for the polypropylene fiber

Source	DF	Type I SS	Mean Square	F Value	Pr > F
Cement	2	2.49119434	1.24559717	5.56	0.0055
Day	1	0.53814899	0.53814899	2.40	0.1252
Day*Day	1	1.14147250	1.14147250	5.09	0.0267
Day*Cement	2	0.41523703	0.20761852	0.93	0.4003
Day*Day*Cement	2	0.68411897	0.34205949	1.53	0.2237

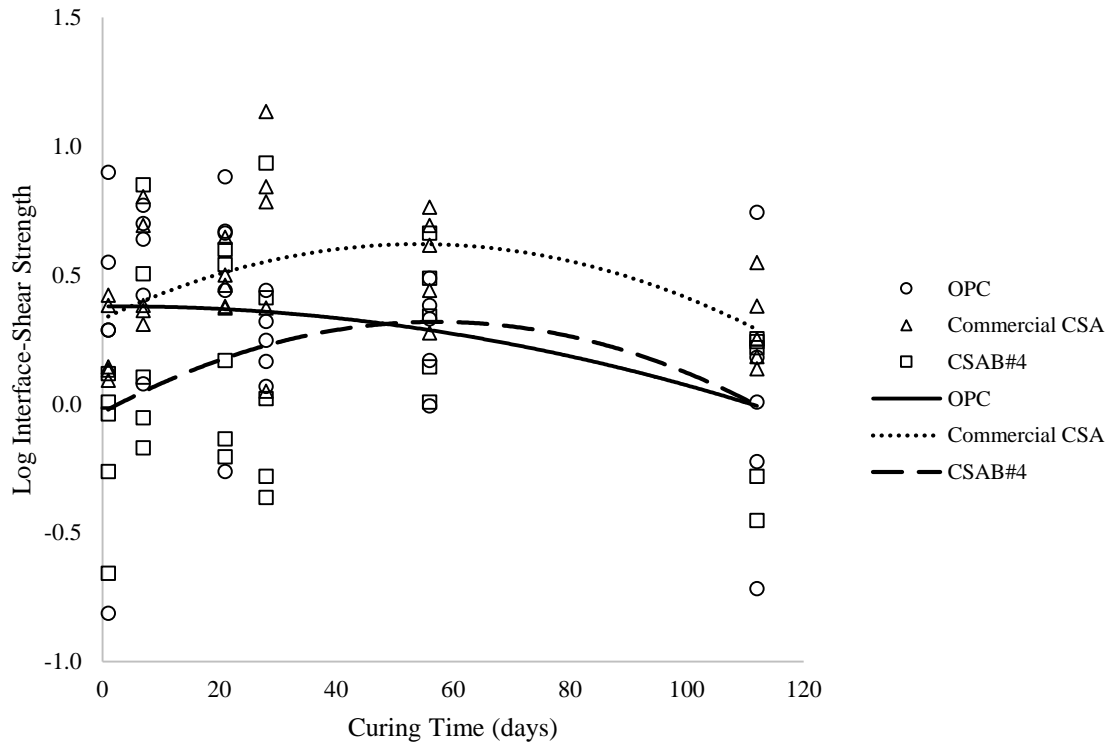


Figure 6-15. Analysis of variance response curves of shear stress for the polypropylene fiber.

There is statistical significance ($P=0.0230$) between cement types with respect to the dependent variable without consideration to the days of curing. The PVA fiber demonstrated increasing quadratic trends for each cement type to 56 days before decreasing to 112 days. Interaction exists after 1 day of curing between the OPC and CSA cements, see Figure 6-16. This figure emphasizes that a reinforcing fiber will not perform the same in calcium sulfoaluminate cement as they do in ordinary portland cement.

Table 6-7. Type I ANOVA for effect of cement type and levels of days of curing on shear stress for the polyvinyl-alcohol fiber

Source	DF	Type I SS	Mean Square	F Value	Pr > F
Cement	2	8.74460881	4.37230441	3.95	0.0230
Day	1	5.91172952	5.91172952	5.34	0.0233
Day*Day	1	19.14380669	19.14380669	17.30	<.0001
Day*Cement	2	1.50925435	0.75462717	0.68	0.5085
Day*Day*Cement	2	1.60415491	0.80207745	0.72	0.4875

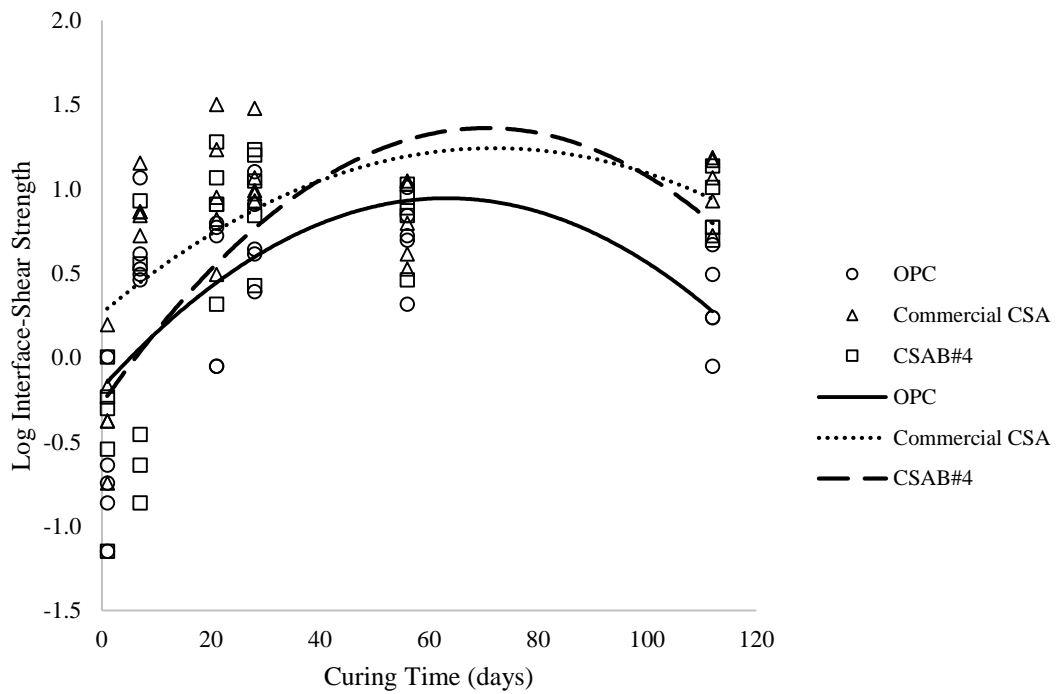


Figure 6-16. Analysis of variance response curves of shear stress for the polyvinyl-alcohol fiber.

6.6. Conclusion

This study examined the interface between four fiber types embedded in three different types of cement. The fiber-matrix bond was evaluated by analysis of the interface shear strength and fracture toughness related to single-fiber pullout.

1. An important factor contributing to the bond strength between fiber and matrix was the ability to transfer interfacial stresses from fiber to matrix. The more rigid-dense morphology of the CSA cement paste related to the ettringite crystal structure yielded higher shear-bond strengths for both steel and synthetic fibers. The morphology of the C-S-H in the OPC matrix provided a good fiber-matrix bond, though lacked the strength and dense-structure found with ettringite in the CSA matrices; this was evident by lower shear-bond strengths.
2. There are two ways to increase the effectiveness of reinforcing fibers, within cementitious matrices, to protract the functional life of the composite and thereby increasing the toughness; both of which involve decreasing the modulus of elasticity ratio of fiber to matrix. First, for the same fiber type a higher modulus cement matrix may be used, i.e. a calcium sulfoaluminate cement instead of an ordinary portland cement. Second the age of the cement matrix will effectively reduce the fiber-matrix elastic modulus ratio as the brittleness of the binder increases.
3. ANOVA results for interfacial shear stress confirm that fibers embedded in calcium sulfoaluminate cement do perform differently than the same type of fibers embedded in ordinary portland cement.

CHAPTER 7 : CONCLUSIONS AND FUTURE WORK

7.1. General Conclusions

Based on the experiments performed in this dissertation several conclusions may be drawn.

Chapter 2 focused on the development of a calcium sulfoaluminate cement fabricated from coal combustion byproducts. A CSA cement was produced that performed similar to a commercially available CSA cement.

Chapter 3 was centered on the evaluation of two primary parameters of the single-fiber pullout test, peak load and toughness associated with complete fiber pullout. Results demonstrated peak loads and overall toughness is enhanced (increased) by utilizing CSA cement in place of ordinary portland cement as the base for the cementitious matrix. Steel fibers achieved strengths much greater than those attained by the synthetic fibers, which was associated with the high modulus of elasticity, and minimal elongation of the steel fibers as compared to the softer synthetic fibers. By pairing a stiff fiber with a stiffer cement than OPC, the CSA-cement/steel fiber combination proved to be an excellent combination for a composite that may sustain high loads. As a result of increased loads before the onset of fiber pullout a tougher material resulted with the steel fiber/CSA cement combination. Even though the synthetic fibers did not achieve high peak loads and were not as tough, these low modulus of elasticity fibers did improve the early-age performance of the composite while demonstrating a more stable/consistent residual strength after the onset of fiber pullout. The use of a CSA cement increased the peak

load and toughness of a fiber-matrix composite as compared to a composite fabricated with OPC.

Chapter 4 and Chapter 5 concentrated on the multiple-cracking behavior, debonding-energy prior to fiber pullout and the interfacial shear and bond stresses that exist at the interface between fiber and matrix when applied to the single-fiber pullout test. An increased debonding-energy density was developed in the CSA matrix as compared to the portland matrix. The CSA matrix was better suited to absorb the energy inflicted on the matrix, through the fiber, from a uniaxial load directed parallel to the embedded length of the fiber. This increased energy absorption resulted in a larger energy density up to peak load, after which point the fiber has become completely debonded from the surrounding matrix and fiber pullout is initiated. In terms of multiple cracking, a larger energy density before fiber pullout suggests the bond developed from the ettringite structure within the transition zone favors the transfer of forces many times between the fiber and matrix; thus influencing the multiple cracking behavior. Again pointing to the heart of this research, reinforcing fibers perform differently in a calcium sulfoaluminate cement as compared to an ordinary portland cement. The stress transition zone between the fiber and matrix plays a pivotal role in defining the bond characteristics of a fiber-matrix composite. Specifically the bond stresses and shear stresses developed within this zone govern at what load and displacement a fiber will begin to debond, to be fully debonded, to begin pullout, to whether frictional forces govern pullout or whether pseudo strain-hardening of the composite will result. The research demonstrated in this dissertation found that the utilization of CSA cements effectively reduced the fiber-matrix bond stress and shear stress by lowering the fiber-matrix modulus of elasticity ratio. By utilizing a

higher modulus of elasticity matrix the effects are witnessed after only 1-day of curing, this behavior continued as the matrix gained strength with time, effectively increasing the modulus of elasticity with time. By lowering the fiber-matrix elastic modulus ratio the stresses within the transition zone were lowered which increases the damage tolerant behavior of the composite allowing for sustaining greater loads and creating a tougher composite.

In summary from all of the research presented, it was determined that reinforcing fibers chosen for an application with ordinary portland cement will not perform the same in a calcium sulfoaluminate cement. The CSA cements, both commercially produced and that produced in the laboratory from coal combustion byproducts, sustained higher peak loads and produced a tougher fiber-matrix composite. This was true for both steel and synthetic fibers.

7.2. Future Work

After having successfully demonstrated that cement type affects the performance of embedded fibers, additional research should be considered to highlight performance/behavior benefits of using CSA cements with fibers to identify unrealized benefits or hidden dangers.

Additional research would include:

- Test a suite of fibers to cover those that are commercially available; including natural fibers, glass, carbon, etc...

- Fibers in the presented research were straight, without any deformation. Mechanically deformed fibers, i.e. hooked end, should be explored to see the impact of the interaction between a CSA-based fiber composite.
- Naturally the presented work should be scaled up to include multiple-fiber composites to evaluate flexural strength, residual strength and compressive strength performance. Additionally the effect of fiber inclination would need to be evaluated as the matrix fracture zone around the fiber deformation would certainly behave different in a CSA cement than for an OPC.
- Specimens prepared in this study utilized only cement and water composites (i.e. paste) to eliminate the effects of particle interaction from fine and coarse aggregates.

APPENDICES

Appendix A : Statistical Analysis

Appendix A-1: List of factors and their levels for the single-fiber pullout test.

Test (levels)	Factors		
	Cement Type	Fiber Type	Curing Days
1	OPC	Polypropylene	1
2	OPC	Polypropylene	7
3	OPC	Polypropylene	21
4	OPC	Polypropylene	28
5	OPC	Polypropylene	56
6	OPC	Polypropylene	112
7	OPC	Polyvinyl Alcohol	1
8	OPC	Polyvinyl Alcohol	7
9	OPC	Polyvinyl Alcohol	21
10	OPC	Polyvinyl Alcohol	28
11	OPC	Polyvinyl Alcohol	56
12	OPC	Polyvinyl Alcohol	112
13	OPC	Cooper-Coated Steel	1
14	OPC	Cooper-Coated Steel	7
15	OPC	Cooper-Coated Steel	21
16	OPC	Cooper-Coated Steel	28
17	OPC	Cooper-Coated Steel	56
18	OPC	Cooper-Coated Steel	112
19	OPC	Plain Steel	1
20	OPC	Plain Steel	7
21	OPC	Plain Steel	21
22	OPC	Plain Steel	28
23	OPC	Plain Steel	56
24	OPC	Plain Steel	112
25	Commercial CSA	Polypropylene	1
26	Commercial CSA	Polypropylene	7
27	Commercial CSA	Polypropylene	21
28	Commercial CSA	Polypropylene	28
29	Commercial CSA	Polypropylene	56
30	Commercial CSA	Polypropylene	112
31	Commercial CSA	Polyvinyl Alcohol	1

Appendix A-1 (continued):

32	Commercial CSA	Polyvinyl Alcohol	7
33	Commercial CSA	Polyvinyl Alcohol	21
34	Commercial CSA	Polyvinyl Alcohol	28
35	Commercial CSA	Polyvinyl Alcohol	56
36	Commercial CSA	Polyvinyl Alcohol	112
37	Commercial CSA	Cooper-Coated Steel	1
38	Commercial CSA	Cooper-Coated Steel	7
39	Commercial CSA	Cooper-Coated Steel	21
40	Commercial CSA	Cooper-Coated Steel	28
41	Commercial CSA	Cooper-Coated Steel	56
42	Commercial CSA	Cooper-Coated Steel	112
43	Commercial CSA	Plain Steel	1
44	Commercial CSA	Plain Steel	7
45	Commercial CSA	Plain Steel	21
46	Commercial CSA	Plain Steel	28
47	Commercial CSA	Plain Steel	56
48	Commercial CSA	Plain Steel	112
49	CAER CSA	Polypropylene	1
50	CAER CSA	Polypropylene	7
51	CAER CSA	Polypropylene	21
52	CAER CSA	Polypropylene	28
53	CAER CSA	Polypropylene	56
54	CAER CSA	Polypropylene	112
55	CAER CSA	Polyvinyl Alcohol	1
56	CAER CSA	Polyvinyl Alcohol	7
57	CAER CSA	Polyvinyl Alcohol	21
58	CAER CSA	Polyvinyl Alcohol	28
59	CAER CSA	Polyvinyl Alcohol	56
60	CAER CSA	Polyvinyl Alcohol	112
61	CAER CSA	Cooper-Coated Steel	1
62	CAER CSA	Cooper-Coated Steel	7
63	CAER CSA	Cooper-Coated Steel	21
64	CAER CSA	Cooper-Coated Steel	28
65	CAER CSA	Cooper-Coated Steel	56
66	CAER CSA	Cooper-Coated Steel	112
67	CAER CSA	Plain Steel	1
68	CAER CSA	Plain Steel	7
69	CAER CSA	Plain Steel	21

Appendix A-1 (continued):

70	CAER CSA	Plain Steel	28
71	CAER CSA	Plain Steel	56
72	CAER CSA	Plain Steel	112

Sample ID	Day	Cement	Fiber	Peak Load (N)	Toughness (mJ)	Interface Shear Stress (MPa)	Debonding -Energy Density (mJ/mm ³)	Bridging Stress (MPa)	Interfacial Shear Stress Distribution (MPa)	Axial Stress Distribution (MPa)
SO1	1	OPC	Csteel	9.2	42.57	3.23	17.41	115.19	-1.29E-04	2.49E-02
SO2	1	OPC	Csteel	6.9	36.93	2.43	14.26	102.01	-1.55E-04	1.97E-02
SO3	1	OPC	Csteel	17.3	91.17	6.08	19.69	119.92	1.34E-05	3.25E-02
SO4	1	OPC	Csteel	7.5	40.19	2.64	2.63	42.66	1.78E-04	6.89E-03
SO5	1	OPC	Csteel	11.3	47.86	3.97	26.82	149.81	-5.34E-04	5.73E-02
SO6	7	OPC	Csteel	18.6	16.28	6.54	9.43	96.74	1.95E-04	7.47E-03
SO7	7	OPC	Csteel	6.9	28.43	3.13	18.48	119.68	-7.71E-05	1.52E-02
SO8	7	OPC	Csteel	24.8	68.19	8.72	6.48	63.93	1.95E-04	9.95E-03
SO9	7	OPC	Csteel	12.9	20.72	4.53	9.03	67.55	9.44E-05	1.14E-02
SO10	7	OPC	Csteel	22.9	74.59	8.05	16.85	121.03	3.66E-05	2.67E-02
SO11	21	OPC	Csteel	29.8	139.24	10.47	22.30	126.07	4.59E-05	2.92E-02
SO12	21	OPC	Csteel	23.7	52.23	8.33	5.75	73.54	1.26E-04	1.46E-02
SO13	21	OPC	Csteel	39.3	135.18	13.81	4.11	83.07	1.49E-04	2.01E-02
SO14	21	OPC	Csteel	17	73.93	5.98	0.80	33.24	2.12E-04	3.81E-03
SO15	21	OPC	Csteel	19	76.34	6.68	20.32	125.84	1.37E-05	2.14E-02

Sample ID	Day	Cement	Fiber	Peak Load (N)	Toughness (mJ)	Interface Shear Stress (MPa)	Debonding -Energy Density (mJ/mm ³)	Bridging Stress (MPa)	Interfacial Shear Stress Distribution (MPa)	Axial Stress Distribution (MPa)
SO16	28	OPC	Csteel	36.5	141.11	12.83	11.66	116.63	1.69E-06	4.18E-02
SO17	28	OPC	Csteel	18.9	69.77	6.64	1.23	32.94	2.14E-04	3.72E-03
SO18	28	OPC	Csteel	39.9	52.11	14.02	2.12	54.87	2.01E-04	1.00E-02
SO19	28	OPC	Csteel	34.6	144.89	12.16	20.80	92.80	4.39E-05	3.31E-02
SO20	28	OPC	Csteel	30	72.94	10.54	1.42	45.75	2.05E-04	7.03E-03
SO21	56	OPC	Csteel	22.5	56.93	7.91	6.67	77.05	1.08E-04	1.48E-02
SO22	56	OPC	Csteel	28.6	90.55	10.05	1.77	55.98	1.79E-04	9.82E-03
SO23	56	OPC	Csteel	46.7	129.82	16.41	0.81	51.34	2.13E-04	8.98E-03
SO24	56	OPC	Csteel	42.4	30.31	14.90	4.11	85.74	1.45E-04	2.09E-02
SO25	56	OPC	Csteel	32.1	84.80	11.28	0.73	49.09	2.00E-04	7.97E-03
SO26	112	OPC	Csteel	32.3	124.19	11.35	0.67	42.91	2.06E-04	6.10E-03
SO27	112	OPC	Csteel	22.7	105.84	7.98	0.35	58.73	1.50E-04	9.83E-03
SO28	112	OPC	Csteel	35.7	113.74	12.55	0.09	41.92	2.12E-04	5.90E-03
SO29	112	OPC	Csteel	28.6	121.31	10.05	0.27	74.31	1.31E-04	1.48E-02
SO30	112	OPC	Csteel	15.1	92.37	5.52	1.07	52.39	1.39E-04	7.55E-03

Sample ID	Day	Cement	Fiber	Peak Load (N)	Toughness (mJ)	Interface Shear Stress (MPa)	Debonding-Energy Density (mJ/mm ³)	Bridging Stress (MPa)	Interfacial Shear Stress Distribution (MPa)	Axial Stress Distribution (MPa)
PPO1	1	OPC	PP	9	29.69	1.33	2.90	15.66	5.14E-05	7.74E-04
PPO2	1	OPC	PP	0.8	2.46	0.44	4.20	19.85	4.89E-08	3.08E-04
PPO3	1	OPC	PP	11.7	50.11	1.73	3.97	18.57	4.43E-05	1.03E-03
PPO4	1	OPC	PP	9	39.90	1.33	1.99	13.77	7.77E-05	6.98E-04
PPO5	1	OPC	PP	16.6	77.91	2.46	6.35	23.74	3.29E-05	1.53E-03
PPO6	7	OPC	PP	12.8	70.88	1.89	3.42	17.34	3.93E-05	7.64E-04
PPO7	7	OPC	PP	7.3	28.08	1.08	6.44	29.41	1.83E-08	5.13E-04
PPO8	7	OPC	PP	10.3	28.76	1.52	4.17	19.47	1.34E-05	6.86E-04
PPO9	7	OPC	PP	14.6	65.18	2.16	5.03	21.22	2.17E-05	9.41E-04
PPO10	7	OPC	PP	13.6	50.13	2.01	5.86	23.10	1.10E-05	9.15E-04
PPO11	21	OPC	PP	13.1	62.04	1.94	7.32	25.80	3.14E-06	8.04E-04
PPO12	21	OPC	PP	5.2	15.35	0.77	2.17	13.42	1.26E-05	3.07E-04
PPO13	21	OPC	PP	16.3	81.43	2.41	5.97	22.67	1.65E-05	9.46E-04
PPO14	21	OPC	PP	10.5	31.28	1.55	2.91	15.83	3.18E-05	5.69E-04
PPO15	21	OPC	PP	13.2	46.35	1.95	3.60	17.90	3.07E-05	7.19E-04

Sample ID	Day	Cement	Fiber	Peak Load (N)	Toughness (mJ)	Interface Shear Stress (MPa)	Debonding -Energy Density (mJ/mm ³)	Bridging Stress (MPa)	Interfacial Shear Stress Distribution (MPa)	Axial Stress Distribution (MPa)
PPO16	28	OPC	PP	10.5	33.57	1.55	6.68	33.20	2.58E-08	6.33E-04
PPO17	28	OPC	PP	6	21.39	1.18	1.13	11.36	5.93E-05	3.64E-04
PPO18	28	OPC	PP	0.8	2.85	1.07	3.48	19.82	2.12E-06	4.32E-04
PPO19	28	OPC	PP	9.3	48.32	1.38	5.58	21.91	2.70E-06	5.55E-04
PPO20	28	OPC	PP	6	13.46	1.28	7.62	30.13	2.58E-08	5.21E-04
PPO21	56	OPC	PP	6	13.46	0.99	3.01	15.86	8.99E-06	3.84E-04
PPO22	56	OPC	PP	9.9	33.67	1.47	5.32	21.35	4.26E-06	5.80E-04
PPO23	56	OPC	PP	8	27.67	1.18	3.09	13.25	3.53E-05	4.07E-04
PPO24	56	OPC	PP	9.4	28.25	1.39	4.28	18.92	8.57E-06	5.40E-04
PPO25	56	OPC	PP	18	40.39	1.63	2.23	14.11	4.95E-05	5.21E-04
PPO26	112	OPC	PP	14.2	13.21	2.10	6.90	28.27	4.91E-09	8.06E-04
PPO27	112	OPC	PP	8.1	19.54	1.20	1.12	9.90	7.97E-05	3.05E-04
PPO28	112	OPC	PP	3.3	16.74	0.49	0.00	6.50	7.46E-05	1.28E-04
PPO29	112	OPC	PP	5.4	8.12	0.80	2.09	14.89	5.89E-06	2.99E-04
PPO30	112	OPC	PP	6.8	9.54	1.01	4.06	18.29	2.84E-06	3.81E-04

Sample ID	Day	Cement	Fiber	Peak Load (N)	Toughness (mJ)	Interface Shear Stress (MPa)	Debonding -Energy Density (mJ/mm ³)	Bridging Stress (MPa)	Interfacial Shear Stress Distribution (MPa)	Axial Stress Distribution (MPa)
PVO1	1	OPC	PVA	1	1.26	0.53	0.10	2.65	1.72E-05	1.20E-04
PVO2	1	OPC	PVA	0.9	0.53	0.48	0.07	2.07	2.46E-05	8.53E-05
PVO3	1	OPC	PVA	0.8	0.69	0.42	0.04	1.53	3.29E-05	5.31E-05
PVO4	1	OPC	PVA	0.6	0.69	0.32	0.03	1.40	3.13E-05	4.32E-05
PVO5	1	OPC	PVA	1.9	2.17	1.00	2.03	11.57	7.95E-10	3.40E-04
PVO6	7	OPC	PVA	3.1	2.17	1.64	3.10	12.46	3.10E-09	3.80E-04
PVO7	7	OPC	PVA	3	1.07	1.58	0.52	6.13	3.98E-06	3.34E-04
PVO8	7	OPC	PVA	5.5	8.23	2.91	7.47	21.01	9.81E-12	6.74E-04
PVO9	7	OPC	PVA	3.2	1.35	1.69	1.18	9.02	3.41E-07	3.89E-04
PVO10	7	OPC	PVA	3.5	1.16	1.85	1.15	8.89	5.86E-07	4.23E-04
PVO11	21	OPC	PVA	4.1	7.92	2.17	4.50	17.51	1.08E-11	4.45E-04
PVO12	21	OPC	PVA	4.2	6.28	2.22	4.91	16.87	-5.64E-13	4.56E-04
PVO13	21	OPC	PVA	1.8	6.66	0.95	2.37	11.03	4.64E-11	1.95E-04
PVO14	21	OPC	PVA	3.9	3.32	2.06	3.22	14.29	1.01E-09	4.23E-04
PVO15	21	OPC	PVA	1.8	3.56	0.95	2.00	10.35	2.36E-10	1.95E-04

Sample ID	Day	Cement	Fiber	Peak Load (N)	Toughness (mJ)	Interface Shear Stress (MPa)	Debonding -Energy Density (mJ/mm ³)	Bridging Stress (MPa)	Interfacial Shear Stress Distribution (MPa)	Axial Stress Distribution (MPa)
PVO16	28	OPC	PVA	5.7	2.45	3.01	3.85	12.85	1.04E-07	5.98E-04
PVO17	28	OPC	PVA	4.7	2.10	2.48	3.05	15.77	3.20E-08	4.94E-04
PVO18	28	OPC	PVA	3.6	9.58	1.90	3.37	15.83	1.42E-10	3.79E-04
PVO19	28	OPC	PVA	2.8	7.43	1.48	4.07	14.17	1.60E-11	2.95E-04
PVO20	28	OPC	PVA	3.5	2.76	1.85	3.61	13.88	2.36E-09	3.68E-04
PVO21	56	OPC	PVA	3.9	8.30	2.06	0.22	12.56	9.33E-09	4.06E-04
PVO22	56	OPC	PVA	2.6	5.85	1.37	5.70	18.66	-1.79E-10	2.70E-04
PVO23	56	OPC	PVA	3.8	1.93	2.01	1.25	9.77	2.21E-07	3.93E-04
PVO24	56	OPC	PVA	5.2	7.27	2.75	10.91	25.13	-1.38E-11	5.41E-04
PVO25	56	OPC	PVA	4.4	2.34	2.32	2.16	13.03	1.36E-08	4.57E-04
PVO26	112	OPC	PVA	2.4	1.63	1.27	1.03	9.85	7.40E-09	2.38E-04
PVO27	112	OPC	PVA	2.4	0.86	1.27	2.88	11.38	4.21E-10	2.38E-04
PVO28	112	OPC	PVA	3.1	2.01	1.64	2.40	13.62	1.22E-10	3.07E-04
PVO29	112	OPC	PVA	1.8	1.05	0.95	1.18	10.89	2.57E-08	1.78E-04
PVO30	112	OPC	PVA	3.7	1.86	1.95	0.41	9.60	5.63E-07	3.61E-04

Sample ID	Day	Cement	Fiber	Peak Load (N)	Toughness (mJ)	Interface Shear Stress (MPa)	Debonding -Energy Density (mJ/mm ³)	Bridging Stress (MPa)	Interfacial Shear Stress Distribution (MPa)	Axial Stress Distribution (MPa)
PSo1	1	OPC	Psteel	15.7	75.07	5.52	28.32	105.03	-5.87E-05	3.31E-02
PSo2	1	OPC	Psteel	8.4	21.73	2.95	7.69	81.21	1.05E-05	1.45E-02
PSo3	1	OPC	Psteel	9.8	41.80	3.44	2.46	90.17	3.16E-06	1.73E-02
PSo4	1	OPC	Psteel	23.4	80.93	8.22	43.25	121.24	-8.28E-05	5.24E-02
PSo5	1	OPC	Psteel	17.7	68.71	6.22	11.55	111.32	2.50E-05	2.90E-02
PSo6	7	OPC	Psteel	8.5	34.55	4.04	10.39	109.05	2.03E-05	1.29E-02
PSo7	7	OPC	Psteel	6.5	17.16	3.34	11.83	107.60	-2.17E-05	1.25E-02
PSo8	7	OPC	Psteel	17.9	73.64	6.29	50.59	116.01	1.46E-05	2.06E-02
PSo9	7	OPC	Psteel	17.7	26.15	6.22	12.32	103.88	2.90E-05	1.92E-02
PSo10	7	OPC	Psteel	27.8	62.41	9.77	16.47	118.41	4.41E-05	2.83E-02
PSo11	21	OPC	Psteel	28.6	61.51	10.05	7.23	124.30	3.28E-05	2.68E-02
PSo12	21	OPC	Psteel	36.4	138.35	12.79	48.61	132.95	2.97E-06	3.88E-02
PSo13	21	OPC	Psteel	52.2	138.49	18.35	16.92	140.06	6.17E-05	4.24E-02
PSo14	21	OPC	Psteel	48.9	174.32	17.19	28.98	138.23	5.84E-05	4.04E-02
PSo15	21	OPC	Psteel	46.8	88.57	16.45	22.58	106.58	5.66E-05	3.91E-02

Sample ID	Day	Cement	Fiber	Peak Load (N)	Toughness (mJ)	Interface Shear Stress (MPa)	Debonding -Energy Density (mJ/mm ³)	Bridging Stress (MPa)	Interfacial Shear Stress Distribution (MPa)	Axial Stress Distribution (MPa)
PSo16	28	OPC	Psteel	51.3	170.64	18.03	3.42	80.58	1.88E-04	1.27E-02
PSo17	28	OPC	Psteel	52.8	166.64	18.56	2.97	86.40	1.79E-04	1.49E-02
PSo18	28	OPC	Psteel	81.4	224.23	28.61	66.15	203.01	-1.67E-05	9.11E-02
PSo19	28	OPC	Psteel	41.4	127.38	14.55	37.89	166.14	1.84E-05	4.01E-02
PSo20	28	OPC	Psteel	47.3	187.92	16.63	20.40	136.75	5.53E-05	3.84E-02
PSo21	56	OPC	Psteel	42.7	126.54	15.01	42.22	163.82	2.14E-05	4.03E-02
PSo22	56	OPC	Psteel	37.2	167.73	13.08	4.04	127.99	4.58E-05	3.13E-02
PSo23	56	OPC	Psteel	56.1	193.19	19.72	20.59	115.83	9.89E-05	3.45E-02
PSo24	56	OPC	Psteel	46.8	138.83	16.45	44.09	126.24	1.27E-05	4.59E-02
PSo25	56	OPC	Psteel	49.2	151.87	17.29	25.02	144.80	4.84E-05	4.08E-02
PSo26	112	OPC	Psteel	18.6	85.61	6.54	10.26	91.66	5.94E-05	1.38E-02
PSo27	112	OPC	Psteel	19.3	56.55	6.78	10.83	92.24	6.13E-05	1.41E-02
PSo28	112	OPC	Psteel	40.2	131.39	14.13	21.43	124.61	5.33E-05	3.08E-02
PSo29	112	OPC	Psteel	60.3	181.79	21.19	76.18	191.87	2.15E-05	5.41E-02
PSo30	112	OPC	Psteel	31.8	105.45	11.18	22.22	135.79	2.45E-05	2.81E-02

Sample ID	Day	Cement	Fiber	Peak Load (N)	Toughness (mJ)	Interface Shear Stress (MPa)	Debonding -Energy Density (mJ/mm ³)	Bridging Stress (MPa)	Interfacial Shear Stress Distribution (MPa)	Axial Stress Distribution (MPa)
SQ1	1	CommCSA	Csteel	45.8	111.16	16.10	24.03	214.19	2.07E-06	5.76E-02
SQ2	1	CommCSA	Csteel	2.4	4.82	1.90	41.32	194.52	4.69E-05	5.66E-03
SQ3	1	CommCSA	Csteel	8.8	30.13	3.09	24.53	165.36	5.84E-05	8.75E-03
SQ4	1	CommCSA	Csteel	15	50.92	5.27	13.46	132.73	2.68E-05	1.71E-02
SQ5	1	CommCSA	Csteel	11.6	32.86	4.08	42.72	182.84	5.14E-05	1.19E-02
SQ6	7	CommCSA	Csteel	41.1	118.32	14.45	19.35	151.98	3.75E-05	3.83E-02
SQ7	7	CommCSA	Csteel	69.2	164.86	24.32	40.06	185.65	4.69E-05	6.16E-02
SQ8	7	CommCSA	Csteel	65.2	158.80	22.92	44.00	191.41	3.75E-05	6.07E-02
SQ9	7	CommCSA	Csteel	47.6	100.22	16.73	10.26	134.69	7.00E-05	3.76E-02
SQ10	7	CommCSA	Csteel	52.2	149.20	18.35	26.97	163.87	4.43E-05	4.71E-02
SQ11	21	CommCSA	Csteel	58.4	109.65	20.53	33.17	194.39	1.84E-05	5.37E-02
SQ12	21	CommCSA	Csteel	61.9	132.29	21.76	16.02	129.35	9.29E-05	3.77E-02
SQ13	21	CommCSA	Csteel	59.1	100.21	20.77	30.41	123.87	1.03E-05	5.63E-02
SQ14	21	CommCSA	Csteel	64.7	180.28	22.74	19.75	147.61	7.36E-05	4.46E-02
SQ15	21	CommCSA	Csteel	63.2	198.41	22.21	32.74	175.76	4.29E-05	5.16E-02

Sample ID	Day	Cement	Fiber	Peak Load (N)	Toughness (mJ)	Interface Shear Stress (MPa)	Debonding -Energy Density (mJ/mm ³)	Bridging Stress (MPa)	Interfacial Shear Stress Distribution (MPa)	Axial Stress Distribution (MPa)
SQ16	28	CommCSA	Csteel	65.5	86.17	23.02	14.90	127.56	9.76E-05	3.71E-02
SQ17	28	CommCSA	Csteel	61.5	96.55	21.62	15.21	134.56	8.28E-05	3.85E-02
SQ18	28	CommCSA	Csteel	70	171.11	24.60	21.12	186.05	4.04E-05	5.60E-02
SQ19	28	CommCSA	Csteel	70.9	86.17	24.92	1.18	103.12	1.80E-04	1.61E-02
SQ20	28	CommCSA	Csteel	71.1	176.43	24.99	75.24	208.07	-6.62E-06	7.06E-02
SQ21	56	CommCSA	Csteel	54.3	99.86	19.09	21.75	133.95	6.91E-05	3.49E-02
SQ22	56	CommCSA	Csteel	56.7	103.36	19.93	10.34	108.87	1.08E-04	2.78E-02
SQ23	56	CommCSA	Csteel	56.4	100.12	19.82	8.40	119.26	1.22E-04	2.44E-02
SQ24	56	CommCSA	Csteel	53.7	102.66	18.87	12.01	110.43	1.01E-04	2.78E-02
SQ25	56	CommCSA	Csteel	62.3	147.83	21.90	23.35	151.43	6.02E-05	4.23E-02
SQ26	112	CommCSA	Csteel	45.87	114.85	16.12	2.26	133.85	5.65E-05	3.24E-02
SQ27	112	CommCSA	Csteel	41.85	98.21	14.71	2.58	112.00	7.85E-05	2.58E-02
SQ28	112	CommCSA	Csteel	36.23	126.24	12.73	1.60	94.32	9.55E-05	1.99E-02
SQ29	112	CommCSA	Csteel	51.56	104.65	18.12	6.55	125.02	7.76E-05	3.20E-02
SQ30	112	CommCSA	Csteel	49.32	111.21	17.34	10.69	142.93	5.18E-05	3.58E-02

Sample ID	Day	Cement	Fiber	Peak Load (N)	Toughness (mJ)	Interface Shear Stress (MPa)	Debonding -Energy Density (mJ/mm ³)	Bridging Stress (MPa)	Interfacial Shear Stress Distribution (MPa)	Axial Stress Distribution (MPa)
PPQ1	1	CommCSA	PP	7.4	20.88	1.10	2.41	14.44	2.46E-05	4.44E-04
PPQ2	1	CommCSA	PP	7.7	17.95	1.14	3.25	17.28	1.02E-05	4.91E-04
PPQ3	1	CommCSA	PP	10.3	41.57	1.52	5.68	21.99	5.18E-06	6.70E-04
PPQ4	1	CommCSA	PP	7.8	21.57	1.15	4.72	19.97	3.65E-06	5.11E-04
PPQ5	1	CommCSA	PP	9.9	30.72	1.47	5.51	21.64	5.01E-06	6.45E-04
PPQ6	7	CommCSA	PP	9.2	38.37	1.36	3.74	12.70	4.94E-05	4.17E-04
PPQ7	7	CommCSA	PP	13.5	51.94	2.00	50.63	43.51	8.45E-10	7.73E-04
PPQ8	7	CommCSA	PP	9.9	31.76	1.47	15.98	35.86	2.12E-09	5.67E-04
PPQ9	7	CommCSA	PP	9.7	27.51	1.44	4.49	19.97	6.00E-06	5.42E-04
PPQ10	7	CommCSA	PP	15.1	42.87	2.24	20.40	41.39	9.27E-09	8.65E-04
PPQ11	21	CommCSA	PP	9.8	33.04	1.45	5.39	21.81	2.39E-06	5.05E-04
PPQ12	21	CommCSA	PP	12.9	41.24	1.91	15.01	34.97	3.10E-08	6.72E-04
PPQ13	21	CommCSA	PP	10.7	36.73	1.58	6.19	22.70	2.46E-06	5.51E-04
PPQ14	21	CommCSA	PP	3.1	7.92	1.46	3.83	31.81	1.49E-08	5.14E-04
PPQ15	21	CommCSA	PP	4.4	14.83	1.65	0.65	21.62	7.27E-05	3.94E-04

Sample ID	Day	Cement	Fiber	Peak Load (N)	Toughness (mJ)	Interface Shear Stress (MPa)	Debonding -Energy Density (mJ/mm ³)	Bridging Stress (MPa)	Interfacial Shear Stress Distribution (MPa)	Axial Stress Distribution (MPa)
PPQ16	28	CommCSA	PP	9.8	42.59	1.45	4.68	19.83	4.88E-06	4.84E-04
PPQ17	28	CommCSA	PP	21	63.19	3.11	12.66	32.77	1.71E-06	1.05E-03
PPQ18	28	CommCSA	PP	14.8	56.11	2.19	7.23	26.39	2.52E-06	7.40E-04
PPQ19	28	CommCSA	PP	7.1	17.97	1.05	2.91	15.73	8.05E-06	3.46E-04
PPQ20	28	CommCSA	PP	15.7	59.95	2.32	36.26	47.31	2.82E-10	7.93E-04
PPQ21	56	CommCSA	PP	8.9	27.21	1.32	6.66	24.03	3.86E-07	4.27E-04
PPQ22	56	CommCSA	PP	12.5	40.50	1.85	5.80	22.82	3.72E-06	5.91E-04
PPQ23	56	CommCSA	PP	10.5	43.16	1.55	7.26	24.99	6.55E-07	5.04E-04
PPQ24	56	CommCSA	PP	13.5	38.22	2.00	5.67	22.44	5.70E-06	6.33E-04
PPQ25	56	CommCSA	PP	14.5	77.35	2.15	52.60	44.58	3.35E-10	6.98E-04
PPQ26	112	CommCSA	PP	9.87	38.69	1.46	9.43	31.52	1.28E-08	4.82E-04
PPQ27	112	CommCSA	PP	8.12	41.56	1.20	6.84	26.21	6.04E-08	3.97E-04
PPQ28	112	CommCSA	PP	11.69	42.58	1.73	17.57	38.30	1.15E-09	5.71E-04
PPQ29	112	CommCSA	PP	7.74	36.63	1.15	2.53	18.07	3.67E-06	3.72E-04
PPQ30	112	CommCSA	PP	8.69	33.99	1.29	4.94	24.12	3.33E-07	4.24E-04

Sample ID	Day	Cement	Fiber	Peak Load (N)	Toughness (mJ)	Interface Shear Stress (MPa)	Debonding -Energy Density (mJ/mm ³)	Bridging Stress (MPa)	Interfacial Shear Stress Distribution (MPa)	Axial Stress Distribution (MPa)
PVAQ1	1	CommCSA	PVA	1.6	2.87	0.85	0.20	3.91	6.49E-06	1.57E-04
PVAQ2	1	CommCSA	PVA	2.3	12.54	1.22	3.14	13.59	6.22E-12	2.67E-04
PVAQ3	1	CommCSA	PVA	1.3	7.11	0.69	2.80	12.43	-2.68E-11	1.51E-04
PVAQ4	1	CommCSA	PVA	0.9	1.29	0.48	0.07	2.42	1.17E-05	7.52E-05
PVAQ5	1	CommCSA	PVA	1.3	2.68	0.69	0.09	2.73	1.37E-05	1.02E-04
PVAQ6	7	CommCSA	PVA	3.9	1.54	2.06	1.38	9.11	4.40E-07	3.86E-04
PVAQ7	7	CommCSA	PVA	6	4.41	3.17	3.73	17.32	1.03E-09	6.00E-04
PVAQ8	7	CommCSA	PVA	4.4	7.80	2.32	5.89	19.31	6.75E-13	4.40E-04
PVAQ9	7	CommCSA	PVA	4.5	4.32	2.38	4.33	16.18	1.84E-10	4.50E-04
PVAQ10	7	CommCSA	PVA	4.5	3.95	2.38	2.69	14.07	3.66E-09	4.50E-04
PVAQ11	21	CommCSA	PVA	8.5	10.53	4.49	9.58	23.01	3.85E-11	7.73E-04
PVAQ12	21	CommCSA	PVA	3.1	8.39	1.64	5.72	14.57	9.90E-12	2.82E-04
PVAQ13	21	CommCSA	PVA	4.3	2.30	2.27	15.22	15.56	1.45E-10	3.91E-04
PVAQ14	21	CommCSA	PVA	6.5	11.11	3.43	12.30	18.59	2.89E-10	5.91E-04
PVAQ15	21	CommCSA	PVA	4.9	4.40	2.59	6.03	14.78	1.94E-09	4.45E-04

Sample ID	Day	Cement	Fiber	Peak Load (N)	Toughness (mJ)	Interface Shear Stress (MPa)	Debonding -Energy Density (mJ/mm ³)	Bridging Stress (MPa)	Interfacial Shear Stress Distribution (MPa)	Axial Stress Distribution (MPa)
PVAQ16	28	CommCSA	PVA	4.8	3.11	2.54	1.22	14.48	2.02E-09	4.23E-04
PVAQ17	28	CommCSA	PVA	8.3	5.15	4.39	4.35	18.81	2.55E-09	7.32E-04
PVAQ18	28	CommCSA	PVA	5.5	2.81	2.91	1.56	15.31	2.55E-09	4.85E-04
PVAQ19	28	CommCSA	PVA	5.1	5.39	2.69	5.27	17.33	6.60E-11	4.50E-04
PVAQ20	28	CommCSA	PVA	5	1.76	2.64	0.93	14.47	3.04E-09	4.41E-04
PVAQ21	56	CommCSA	PVA	5.3	4.76	2.80	4.47	18.38	1.52E-11	4.45E-04
PVAQ22	56	CommCSA	PVA	5.4	3.95	2.85	3.84	16.28	4.42E-10	4.53E-04
PVAQ23	56	CommCSA	PVA	3.2	2.87	1.69	0.51	11.38	1.92E-06	2.54E-04
PVAQ24	56	CommCSA	PVA	4.2	8.99	2.22	6.73	22.01	-2.68E-13	3.53E-04
PVAQ25	56	CommCSA	PVA	3.5	1.70	1.85	0.97	9.51	9.40E-08	2.93E-04
PVAQ26	112	CommCSA	PVA	6.2	8.69	3.28	9.50	21.43	1.63E-12	5.29E-04
PVAQ27	112	CommCSA	PVA	5.5	7.21	2.91	5.46	16.33	5.58E-10	4.69E-04
PVAQ28	112	CommCSA	PVA	6.1	6.69	3.22	4.42	16.68	1.08E-09	5.20E-04
PVAQ29	112	CommCSA	PVA	3.9	7.22	2.06	1.84	14.52	1.57E-10	3.33E-04
PVAQ30	112	CommCSA	PVA	4.8	9.13	2.54	3.04	15.07	7.26E-10	4.09E-04

Sample ID	Day	Cement	Fiber	Peak Load (N)	Toughness (mJ)	Interface Shear Stress (MPa)	Debonding-Energy Density (mJ/mm ³)	Bridging Stress (MPa)	Interfacial Shear Stress Distribution (MPa)	Axial Stress Distribution (MPa)
PSQ1	1	CommCS Δ	Psteel	28.2	61.02	9.91	18.92	124.07	3.50E-05	2.81E-02
PSQ2	1	CommCS Δ	Psteel	51.8	198.83	18.21	38.93	146.96	3.61E-05	5.14E-02
PSQ3	1	CommCS Δ	Psteel	43.9	147.53	15.43	58.16	120.88	2.89E-05	4.50E-02
PSQ4	1	CommCS Δ	Psteel	45.9	132.39	16.13	20.29	127.11	7.26E-05	3.80E-02
PSQ5	1	CommCS Δ	Psteel	41.6	128.96	14.62	31.14	154.70	3.11E-05	4.22E-02
PSQ6	7	CommCS Δ	Psteel	38.1	171.95	13.39	4.05	77.31	1.31E-04	1.72E-02
PSQ7	7	CommCS Δ	Psteel	75.5	134.54	26.54	5.70	91.27	1.57E-04	2.60E-02
PSQ8	7	CommCS Δ	Psteel	52.5	202.88	18.45	26.05	139.63	5.71E-05	3.98E-02
PSQ9	7	CommCS Δ	Psteel	55.2	99.82	19.40	6.24	82.38	1.49E-04	2.07E-02
PSQ10	7	CommCS Δ	Psteel	39.7	182.35	13.95	18.97	128.64	4.78E-05	3.16E-02
PSQ11	21	CommCS Δ	Psteel	78.4	53.48	27.56	5.80	84.41	1.58E-04	2.18E-02
PSQ12	21	CommCS Δ	Psteel	86.6	125.61	30.44	10.94	100.00	1.43E-04	2.92E-02
PSQ13	21	CommCS Δ	Psteel	69.6	94.35	24.46	4.73	74.16	1.66E-04	1.72E-02
PSQ14	21	CommCS Δ	Psteel	74.3	93.54	26.12	0.89	74.35	1.69E-04	1.74E-02
PSQ15	21	CommCS Δ	Psteel	62.6	42.78	22.00	1.00	66.61	1.86E-04	1.06E-02

Sample ID	Day	Cement	Fiber	Peak Load (N)	Toughness (mJ)	Interface Shear Stress (MPa)	Debonding -Energy Density (mJ/mm ³)	Bridging Stress (MPa)	Interfacial Shear Stress Distribution (MPa)	Axial Stress Distribution (MPa)
PSQ16	28	CommCS Δ	Psteel	71.2	78.63	25.03	4.17	74.15	1.64E-04	1.69E-02
PSQ17	28	CommCS Δ	Psteel	76.8	85.40	26.99	5.73	84.30	1.54E-04	2.13E-02
PSQ18	28	CommCS Δ	Psteel	64.2	68.44	22.57	0.68	78.57	1.87E-04	9.43E-03
PSQ19	28	CommCS Δ	Psteel	72.9	89.41	25.62	0.83	90.16	1.42E-04	2.35E-02
PSQ20	28	CommCS Δ	Psteel	70.4	71.22	24.74	0.33	65.14	1.88E-04	1.00E-02
PSQ21	56	CommCS Δ	Psteel	54.6	63.17	19.19	1.69	51.44	1.79E-04	8.40E-03
PSQ22	56	CommCS Δ	Psteel	61.5	86.17	21.62	0.98	66.52	1.62E-04	1.34E-02
PSQ23	56	CommCS Δ	Psteel	98.8	99.47	34.73	1.25	95.95	1.48E-04	2.67E-02
PSQ24	56	CommCS Δ	Psteel	55.3	46.35	19.44	0.41	67.35	1.56E-04	1.35E-02
PSQ25	56	CommCS Δ	Psteel	83.4	71.87	29.31	1.34	70.42	1.71E-04	1.54E-02
PSQ26	112	CommCS Δ	Psteel	61.5	54.23	21.62	0.42	77.14	1.48E-04	1.73E-02
PSQ27	112	CommCS Δ	Psteel	78.9	59.47	27.73	2.14	71.44	1.57E-04	1.94E-02
PSQ28	112	CommCS Δ	Psteel	65.5	71.57	23.02	1.52	83.32	1.42E-04	1.98E-02
PSQ29	112	CommCS Δ	Psteel	71.2	49.14	25.03	0.83	78.38	1.54E-04	1.82E-02
PSQ30	112	CommCS Δ	Psteel	61.1	52.87	21.48	0.25	66.56	1.63E-04	1.35E-02

Sample ID	Day	Cement	Fiber	Peak Load (N)	Toughness (mJ)	Interface Shear Stress (MPa)	Debonding -Energy Density (mJ/mm ³)	Bridging Stress (MPa)	Interfacial Shear Stress Distribution (MPa)	Axial Stress Distribution (MPa)
S4_1	1	CSAB#4	Csteel	18.40	97.99	6.47	14.91	105.13	4.15E-05	2.07E-02
S4_2	1	CSAB#4	Csteel	35.20	110.23	12.37	19.39	132.55	5.87E-05	3.67E-02
S4_3	1	CSAB#4	Csteel	25.80	123.65	9.07	29.21	180.79	-2.11E-05	3.68E-02
S4_4	1	CSAB#4	Csteel	37.10	128.36	13.04	28.74	172.44	1.80E-05	4.60E-02
S4_5	1	CSAB#4	Csteel	16.6	56.74	5.83	21.99	127.40	3.20E-06	2.17E-02
S4_6	7	CSAB#4	Csteel	43.10	171.85	15.15	6.92	84.86	1.94E-04	1.40E-02
S4_7	7	CSAB#4	Csteel	25.20	83.11	8.86	8.31	86.99	1.02E-04	1.89E-02
S4_8	7	CSAB#4	Csteel	39.40	127.89	13.85	12.37	105.45	1.08E-04	2.84E-02
S4_9	7	CSAB#4	Csteel	16.20	62.67	5.69	11.06	94.36	4.49E-05	1.64E-02
S4_10	7	CSAB#4	Csteel	61.90	177.52	21.76	18.19	144.31	9.08E-05	4.96E-02
S4_11	21	CSAB#4	Csteel	54.50	159.61	19.16	6.72	81.89	1.72E-04	2.07E-02
S4_12	21	CSAB#4	Csteel	69.10	107.25	24.29	25.30	159.02	7.77E-05	5.55E-02
S4_13	21	CSAB#4	Csteel	49.60	119.48	17.43	7.35	86.55	1.75E-04	1.82E-02
S4_14	21	CSAB#4	Csteel	57.9	109.12	20.35	6.40	78.44	1.98E-04	1.54E-02
S4_15	21	CSAB#4	Csteel	62.8	112.87	22.07	5.06	85.25	1.77E-04	2.27E-02

Sample ID	Day	Cement	Fiber	Peak Load (N)	Toughness (mJ)	Interface Shear Stress (MPa)	Debonding -Energy Density (mJ/mm ³)	Bridging Stress (MPa)	Interfacial Shear Stress Distribution (MPa)	Axial Stress Distribution (MPa)
S4_16	28	CSAB#4	Csteel	94.30	201.14	33.14	11.30	92.14	9.07E-05	6.88E-02
S4_17	28	CSAB#4	Csteel	82.00	161.73	28.82	10.71	105.85	9.63E-05	5.78E-02
S4_18	28	CSAB#4	Csteel	61.50	148.39	21.62	9.36	92.34	1.62E-04	2.55E-02
S4_19	28	CSAB#4	Csteel	59.40	213.31	20.88	7.38	84.95	1.71E-04	2.21E-02
S4_20	28	CSAB#4	Csteel	98.50	188.96	34.62	11.96	102.70	1.29E-04	5.50E-02
S4_21	56	CSAB#4	Csteel	92.60	203.49	32.55	6.14	85.31	1.40E-04	4.48E-02
S4_22	56	CSAB#4	Csteel	82.80	199.48	29.10	15.80	105.88	1.42E-04	3.94E-02
S4_23	56	CSAB#4	Csteel	77.90	171.19	27.38	9.67	90.80	1.34E-04	3.97E-02
S4_24	56	CSAB#4	Csteel	65.8	165.98	23.13	10.06	74.48	1.60E-04	2.62E-02
S4_25	56	CSAB#4	Csteel	72.9	176.15	25.62	8.50	108.95	1.04E-04	4.69E-02
S4_26	112	CSAB#4	Csteel	95.2	200.14	26.43	12.61	69.93	6.55E-05	5.73E-02
S4_27	112	CSAB#4	Csteel	97.3	206.11	27.17	9.85	103.93	8.56E-05	5.23E-02
S4_28	112	CSAB#4	Csteel	85.7	184.26	23.09	14.37	81.10	1.08E-04	3.82E-02
S4_29	112	CSAB#4	Csteel	91.9	192.44	28.79	4.55	75.17	1.27E-04	4.09E-02
S4_30	112	CSAB#4	Csteel	100.5	189.34	24.78	7.58	106.31	9.92E-05	4.36E-02

Sample ID	Day	Cement	Fiber	Peak Load (N)	Toughness (mJ)	Interface Shear Stress (MPa)	Debonding -Energy Density (mJ/mm ³)	Bridging Stress (MPa)	Interfacial Shear Stress Distribution (MPa)	Axial Stress Distribution (MPa)
PP4_1	1	CSAB#4	PP	6.5	19.32	0.96	3.13	16.30	9.44E-06	4.35E-04
PP4_2	1	CSAB#4	PP	3.5	15.74	0.52	0.36	5.74	1.22E-04	1.30E-04
PP4_3	1	CSAB#4	PP	7.6	34.49	1.13	17.94	39.33	-2.00E-10	5.28E-04
PP4_4	1	CSAB#4	PP	6.8	27.50	1.01	0.80	8.67	1.06E-04	2.80E-04
PP4_5	1	CSAB#4	PP	5.2	13.87	0.77	14.62	37.26	-3.78E-08	3.61E-04
PP4_6	7	CSAB#4	PP	6.4	42.68	0.95	0.00	15.19	1.18E-05	3.89E-04
PP4_7	7	CSAB#4	PP	11.2	50.62	1.66	6.81	23.93	3.29E-06	7.06E-04
PP4_8	7	CSAB#4	PP	7.5	27.90	1.11	2.46	14.46	2.36E-05	4.34E-04
PP4_9	7	CSAB#4	PP	15.8	37.63	2.34	1.85	16.87	5.44E-05	7.90E-04
PP4_10	7	CSAB#4	PP	5.7	18.91	0.84	1.31	10.40	5.02E-05	2.91E-04
PP4_11	21	CSAB#4	PP	5.9	18.57	0.87	3.59	18.27	1.75E-06	3.53E-04
PP4_12	21	CSAB#4	PP	11.6	24.81	1.72	3.68	18.16	2.04E-05	6.41E-04
PP4_13	21	CSAB#4	PP	5.5	13.21	0.81	0.72	8.26	8.26E-05	2.19E-04
PP4_14	21	CSAB#4	PP	12.3	21.47	1.82	2.02	13.04	7.29E-05	5.19E-04
PP4_15	21	CSAB#4	PP	8.0	16.62	1.18	2.02	13.91	2.95E-05	4.24E-04

Sample ID	Day	Cement	Fiber	Peak Load (N)	Toughness (mJ)	Interface Shear Stress (MPa)	Debonding -Energy Density (mJ/mm ³)	Bridging Stress (MPa)	Interfacial Shear Stress Distribution (MPa)	Axial Stress Distribution (MPa)
PP4_16	28	CSAB#4	PP	10.2	19.51	1.51	3.00	16.51	2.30E-05	5.47E-04
PP4_17	28	CSAB#4	PP	5.1	12.14	0.76	4.36	19.04	4.63E-07	3.02E-04
PP4_18	28	CSAB#4	PP	4.7	10.75	0.70	0.54	7.03	9.58E-05	1.68E-04
PP4_19	28	CSAB#4	PP	17.2	31.72	2.55	1.02	9.57	1.51E-04	3.81E-04
PP4_20	28	CSAB#4	PP	6.9	20.62	1.02	2.64	15.18	1.28E-05	3.87E-04
PP4_21	56	CSAB#4	PP	6.8	19.25	1.01	1.68	11.91	3.68E-05	3.30E-04
PP4_22	56	CSAB#4	PP	13.1	28.74	1.94	2.97	19.09	1.98E-05	6.89E-04
PP4_23	56	CSAB#4	PP	9.5	27.28	1.41	2.39	17.50	1.33E-05	5.14E-04
PP4_24	56	CSAB#4	PP	11	24.44	1.63	2.43	16.86	2.35E-05	5.68E-04
PP4_25	56	CSAB#4	PP	7.8	24.81	1.15	1.86	15.05	1.77E-05	4.14E-04
PP4_26	112	CSAB#4	PP	4.3	26.87	0.64	0.46	8.16	5.59E-05	1.78E-04
PP4_27	112	CSAB#4	PP	8.7	30.44	1.29	0.27	10.62	7.04E-05	3.30E-04
PP4_28	112	CSAB#4	PP	8.4	31.69	1.24	0.23	12.92	3.74E-05	3.83E-04
PP4_29	112	CSAB#4	PP	5.1	32.74	0.76	0.24	10.21	3.55E-05	2.35E-04
PP4_30	112	CSAB#4	PP	8.6	28.11	1.27	3.40	19.81	3.51E-06	4.61E-04

Sample ID	Day	Cement	Fiber	Peak Load (N)	Toughness (mJ)	Interface Shear Stress (MPa)	Debonding -Energy Density (mJ/mm ³)	Bridging Stress (MPa)	Interfacial Shear Stress Distribution (MPa)	Axial Stress Distribution (MPa)
PVA4_1	1	CSAB#4	PVA	1.4	1.34	0.74	0.15	3.37	9.10E-06	1.34E-04
PVA4_2	1	CSAB#4	PVA	1.9	1.37	1.00	0.30	4.84	4.03E-06	2.09E-04
PVA4_3	1	CSAB#4	PVA	1.5	1.64	0.79	0.18	3.70	7.48E-06	1.50E-04
PVA4_4	1	CSAB#4	PVA	1.1	0.90	0.58	0.16	3.80	3.45E-06	1.23E-04
PVA4_5	1	CSAB#4	PVA	0.6	0.31	0.32	0.04	1.65	1.79E-05	4.24E-05
PVA4_6	7	CSAB#4	PVA	4.8	21.94	2.54	13.96	26.41	-3.43E-09	5.35E-04
PVA4_7	7	CSAB#4	PVA	0.8	0.60	0.42	0.08	2.17	1.28E-05	6.16E-05
PVA4_8	7	CSAB#4	PVA	1.2	2.42	0.63	0.07	2.07	2.01E-05	6.84E-05
PVA4_9	7	CSAB#4	PVA	1	1.62	0.53	0.08	2.42	1.28E-05	7.69E-05
PVA4_10	7	CSAB#4	PVA	3.3	16.34	1.74	4.54	16.77	1.65E-12	3.68E-04
PVA4_11	21	CSAB#4	PVA	6.8	12.00	3.59	9.23	21.51	3.34E-11	7.15E-04
PVA4_12	21	CSAB#4	PVA	5.5	3.39	2.91	3.15	15.13	7.71E-09	5.78E-04
PVA4_13	21	CSAB#4	PVA	2.6	0.55	1.37	0.48	6.54	1.37E-06	2.64E-04
PVA4_14	21	CSAB#4	PVA	4.7	5.88	2.48	5.69	19.31	3.30E-12	4.94E-04
PVA4_15	21	CSAB#4	PVA	4.7	17.70	2.48	12.60	21.57	-9.38E-14	4.94E-04

Sample ID	Day	Cement	Fiber	Peak Load (N)	Toughness (mJ)	Interface Shear Stress (MPa)	Debonding -Energy Density (mJ/mm ³)	Bridging Stress (MPa)	Interfacial Shear Stress Distribution (MPa)	Axial Stress Distribution (MPa)
PVA4_16	28	CSAB#4	PVA	2.9	1.14	1.53	0.99	13.64	6.63E-11	3.00E-04
PVA4_17	28	CSAB#4	PVA	4.4	2.67	2.32	10.52	14.01	3.80E-09	4.55E-04
PVA4_18	28	CSAB#4	PVA	6.5	6.27	3.43	6.23	21.76	1.10E-11	6.72E-04
PVA4_19	28	CSAB#4	PVA	17.1	27.55	9.03	6.57	24.84	2.24E-08	1.77E-03
PVA4_20	28	CSAB#4	PVA	5.4	19.84	2.85	11.30	27.12	-2.76E-10	5.58E-04
PVA4_21	56	CSAB#4	PVA	4.6	16.79	2.43	11.48	24.70	-9.30E-11	4.60E-04
PVA4_22	56	CSAB#4	PVA	3	3.80	1.58	9.86	14.37	1.95E-11	3.00E-04
PVA4_23	56	CSAB#4	PVA	4.4	7.13	2.32	6.86	22.24	-1.31E-12	4.40E-04
PVA4_24	56	CSAB#4	PVA	5.3	6.03	2.80	5.51	21.46	4.30E-13	5.31E-04
PVA4_25	56	CSAB#4	PVA	4.9	6.38	2.59	6.13	21.55	5.08E-14	4.90E-04
PVA4_26	112	CSAB#4	PVA	4.1	15.11	2.17	8.26	22.30	-4.64E-12	3.90E-04
PVA4_27	112	CSAB#4	PVA	3.8	6.21	2.01	6.01	20.24	-2.48E-13	3.61E-04
PVA4_28	112	CSAB#4	PVA	5.2	5.87	2.75	10.87	25.01	-3.76E-12	4.94E-04
PVA4_29	112	CSAB#4	PVA	5.9	10.88	3.12	7.89	23.53	4.61E-14	5.61E-04
PVA4_30	112	CSAB#4	PVA	4.1	9.41	2.17	6.06	28.47	5.79E-13	3.90E-04

REFERENCES

- ACI, "Report on the Physical Properties and Durability of Fiber-Reinforced Concrete," ACI 5445R-10, March. 2010, pp. 35.
- Arjunan P, Silsbee MR, Della MR, "Sulfoaluminate-belite cement from low-calcium fly ash and sulfur-rich and other industrial by-products," *Cement and Concrete Research*, V. 29, No. 8. 1999, pp. 1305-11.
- ASTM Standard C 109, 2011, "Standard Test Method for Compressive Strength of Hydraulic Cement Mortars (Using 2-in. or [50-mm] Cube Specimens)," ASTM International, West Conshohocken, PA, 2008, DOI: 10.1520/C0109_C0109M-11, www.astm.org
- Atkins AG, "Intermittent bonding for high toughness/ high strength composites," *Journal of Materials Science*, V. 10, No. 5, 1975/05/01. 1975, pp. 819-32.
- Aveston J, Cooper GA, Kelly A, "Single and Multiple Fracture," In: *Proceedings of the The Properties of Fiber Composites*, Surrey, U.K., 1971, pp. 15-26.
- Bartos P, "Review paper: Bond in fibre reinforced cements and concretes," *International Journal of Cement Composites and Lightweight Concrete*, V. 3, No. 3. 1981, pp. 159-77.
- Becher PF, Hsueh CH, Angelini P, Tiegs TN, "Toughening Behavior in Whisker-Reinforced Ceramic Matrix Composites," *Journal of the American Ceramic Society*, V. 71, No. 12. 1988, pp. 1050-61.
- Bentur A, Mindess S, Vondran G, "Bonding in polypropylene fibre reinforced concretes," *International Journal of Cement Composites and Lightweight Concrete*, V. 11, No. 3. 1989, pp. 153-8.
- Beretka J, de Vito B, Santoro L, Sherman N, Valenti GL, "Hydraulic behaviour of calcium sulfoaluminate-based cements derived from industrial process wastes," *Cement and Concrete Research*, V. 23, No. 5. 1993, pp. 1205-14.
- Bernardo G, Marroccoli M, Montagnaro F, Valenti GL, "Use of Fluidized Bed Combustion Ash as Raw Feed in the Manufacture of Calcium Sulfoaluminate Cements," *Fly Ash, Silica Fume, Slag, and Natural Pozzolans in Concrete*, Malhotra VM, ed., 2004, pp. 169-80.
- Bernardo G, Telesca A, Valenti GL, "A porosimetric study of calcium sulfoaluminate cement pastes cured at early ages," *Cement and Concrete Research*, V. 36, No. 6. 2006, pp. 1042-7.
- Betterman LR, Ouyang C, Shah SP, "Fiber-matrix interaction in microfiber-reinforced mortar," *Advanced Cement Based Materials*, V. 2, No. 2. 1995, pp. 53-61.
- Beyerlein IJ, Zhu YT, Mahesh S, "On the influence of fiber shape in bone-shaped short-fiber composites," *Composites Science and Technology*, V. 61, No. 10. 2001, pp. 1341-57.

Bin Y, Mine M, Koganemaru A, Jiang X, Matsuo M, "Morphology and mechanical and electrical properties of oriented PVA-VGCF and PVA-MWNT composites," *Polymer*, V. 47, No. 4. 2006, pp. 1308-17.

Box GE, Cox DR, "An analysis of transformations," *Journal of the Royal Statistical Society Series B (Methodological)*. 1964, pp. 211-52.

Brandt AM, "Fibre reinforced cement-based (FRC) composites after over 40 years of development in building and civil engineering," *Composite Structures*, V. 86, No. 1-3. 2008, pp. 3-9.

Brogren C, Karlsson HT, "Modeling the absorption of SO₂ in a spray scrubber using the penetration theory," *Chemical Engineering Science*, V. 52, No. 18. 1997, pp. 3085-99.

Brown ADR, "Application of Calcium Sulfoaluminate Cements in the 21st Century," In: *Proceedings of the Concrete 2000*, Dundee, UK, 1993, pp. 1773-8.

Brown R, Shukla A, Natarajan KR, "Fiber Reinforcement of Concrete Structures," University of Rhode Island, Dept. of Chemical Engineering, City, 2002, pp. 51.

Brunner, E., Dette, H., and A. Munk, "Box-Type Approximations in Nonparametric Factorial Designs," *Journal of the American Statistical Association*, V. 92, 1997, pp. 1494-1502.

Cadek M, Coleman JN, Barron V, Hedicke K, Blau WJ, "Morphological and mechanical properties of carbon-nanotube-reinforced semicrystalline and amorphous polymer composites," *Applied Physics Letters*, V. 81, No. 27. 2002, pp. 5123-5.

Chan Y-W, Chu S-H, "Effect of silica fume on steel fiber bond characteristics in reactive powder concrete," *Cement and Concrete Research*, V. 34, No. 7. 2004, pp. 1167-72.

Chanvillard, G., Aïtcin, P-C., "Pull-out behavior of corrugated steel fibers : Qualitative and statistical analysis," *Advanced Cement Based Materials*, V. 4, No. 1. 1996, pp. 28-41.

Chu TJ, Robertson RE, Najm H, Naaman AE, "Effects of poly(vinyl alcohol) on fiber cement interfaces. Part II: Microstructures," *Advanced Cement Based Materials*, V. 1, No. 3. 1994, pp. 122-30.

Cox HL, "The elasticity and strength of paper and other fibrous materials," *British Journal of Applied Physics*, V. 3, No. 3. 1952, pp. 72.

Cox DR, McCullagh P, "A biometrics invited paper with discussion. Some aspects of analysis of covariance," *Biometrics*. 1982, pp. 541-61.

Damtoft JS, Lukasik J, Herfort D, Sorrentino D, Gartner EM, "Sustainable development and climate change initiatives," *Cement and Concrete Research*, V. 38, No. 2. 2008, pp. 115-27.

Evans AG, McMeeking RM, "On the toughening of ceramics by strong reinforcements," *Acta Metallurgica*, V. 34, No. 12. 1986, pp. 2435-41.

Fahlman BD, "What is Materials Chemistry?." Springer; 2011.

Gartner EM, Macphee DE, "A physico-chemical basis for novel cementitious binders," *Cement and Concrete Research*, V. 41, No. 7. 2011, pp. 736-49.

Glasser FP, Zhang L, "High-performance cement matrices based on calcium sulfoaluminate-belite compositions," *Cement and Concrete Research*, V. 31, No. 12. 2001, pp. 1881-6.

Gray RJ, "Analysis of the effect of embedded fibre length on fibre debonding and pull-out from an elastic matrix," *Journal of Materials Science*, V. 19, No. 3, 1984/03/01. 1984, pp. 861-70.

Greszczuk L, "Theoretical studies of the mechanics of the fiber-matrix interface in composites," *Interfaces in composites*, ASTM STP, V. 452. 1969, pp. 42-58.

Grier D, Jarabek E, Peterson R, Mergen L, McCarthy G, "Rietveld structure refinement of carbonate and sulfite ettringite," *Advances in X-ray Analysis*, V. 45. 2002, pp. 194-9.

Hamoush S, Abu-Lebdeh T, Cummins T, Zornig B, "Pullout Characterizations of Various Steel Fibers Embedded in Very High-Strength Concrete," *American Journal of Engineering and Applied Sciences*, V. 3, No. 2. 2010, pp. 418-26.

Hannant DJ, "4.11 - Cement-based Composites," *Comprehensive Composite Materials*, Kelly A, Zweben C, eds., Pergamon, Oxford, 2000, pp. 323-62.

Hartman MR, Berliner R, "Investigation of the structure of ettringite by time-of-flight neutron powder diffraction techniques," *Cement and Concrete Research*, V. 36, No. 2, 2006, pp. 364-70.

Herrera-Franco PJ, Drzal LT, "Comparison of methods for the measurement of fibre/matrix adhesion in composites," *Composites*, V. 23, No. 1. 1992, pp. 2-27.

Hertzberg RW, "Deformation and Fracture Mechanics of Engineering Materials." 4th ed. Canada: John Wiley & Sons, Inc.; 1996.

Horikoshi, T., Ogawa, A., Saito, T., Hoshiro, H., "Properties of Polyvinylalcohol Fiber as Reinforcing Materials for Cementitious Composites", Kuraray Co., Ltd., City, 2008, pp. 8.

Hsueh C-H, "Elastic load transfer from partially embedded axially loaded fibre to matrix," *Journal of Materials Science Letters*, V. 7, No. 5, 1988/05/01. 1988, pp. 497-500.

Hsueh C-H, "Interfacial debonding and fiber pull-out stresses of fiber-reinforced composites," *Materials Science and Engineering: A*, V. 123, No. 1. 1990, pp. 1-11.

Hsueh CH, Becher PF, "Interfacial shear debonding problems in fiber-reinforced ceramic composites," *Acta Materialia*, V. 46, No. 9. 1998, pp. 3237-45.

Ikeda K, "Cements along the join $C_4A_3S-C_2S$," In: *Proceedings of the 7th International Congress on the Chemistry of Cement*, Paris, 1980, pp. 31-6.

Janotka I, Krajci L, Ray A, Mojumdar SC, "The hydration phase and pore structure formation in the blends of sulfoaluminate-belite cement with Portland cement," *Cement and Concrete Research*, V. 33, No. 4. 2003, pp. 489-97.

Jewell RB, Mahboub KC, Robl TR, Bathke AC, "Interfacial Bond between Reinforcing Fibers and Calcium Sulfoaluminate Cements: Fiber Pullout Characteristics," *ACI Materials Journal*, V. 112, No. 1. 2015, pp. 39-48.

Johnston CD, "Fiber-Reinforced Cements and Concretes." Calgary: Gordon and Breach Science Publishers; 2001.

Juenger MCG, Winnefeld F, Provis JL, Ideker JH, "Advances in alternative cementitious binders," *Cement and Concrete Research*, V. 41, No. 12. 2011, pp. 1232-43.

Kanda T, Li VC, "Interface Property and Apparent Strength of High-Strength Hydrophilic Fiber in Cement Matrix." ASCE; 1998.

Kim J-K, Kim J-S, Ha GJ, Kim YY, "Tensile and fiber dispersion performance of ECC (engineered cementitious composites) produced with ground granulated blast furnace slag," *Cement and Concrete Research*, V. 37, No. 7. 2007, pp. 1096-105.

Kim J-K, Mai Y-w, "High strength, high fracture toughness fibre composites with interface control - A Review," *Composites Science and Technology*, V. 41, No. 4. 1991, pp. 333-78.

Kim J, Mai Y, "Engineered Interfaces in Fiber Reinforced Composites." New York: Elsevier; 1998.

Komatsu R, Mizukoshi N, Makida K, Tsukamoto K, "In-situ observation of ettringite crystals," *Journal of Crystal Growth*, V. 311, No. 3. 2009, pp. 1005-8.

Leung CKY, Li VC, "Applications of a two-way debonding theory to short fibre composites," *Composites*, V. 21, No. 4. 1990, pp. 305-17.

Li VC, Fischer G, "Reinforced ECC - An Evolution From Materials to Structures," In: *Proceedings of the First FIB Congress*, Osaka, Japan, 2002, pp. 18.

Li VC, Kanda T, Lin Z, "The Influence of Fiber/Matrix Interface Properties on Complementary Energy and Composite Damage Tolerance," In: *Proceedings of the Key Engineering Materials: Proceedings, 3rd Conf on Frac & Strength of Solids*, Hong Kong, 1997, pp. 9.

Li V, Leung C, "Steady-State and Multiple Cracking of Short Random Fiber Composites," *Journal of Engineering Mechanics*, V. 118, No. 11. 1992, pp. 2246-64.

Li VC, Stang H, "Interface property characterization and strengthening mechanisms in fiber reinforced cement based composites," *Advanced Cement Based Materials*, V. 6, No. 1. 1997, pp. 1-20.

Li VC, Wu H-C, "Conditions for Pseudo Strain-Hardening in Fiber Reinforced Brittle Matrix Composites," *Applied Mechanics Reviews*, V. 45, No. 8. 1992, pp. 390-8.

Li Z-F, Grubb DT, "Single-fibre polymer composites," *Journal of Materials Science*, V. 29, No. 1, 1994/01/01. 1994, pp. 189-202.

Lin Z, Li VC, "Crack bridging in fiber reinforced cementitious composites with slip-hardening interfaces," *Journal of the Mechanics and Physics of Solids*, V. 45, No. 5. 1997, pp. 763-87.

Littell, R, Henry, P, Ammerman, C, "Statistical Analysis of Repeated Measures Data Using SAS Procedures," *Journal of Animal Science*, V. 76. 1998, pp. 1216-31.

Majling J, Znásik P, Gabrisová A, Svetík S, "The influence of anhydrite activity upon the hydration of calcium sulphoaluminate cement clinker," *Thermochimica Acta*, V. 92. 1985, pp. 349-52.

Markovic I, "High-Performance Hybrid-Fibre Concrete-Development and Utilisation," *Book High-Performance Hybrid-Fibre Concrete-Development and Utilisation, (Doctoral Dissertation)*, Delft University of Technology, City, 2006, pp. 228.

Marrocchi M, Nobili M, Telesca A, Valenti GL, "Early Hydration of Calcium Sulfoaluminate-Based Cements for Structural Applications." London: Taylor & Francis Group; 2007.

Marshall DB, Cox BN, "A J-integral method for calculating steady-state matrix cracking stresses in composites," *Mechanics of Materials*, V. 7, No. 2. 1988, pp. 127-33.

Marshall DB, Cox BN, Evans AG, "The mechanics of matrix cracking in brittle-matrix fiber composites," *Acta Metallurgica*, V. 33, No. 11. 1985, pp. 2013-21.

Marston TU, Atkins AG, Felbeck DK, "Interfacial fracture energy and the toughness of composites," *Journal of Materials Science*, V. 9, No. 3, 1974/03/01. 1974, pp. 447-55.

McDonald JH, "Handbook of biological statistics." Sparky House Publishing Baltimore, MD; 2009.

Mehta PK, "Mechanism of expansion associated with ettringite formation," *Cement and Concrete Research*, V. 3, No. 1. 1973, pp. 1-6.

Mehta PK, Monteiro PJM, "Concrete, Microstructure, Properties and Materials." 3rd ed.: McGraw-Hill, USA; 2006.

Mobasher B, Cheng Yu L, "Effect of interfacial properties on the crack propagation in cementitious composites," *Advanced Cement Based Materials*, V. 4, No. 3-4. 1996, pp. 93-105.

Mobasher B, Stang H, Shah SP, "Microcracking in fiber reinforced concrete," *Cement and Concrete Research*, V. 20, No. 5. 1990, pp. 665-76.

Montgomery MD, "How does cement stabilisation work?." *Stabilised Soil Research Progress Report (SSRPR2)*. Warwick: School of Engineering Development Technology Unit, University of Warwick, Warwick; 1998.

Moore A, Taylor HFW, "Crystal Structure of Ettringite," *Nature*, V. 218, No. 5146, 06/15/print. 1968, pp. 1048-9.

Naaman AE, Namur GG, Alwan JM, Najm HS, "Fiber Pullout and Bond Slip. I: Analytical Study," *Journal of Structural Engineering*, V. 117, No. 9. 1991, pp. 2769-90.

Naebe M, Lin T, Staiger MP, Dai L, Wang X, "Electrospun single-walled carbon nanotube/polyvinyl alcohol composite nanofibers: structure-property relationships," *Nanotechnology*, V. 19, No. 30. 2008, pp. 8.

Nairn JA, "A variational mechanics analysis of the stresses around breaks in embedded fibers," *Mechanics of Materials*, V. 13, No. 2. 1992, pp. 131-54.

Nairn JA, Liu C-H, Mendels DA, Zhandarov S, "Fracture Mechanics Analysis of the Single-Fiber Pull-Out Test and the Microbond Test Including The Effects of Friction and Thermal Stresses," In: *Proceedings of the 16th Ann Tech Conf of the Amer Soc Composites*, VPI, Blacksburg, VA, 2001, pp. 12.

Najm H, Naaman AE, Chu TJ, Robertson RE, "Effects of poly(vinyl alcohol) on fiber cement interfaces. Part I: Bond stress-slip response," *Advanced Cement Based Materials*, V. 1, No. 3. 1994, pp. 115-21.

Neville, A.M., "Properties of Concrete." Fourth ed. Singapore: Pearson Education Ltd.; 1995.

Pan N, "Theoretical Modeling and Analysis of Fiber-pull-out Behaviour from a Bonded Fibrous Matrix: The Elastic-bond Case," *Journal of the Textile Institute*, V. 84, No. 3. 1993, pp. 472-85.

Pitkethly MJ, Doble JB, "Characterizing the fibre/matrix interface of carbon fibre-reinforced composites using a single fibre pull-out test," *Composites*, V. 21, No. 5. 1990, pp. 389-95.

Redon C, Li VC, Wu C, Hoshiro H, Saito T, Ogawa A, "Measuring and Modifying Interface Properties of PVA Fibers in ECC Matrix," *Journal of Materials in Civil Engineering*, V. 13, No. 6. 2001, pp. 399-406.

Richardson IG, "The nature of C-S-H in hardened cements," *Cement and Concrete Research*, V. 29, No. 8. 1999, pp. 1131-47.

Roy DM, Silsbee MR, Xie Z, "Influences of Surplus SO₃ in FBC Ash on Formation of Belite-Rich Sulfoaluminate Clinker," *Book Influences of Surplus SO₃ in FBC Ash on Formation of Belite-Rich Sulfoaluminate Clinker*, Editor, ed.^eds., City, 1999, pp. 5.

Sahu S, Majling Jn, "Preparation of sulphoaluminate belite cement from fly ash," *Cement and Concrete Research*, V. 24, No. 6. 1994, pp. 1065-72.

Schneider M, Romer M, Tschudin M, Bolio H, "Sustainable cement production-present and future," *Cement and Concrete Research*, V. 41, No. 7. 2011, pp. 642-50.

Shah SP, "Do Fibers Increase the Tensile Strength of Cement-Based Matrixes?," *American Concrete Institute Materials Journal*, V. 88, No. 6, Nov-Dec 1991, pp. 595-602.

Sherman N, Beretka J, Santoro L, Valenti GL, "Long-term behaviour of hydraulic binders based on calcium sulfoaluminate and calcium sulfoasilicate," *Cement and Concrete Research*, V. 25, No. 1. 1994, pp. 113-26.

Silknitter KO, Wisnowski JW, Montgomery DC, "The analysis of covariance: a useful technique for analysing quality improvement experiments," *Quality and reliability engineering international*, V. 15, No. 4. 1999, pp. 303-16.

Stang H, Li Z, Shah SP, "Pullout Problem: Stress versus Fracture Mechanical Approach," *Journal of Engineering Mechanics*, V. 116, No. 10. 1990, pp. 2136-50.

Stark J, Bollmann K, "Delayed ettringite formation in concrete," *NORDIC CONCRETE RESEARCH-PUBLICATIONS-*, V. 23. 2000, pp. 4-28.

Stark J, Möser B, Bellmann F, "Nucleation and growth of C-S-H phases on mineral admixtures," *Advances in Construction Materials 2007*, Grosse C, ed., Springer Berlin Heidelberg, 2007, pp. 531-8.

Stengel, T., "Fibre Reinforced Civil Engineering Materials: A Model for Fibre Pull-Out Based on Tribological Mechanisms and Contact Mechanics", 2010, pp. 9.

Subramani S, Gaurav N, "Fiber-Matrix Interface Characterization through the Microbond Test," *International Journal Aeronautical and Space Sciences*, V. 13, No. 3. 2012, pp. 282-95.

Takaku A, Arridge RGC, "The effect of interfacial radial and shear stress on fibre pull-out in composite materials," *Journal of Physics D: Applied Physics*, V. 6, No. 17. 1973, pp. 2038.

Taylor HFW, "Cement Chemistry." 2nd ed. London: Thomas Telford; 1997.

Taylor HFW, Famy C, Scrivener KL, "Delayed ettringite formation," *Cement and Concrete Research*, V. 31, No. 5. 2001, pp. 683-93.

Torre AFdl, Aranda MAG, Aza Moya AHd, Aza Pendas Sd, Pena Castro MdP, "Belite Portland Clinkers. Synthesis and Mineralogical Analysis," *Bol Soc Esp Ceram*, V. 44, No. 3, May. 2005, pp. 185-91.

Ukrainezyk N, Frankoviæ Mihelj N, Šipušić J, "Calcium Sulfoaluminate Eco-Cement from Industrial Waste," *Chemical and Biochemical Engineering Quarterly*, V. 27, No. 1. 2013, pp. 83-93.

van Zijl GP, "Durability under mechanical load—micro-crack formation (ductility)," Durability of Strain-Hardening Fibre-Reinforced Cement-Based Composites (SHCC), Springer, 2011, pp. 9-39.

Vano M, Goracci C, Monticelli F, Tognini F, Gabriele M, Tay F, et al., "The adhesion between fibre posts and composite resin cores: the evaluation of microtensile bond strength following various surface chemical treatments to posts," International Endodontic Journal, V. 39, No. 1. 2006, pp. 31-9.

Wang Y, Li VC, Backer S, "Modelling of fibre pull-out from a cement matrix," International Journal of Cement Composites and Lightweight Concrete, V. 10, No. 3. 1988, pp. 143-9.

Wille K, Naaman AE, "Pullout Behavior of High-Strength Steel Fibers Embedded in Ultra-High-Performance Concrete," ACI Materials Journal, V. 109, No. 4, July 1. 2012, pp. 479-88.

Winnefeld F, Lothenbach B, "Hydration of calcium sulfoaluminate cements -- Experimental findings and thermodynamic modelling," Cement and Concrete Research, V. In Press, Corrected Proof. 2010.

Woodson RD, "Chapter 2 - Concrete Materials," Concrete Portable Handbook, Butterworth-Heinemann, Boston, 2012, pp. 5-18.

Xu Q, Stark J, "Early hydration of ordinary Portland cement with an alkaline shotcrete accelerator," Advances in cement research, V. 17, No. 1. 2005, pp. 1-8.

Xu S, Zhang X, "Determination of fracture parameters for crack propagation in concrete using an energy approach," Engineering Fracture Mechanics, V. 75, No. 15. 2008, pp. 4292-308.

Yamazaki T, Schricker SR, Brantley WA, Culbertson BM, Johnston W, "Viscoelastic behavior and fracture toughness of six glass-ionomer cements," The Journal of prosthetic dentistry, V. 96, No. 4. 2006, pp. 266-72.

Yang E-H, Wang S, Yang Y, Li VC, "Fiber-bridging constitutive law of engineered cementitious composites," Journal of advanced concrete technology, V. 6, No. 1. 2008, pp. 181-93.

Zhang L, Glasser FP, "Modern Concrete Materials: Binders, Additions and Admixtures." London: Thomas Telford Publishing; 1999.

Zhang L, Su M, Wang Y, "Development of the use of sulfo- and ferroaluminate cements in China," Advances in Cement Research, V. 11, No. 1, January, 1. 1999, pp. 15-21.

Zhou L-M, Kim J-K, Mai Y-W, "Micromechanical characterisation of fibre/matrix interfaces," Composites Science and Technology, V. 48, No. 1–4. 1993, pp. 227-36.

Zucchini A, Hui CY, "Detailed analysis of the fibre pull-out test," Journal of Materials Science, V. 31, No. 21. 1996, pp. 5631-41.

VITA

Robert Benjamin Jewell (Bob)

RESEARCH INTERESTS

Research Interests include process development for ash beneficiation including ash sampling techniques, the fabrication of new low energy, low CO₂ emitting construction materials including cements and concretes from coal by products. Additional interests include the development of smart energy-harvesting cementitious materials for civil engineering structures.

EDUCATION

Ph.D., Civil Engineering, 2015, University of Kentucky, Lexington, Kentucky.

M.S., Geology, 2004, University of Kentucky, Lexington, Kentucky.

B.S., Geology, 2002, University of Kentucky, Lexington, Kentucky.

GRADUATE ADVISOR

Prof. Kamyar Mahboub, PhD advisor, Civil Engineering, University of Kentucky.

EXPERIENCE

2002-2004 Research Assistant, Environmental and Coal Technologies Group, Center for Applied Energy Research, University of Kentucky.

2004-2012 Scientist I – Research, Center for Applied Energy Research, University of Kentucky.

2012-Present Associate Research Scientist, Center for Applied Energy Research,
University of Kentucky.

SYNERGISTIC ACTIVITIES

Delegate, Asian Coal Ash Association: Utilization of Dry Scrubber Materials in Portland
Cement Concrete, Coal Ash Asia Conference, Shuozhou, Shanxi Province, China,
September, 2014.

Lecturer, Coal Combustion Products Utilization and Management: A Practical
Workshop, April 2014, Lexington, KY.

Delegate, Asian Coal Ash Association: An Overview of Fluidized Bed Combustion Spent
Bed Material Utilization in the U.S., Coal Ash Asia Conference, Shuozhou, Shanxi
Province, China, September, 2013.

Lecturer, Coal Combustion Products Utilization and Management: A Practical
Workshop, October 2012, Lexington, KY.

Co-organizer and speaker for the World of Coal Ash Conference and Coal Ash Short
Course, 2007 – present.

Organizer for UK CAER Outreach Program to Elementary-age children, 2004 – present.

Development of Tekcrete Fast® and Teckcrete Fast M®. Working with a team that
included Peter Mills of Minova USA, developed and jointly patented an ultrafast strength
developing shotcrete for mining and civil engineering. This product is helping provide
added safety in mines with weak and unstable roof conditions.

GRANTS AND CONTRACTS

Active Grants

Jewell, R. (PI). “Ettringite, a Novel Piezoelectric Source Crystal for Energy Harvesting Materials”, National Science Foundation, \$309,737, 8/1/14-7/30/17.

Jewell, R. (PI). “Use of Spray Dryer Absorber Material as a Replacement for Portland Cement in Concrete”, Electric Power Research Institute, \$151,964, 5/1/13-10/30/14.

Jewell, R. (PI). “Evaluation of Dry Flue Gas Desulfurization Byproducts in Cement Applications”, Lonjing Environment Technology Co., Ltd., \$25,000, 1/3/14-7/30/14.

Jewell, R. (PI). “Evaluation of Pure Ettringite/MWCNT Array Layered Composite for Piezoelectric Effect”, Seed Grant from the University of Kentucky Center for Applied Energy Research, \$34,976, 2/28/14-7/28/14.

Completed Grants

Robl, T. (PI), Rathbone, R. (Co-PI), **Jewell, R.** (Co-PI). “Center for Coal-Derived Low Energy Materials for Sustainable Construction”, U.S. Department of Energy/NETL, \$913,985, Kentucky Energy and Environment Cabinet, \$114,248, 2008.

Robl, T. (PI), Rathbone, R. (Co-PI), **Jewell, R.** (Co-PI). “Rapidly Deployable System for the Structural Stabilization of Shock Damaged Structures”, Department of Homeland Security/NIHS, \$991,408.

PATENTS

Mills, P., Robl, T., Rathbone, R., **Jewell, R.**, Cementitious Composites, U.S. Patent Application Publication, US 2012/0145044 A1, July 14, 2012.

PUBLICATIONS

Jewell, R.B., Mahboub, K.C., Robl, T.L., Bathke, A.C., “Interfacial Bond between Reinforcing Fibers and Calcium Sulfoaluminate Cements: Fiber Pullout Characteristics,” *ACI Materials Journal*, 111(1-6), 2014.

Jewell, R. "Micromechanics and Complementary Energy of Fibers Embedded in a Low-Energy CSA Cement Matrix," *World of Coal Ash*, Apr. 23-25, Lexington, KY, 2013.

Muh-Cheng, M.W, Jiang, Y., Su. Q., Robl, T., **Jewell R.**, Butalia, T.S., Zhang, W., Wolfe, W., *Dry FGD By-Product Characteristics and Utilization – International Perspective*, *World of Coal Ash*, Lexington, KY, 2013.

Robl, T., **Jewell, R.**, Oberlink, A., Value Added and Advance Uses for Coal Combustion Fly Ash, *in Proceedings of the Asian Coal Ash Conference*, held in Shuozhou City, Shanxi Province, China, September, 2013.

Jewell, R., Oberlink, A., Robl, T., An Overview of Fluidized Bed Combustion Spent Bed Material Utilization in the U.S., *in Proceedings of the Asian Coal Ash Conference*, held in Shuozhou City, Shanxi Province, China, September, 2013.

Jewell, R.B., Mahboub, K.C., Robl, T.L., Interfacial Bond between Reinforcing Fibres and CSA Cements: An Examination of its Influence on Fibre Pullout Characteristics, *in*

Proceedings of the Concrete in a Low Carbon Era Conference, held at the University of Dundee, Scotland, UK, 2012.

Jewell, R.B., Oberlink, A., Robl, T., Rapidly Deployable System Including a CSA Guniting Material for the Structural Stabilization of Shock Damaged Structures, *in* Proceedings of the Concrete in a Low Carbon Era Conference, held at the University of Dundee, Scotland, UK, 2012.

Silva, L.F.O.; Jasper, A.; Andrade, M.L.; Sampaio, C.H.; Dai, S.; Li., X.; Li, T.; Chen, W.; Wang, X.; Liu, H.; Zhao, L.; Hopps, S.G.; **Jewell, R.B.**; Hower, J.C. "Applied investigation on the interaction of hazardous elements binding on ultrafine and nanoparticles in Chinese anthracite-derived fly ash," *The Science of the Total Environment*, 419, 250-264, 2012.

Duvallet, T.; Rathbone, R. F.; Henke, K. R.; **Jewell, R. B.** "Low-Energy, Low CO₂-Emitting Cements Produced from Coal Combustion By-Products and Red Mud," *World of Coal Ash: Science Applications and Sustainability*, May 4-7, Lexington, KY, WOCA 2009 Proceedings, CD, 2009.

Jewell, R.; Robl, T.; Rathbone, R.; Groppo, J.; Hower, J.C. "The sedimentation, stratigraphy and petrography of a coal-ash pond in Carroll County, Kentucky," *World of Coal Ash: Science Applications and Sustainability*, May 4-7, Lexington, KY, WOCA 2009 Proceedings, CD, 2009.

Jewell, R. B.; Rathbone, R. F.; Robl, T. L.; Henke, K. R. "Fabrication and Testing of CSAB Cements in Mortar and Concrete that Utilize Circulating Fluidized Bed

Combustion Byproducts," World of Coal Ash: Science Applications and Sustainability, May 4-7, Lexington, KY, WOCA 2009 Proceedings, CD, 2009.

Jewell, R.B.; Rathbone, R.F. "Optical Properties of Coal Combustion Byproducts for Particle-Size Analysis by Laser Diffraction," Coal Combustion and Gasification Products (CCGP) 1, <http://www.coalccgp-journal.org/papers/2009/CCGP-D-09-00001-Jewell.pdf>, 2009.

Jewell, R.; Rathbone, R.; Robl, T. "The Fabrication of Value Added Cement Products from Circulating Fluidized Bed Combustion Ash," 2007 World of Coal Ash Conference (WOCA) May 7-10, Covington, KY, Proceedings CD, Paper 90, 2007.

Jewell, R.B. "Digital Mapping of the Sedimentation and Stratigraphy of a Coal-ash Pond Using Vibracore and Ground-penetrating Radar Analysis," Regional Geological Society of America Meeting, Mar 24-27, Tyson's Corner, Virginia, Geological Society of America Abstracts with Programs, 36(2) 136, 2004.

Jewell, R. B. Lexington, KY, The Sedimentation, Stratigraphy, and Petrography of a Coal-Ash Pond in Carroll County, Kentucky, Masters Thesis, University of Kentucky, 156 leaves, 2004.

Jewell, R. "Vibracore Sampling in a Coal Ash Pond," 2003 International Ash Utilization Symposium, Oct. 20-22, Lexington, KY, 2003.

PUBLICATIONS (IN PROGRESS OR SUBMITTED FOR PEER REVIEW)

Jewell, R.B.; Rathbone, R.; Robl, T.L.; Duvallet, T., Mahboub, K.C., “Fabrication and Testing of Low-Energy CSAB Cements that Utilize Circulating Fluidized Bed Combustions Byproducts,” Coal Combustion and Gasification Products (CCPG) Journal, 2015.

Jewell, R.B.; Mahboub, K.C.; Robl, T.L.; (et al.), “Influence of Cement on Multiple Cracking Behavior in Fiber Composites,” American Society of Civil Engineers (ASCE), Materials Journal, 2015.

Jewell, R.B.; Mahboub, K.C.; Robl, T.L.; (et al.), “Influence of Cement Type on Fiber-Matrix Interface Bond Strengths,” American Society of Civil Engineers (ASCE), Materials Journal, 2015.